Uses of Statistical Muscle Models, including a Test of an Equilibrium Point Control Theory of Spinal Cord Function in *Rana Catesbiana.*

by

Eric Peter Loeb

Submitted to the Department of Brain and Cognitive Sciences
in partial fulfillment of the requirements for the degree of

Doctor of Philosophy in Cognitive Neuroscience

at the

MASSACHUSETTS INSTITUTE OF TECHNOLOGY

May 1995

Signature of Author .....
Department of Brain and Cognitive Sciences
May 15, 1995

Certified by .....
Dr. Emilio Bizzi
Professor
Thesis Supervisor

Accepted by .....
Gerald Schneider
Chairman, Departmental Committee on Graduate Students

Uses of Statistical Muscle Models, including a Test of an Equilibrium Point Control Theory of Spinal Cord Function in *Rana Catesbiana.*

by

Eric Peter Loeb

Submitted to the Department of Brain and Cognitive Sciences
on May 15, 1995, in partial fulfillment of the
requirements for the degree of
Doctor of Philosophy in Cognitive Neuroscience

Abstract

Spinal stimulation experiments were recently undertaken in an attempt to elucidate the coordinate transformations being performed by the frog spinal cord (Bizzi, et al, 1991; Giszter, et al, 1993; Loeb, et al, 1993; Saltiel & Bizzi 1994). These experiments have demonstrated that the spinal cord of the frog contains a limited number of "modules". That is, we measured the hindlimb forces evoked by spinal interneuronal stimulation, and observed that the evoked forces occurred in a few discrete clusters of orientations. This result is unexpected because forces which result from random activation of the frog's hindlimb muscles do not fall into discrete clusters. The structure of the hindlimb musculature does not, therefore, predict the striking regularity we have observed after thousands of microstimulation experiments. The small number of force patterns suggests that the spinal cord preferentially represents a limited number of classes of muscle combinations. We theorize that the limited number of spinal modules serve as the basic building blocks of posture and movement (Mussa-Ivaldi, 1992). Descending fibers from supra-spinal structures could conceivably activate simple combinations of the spinal modules in order to produce forces that are not directly represented as modules.

My thesis is devoted to formulating and preliminarily executing a statistical test of that theory. We can stimulate supra-spinal descending axons in order to elicit muscle contractions in the leg, and try to explain the forces resulting from those contractions as being produced by the spinal modules. If we can explain what happened using just the spinal modules, then we cannot rule out the hypothesis that the spinal modules are acting as building blocks. If, however, the muscles provide a significantly better explanation than do the spinal modules, we will have evidence that the spinal modules are being bypassed somehow by the supra-spinal systems, and thus are not acting as building blocks.

The body of the thesis is organized as a march up the neuroaxis. In order to enable computations involving the muscles and the spinal modules, I built computer models

of them. I did this by stimulating isolated muscles and spinal cords in order to observe the effects of activation of the muscles and the spinal modules. I then confirmed that the spinal modules could be found in decerebrate animals by stimulating the spinal cords of decerebrate animals and verifying that the computer models were still valid in that context. Finally, I present the promising preliminary results of the supra-spinal stimulation experiment.

Thesis Supervisor: Dr. Emilio Bizzi
Title: Professor

Acknowledgments

I don't know how it works in the humanities, but I perceive this section of a scientific thesis as the only place where the author has the option of being a human being. We come here to wave farewell, before the soul is sacrificed to the dictates of scientific precision! This is the the place where the I am given a cigarette, and allowed to say a few last words before the firing squad commences its work. Naturally, the "last words" ritual is organized for the pleasure of the executioners, and the acknowledgements are for your benefit, not mine. I may escape the confines of scientific prose for a moment, but what human being can escape the needs of the human community, and who would wish to? So, here is the product of the estimated probability that you are reading these acknowledgements and the extent of my gratitude thresholded by the fact that I have to print the final document in about an hour from now....

I would like to begin by acknowledging God, who created the heavens and earth in six days. By way of comparison, it took me six years to finish this thesis. So much for the reputed God-like qualities of MIT PhDs.

I am grateful to my family. Drs. Jane and Peter Loeb helped me throughout my graduate career financially, emotionally, and professionally. My Mom helped me work out the power analysis in chapter 4, and my Dad confirmed the deep relation between finite-dimensional coordinate transformations and basis function representations (chapter 1). My parents convinced me to remain in this program when I considered switching to AI in 1993. My sister, Gwen, argued equally correctly that I should switch. Gwen is a magical, cheer-bringing woman. Aaron is a fire-eating philosopher and adventurer. He will be a great author, and he is already a great brother! My Grandmother, the venerated Virginia "CyberGranny" Watkins, inspires me with her calm, thoughtful discernment and erudition. My Aunt, Catherine "Cato" Watkins rules the airwaves with her ready sense of humor. My cousins Glen Smith and Alejo Loeb could hardly be more different. I'm not surprised they've never run into each other, despite living on opposite sides of the country. I will be very grateful to my Aunts and Uncles Sarah & John Shirley-Quirk and Alison & David Davis-

Shardt when I finally go down to Washington and stay at their respective houses. It has been too long since I have seen Cousin Amy (and Mitch, Ben, and Nick), but not long enough since I last saw my evil, nasty, demented Aunt Barbara. I hope her brilliant children, Simon and Mia will forgive my thinking there is something wrong with me for liking their Mother as much as I do. I know I have everything to thank Jack, Edwin, and Lisle for. Goodbye, too, to Ella Marie, who launched my graduate career with a quixotic gift.

Dr. Bronwen Brown has been an extraordinary, awesome, indispensable, patient, devoted, instructive editing Godsend. I would confess here that she has taught me to write, except that she would then be in the position of having to disown the previous sentence.

My roommate, Dr. Cindy Wible cooked some food, threw some parties, borrowed some money, bought some wine, washed some dishes, cleaned up some messes in the apartment, bought some plants, broke up with some boyfriends, got back together with some boyfriends, broke up with some boyfriends, rented some movies, watched some TV, went for some walks, and threatened on several occasions to castrate me without ever once asking me about my work. Thank you, Cindy.

I like Jan Ellertsen. She's helpfully answered my many stupid questions as I've finished this thing...in fact, she's been answering my stupid questions for years. More to the point, though, she's really really nice.

As is typical for many graduate students, I have come close to hating my advisor at times. I knew at some level, though, that anyone who didn't like Emilio had some kind of problem. Emilio is a dignified, charming, professional, thoughtful (when he has the time), humane (when he has the option), introspective, observant, literate, and wise man. Despite tremendous temptation to leave, I stuck around in the hopes that I would learn from him the maturity I needed in order to learn from him. I can see now that that was an idiotic way to run my life, so I think I've at least been able to learn a little something of Emilio's practical outlook.

My thesis defense was the best talk I've ever given, and I think some of the credit is due to Mike Jordan. Mike pointed out that it is ignoble either to receive credit

beyond one's merit or to permit only a murky impression of one's merit to be formed by performing at less than one's capacity. In retrospect I find that I feel that Mike's personal comments were an act of true friendship, and that I am looking forward to acting as Mike's friend after this thesis is completed.

I am indebted to Joe Perkell, who read this thesis closely, and provided me with a clear critique.

I am in professional debt to Simon Giszter, Sandro Mussa-Ivaldi, and Phillipe Saltiel. The muscle work was inspired by Philippe, who pointed out that the muscle force fields in the Journal of Neuroscience paper look like the spinal force fields. Hmmm. That was a little over 1 year ago. Philippe set out to understand the muscles by looking at 30 billion EMG patterns. I modelled the muscles. Phillipe's understanding has helped me to proceed, and my models have helped confirm his beliefs. Ours has been a productive muscle synergy. Sandro refuses to accept credit for the form of the muscle models, but he's the one who patiently explained that the gradient of the muscle length determines the joint torque. Actually, he explained it about 5 times before I finally got it. Sandro is a calm, encouraging, compassionate, supportive, brilliant, nice guy. Simon, on the other hand, ... ! Simon has taught me most of what I know about practical physiology. He's put up with all sorts of blathering when I've blathered (like, you know, now, for example?), dithering when I've dithered, slithering, slathering and even kibitzing. For this he's earned nothing more than a bottle of scotch. Life is unfair. Thank you, Simon.

I would especially like to thank Francesca Gandolfo, for making the Bizzi lab the exciting place to work that it has been in the last few years. Midnight naked coed bungee cord jumping off the roof of E25 just would never have been the same without her. Judy Schotland deserves better than to mentioned in a paragraph that contains the preceding sentence, but James Galagan deserves exactly that. Margo Cantor gave the place spirit and a hard time. Brian Bendah taught impromptu courses in skeletal and divorce mechanics. Any scholarship in this thesis is either an accident or due to Matt Tresch (or, as Cindy put it, he walks on clouds). Terry Sanger is some kind of freak of nature – he's just way too damn smart. Reza Schadmehr is turquoise blue

and oblong. Paul Borghesani and Gina Kang provided valuable assistance at various stages along the way.

My office mate, Tom Brashers-Krug, and I have been having fun in the trenches these last few stressful months. I have quite a lot to thank Tom for personally and professionally. He has just now defended his thesis! Congratulations, Tom. I am sure that your measured ethical outlook, wry humor, and personal integrity will get you in a *lot* of trouble. But keep it up, all the same.

You know what? I want to acknowledge Chris Atkeson. It's not been the same around here since he left. Have you heard from him lately? How's he doing?

Patrick Winston took a chance on me and helped start my *other* PhD in motion. Susie Wallerstein and Barry Cronin at WGBH have also recently taken a chance on me. John Mallery is definitely the biggest pain in the ass I have ever worked with, but I nevertheless enjoy his bizarre outlook. I shared with John one of the two happiest professional moments of my graduate career. One moment came at 3 or 4 in the morning, when I danced around the lab overjoyed because a prototype of the muscle model in chapter 2 proved itself to be *both* the best at capturing the muscle data *and* a good representation of the structure of the muscle itself. The other professional "moment" lasted over several months at the end of 1992 when John and I discovered to our astonishment that we really had founded the email publishing system of the transition team and then of the White House. I have always since then felt that absolutely anything is possible.

My Cousin Paul Loeb probably does not want to mentioned here. As I love and admire Paul, tremendously, I really have no choice than to respect his wishes. I could perhaps say that it is profoundly pleasurable to have as a close friend a cousin of one's own age, but I certainly would not mention the influence he has had on my thinking during our long talks about his work.

My dear friend Davy Temperley probably would not mind at all being mentioned here. I have relied on Davy as my sounding board and friendly creative genius for so many years now that I'm able to consult with him when he's not even around. I just think, "what would Davy say" and immediately the answer is available: "something

incredibly clever". At that point, I call Davy to learn the details. Actually, I owe approximately 1,243,558 thanks to the whole Sleator-Temperley family. Mary and Nicholas have been like a second set of parents to me (could I borrow some money?). Lucy is great. Sylvie is wonderful. I don't have time now to call Davy for cleverer things to say than that. Congratulations to Ernie and John! Congratulations too to Danny and Lylia Sleator, whose company I enjoy so much (not the internet-raping one). I will be grateful if Billy lives to be 70. I will be grateful to Tycho and Marina when I stay at their house this summer. I owe Bill and Esther more fond memories of Christmas parties and late-night gatherings than I can ever repay.

Now, is it acceptable to say a few words about Bill Burkholder, Richard and Hara Blaylock (yeah, sure Hara, like I'm going to try to spell it), Kris Gunsalus, Jeff Terstriep, Paulie Profett, Carl Lambarth, Mike Winsell, Peter Krause, and Rosana Francescato in one paragraph? No, it's not. Bill deserves professional citation for the difficult questions he consistently asks whenever I make the mistake of talking about my work around him. He's another one of those freaks of nature. Richard has called me up, made me run, listened to my complaints, and generally put up with me. Hara is the most judgemental person I've ever really liked. Kris will live forever, and I look forward to having more time to hang out together then. Jeff has 3 children and a farm. So he's still, 20 years after we first met, leading the way. Paulie is an eagle and a sparrow, a kitten and a lioness except for her laughter, which is that of a free and happy woman. Carl is another freakishly smart person, and an American philosopher. I am grateful to Mike for his well-timed words of wisdom, "Albert, life is like a sleazy bar in a slum." Peter is still fascinating after all these years. I am grateful to Rosana for remaining in touch despite my being such a poor correspondent. I should go on for pages about every one of my friends, but it might harm the rock that I stand on to show off the sparkle in its heart.

I owe special thanks to Maria-Lisa Abundo, who thinks I am an intellectual. I hope that despite the proof to the contrary contained in this thesis, that we can still be friends.

I want to mention everybody in the department because I have never enjoyed

a crowd of people more than this one. Daniel Emerling, comes first because he can blackmail me. Those nutty, nutty boys of the Jordan lab Zoubin, Flip, and John should put on a musical review, but will instead all disperse into separate but brilliant post-docs. This is going to be a very sad thing, no longer to not see you as a result of your not being here. Annie Senghas helped me out. Michael Ulman will always have a blond place in my heart. I enjoyed my coffee dates with Karina. It seems I never saw as much as I wanted of David and Amy Poeppel, despite some notable efforts to those ends. It's always great fun to run into Ed Tehovnik and talk about life. I've also enjoyed running into Peter Chefalo frequently over the last few years and getting to know each other during our long loud talks in the hall. I am grateful to Diana Smetters for her helpful "den-mother duty" last year, and also for introducing me to Barbara Ahern. I enjoy tormenting Chris Moore, but Bavin Sheth takes it better. In the good old days there were Sandeep, Josh, Anita, Martyn, Elliot, Mike N, and Bob who titrated their teachings so perfectly that what I learned from them of science was exactly wiped clean by what I learned from them of drinking. In those ancient times also there were Greg Belmont, Jonathan Wallach, Hemai Parthasarathy, Gary Marcus, and Corrie Latham, all of whom I would be more pleased to see on less rare occasions. I-han Chou is extraordinary (or, as Cindy put it, she walks on clouds). I owe Pietro Mazzoni many thanks still for giving me a place to live when I was homeless. Stephan Treue taught me to play GO. Bobby Dolan taught me to just say no. Janine Mendola, Josh Tenenbaum, Todd Holmes, Gavin and Beth Huntley-Fenner were all part of the music. I hope we can all jam again some day.

I am grateful to the voters of Massachusetts for re-electing Senator Kennedy! He is a better leader, even, than Emilio Bizzi. One effect of his leadership is a talented, skilled, and lively organization. Like the department of Brain and Cognitive Sciences, Kennedy's organization is reputed among its members to be reputed by those outside the organization to be an excellent organization. That is apparently a very good sign, because both organizations really are excellent. I am particularly grateful to Jiwon Parks, Chris Casey, and Pam Hughes, who inspired me.

If your name isn't here, you shouldn't have laughed at my price.

Last and least, I must acknowledge the remainder of my Todo list

1. Put references in bibtex format.

2. Add appendix with software.

3. Add appendix listing potential applications of the models.

Contents

List of Figures

List of Tables

Chapter 1

Introduction

The control of movement, like most functions of the brain, appears by introspection to be easy but is revealed by science to be tremendously difficult. Because we move our hands in straight-line paths, the angles of the joints in our skeletons sometimes must change in counter-intuitive ways, and the way that the muscles contract to perform these movements is almost incomprehensibly complex (see part VI of Kandel, Schwartz, and Jessell, 1991). It is not unreasonable to think the spinal cord helps to simplify the problems of movement by providing the rest of the brain with abstractions for the control of movement: everything we do is done by the muscles, which are controlled by the motor neurons, which receive the vast majority of their inputs from spinal interneurons. Recently a series of experiments in which the spinal cord was examined for its role in the simplification of movement was initiated by Emilio Bizzi and colleagues. Bizzi, et al. (1991) have found that the spinal cord contains a limited number of "modules" (see below). Because these modules could be added together in simple ways to produce new modules, Bizzi, et al have hypothesized that the modules are the building blocks of movement provided by the spinal cord to the rest of the brain.

My thesis is devoted to formulating and preliminarily executing a test of that hypothesis. The test appears to be easy: I stimulate supra-spinal descending axons in order to elicit movements of the leg. I can then try to explain those movements as being produced by the spinal modules. If I can explain what happened using just

the spinal modules, then I cannot rule out the hypothesis that the spinal modules are acting as building blocks. If, however, the muscles provide a significantly better explanation than do the spinal modules, I will have evidence that the spinal modules are being bypassed somehow by the supra-spinal systems, and thus are not acting as building blocks.

In this introduction, I describe the key concepts of coordinate transformations, basis functions, and the results of our previous spinal stimulation studies. The body of the thesis is organized as a march up the neuroaxis (figure 1-1). In order to enable computations involving the muscles and the spinal modules, I built computer models of them. I did this by stimulating isolated muscles and spinal cords in order to observe the effects of activation of the muscles and the spinal modules (chapter 2). I confirmed that the spinal modules could be found in decerebrate animals by stimulating the spinal cords of decerebrate animals and verifying that the computer models were still valid in that context (chapter 3). In chapter 4, I present the promising preliminary results of the supra-spinal stimulation experiment.

Coordinate Transformations

One can not get anywhere in motor control without understanding coordinate transformation. A coordinate transformation is a mapping from one coordinate system, such as cartesian coordinates, to another coordinate system, such as polar coordinates. A simple experiment demonstrates the importance of coordinate transformations in the control of movement. Tilt your head, rotate your eyes in their sockets, and focus on some object within reach. Now close your eyes and touch the object. You may not hit it exactly, but you will probably be close. Your brain had to perform several coordinate transformations in order to do this. The location of the object in space has to be computed from its location on your retinas, the rotation of your eyes in their sockets, and the tilt of your head. For the sake of argument, suppose that the representation in your brain of the location of the object is a cartesian grid. The position of your finger when it touches the object is given by the (x, y, z) location

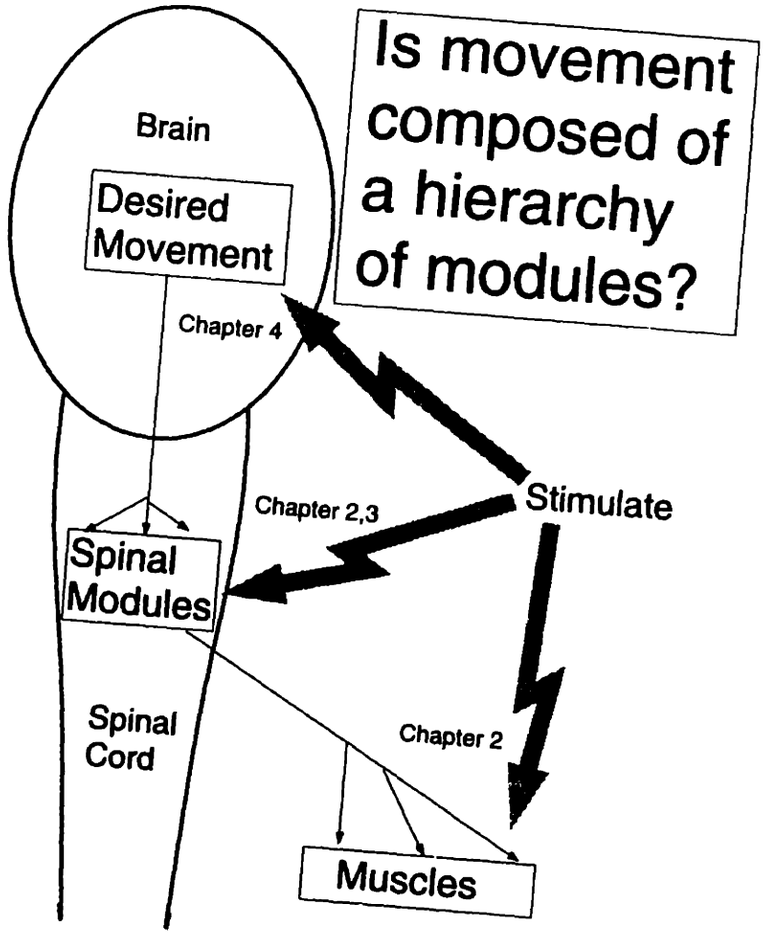

Figure 1-1: The Big Question: Is movement composed of a hierarchy of modules? In this thesis I provide a new method for testing hypothesized modular control circuits. In chapter two I build statistical models of the effects of muscle stimulation and spinal stimulation. In chapter 3 I show that the models of spinal stimulation built in chapter 2 are valid for the spinal cords of decerebrate frogs. In chapter 4 I show how the spinal and muscle models can be used to test whether the spinal models suffice to explain the effects of supra-spinal stimulation in decerebrate frogs.

of the object. Getting your finger to that point required coordinate transformations from the (x, y, z) location of the object to the angles of your shoulder, elbow, wrist, and finger joints, and then from these angles into the lengths of all the muscles in your back, shoulder, arm, and hand. Thus, we can recognize several distinct sensory and motor coordinate systems needed to perform the seemingly simple task of touching an object.

The same coordinate transformations that allow us to determine how to touch an object also allow us to compute the static forces needed to maintain the arm's posture against the force of gravity. The transformation from hand positions to the angles of the arm joints is important in converting between forces on the arm and torques about the joints. The coordinate transformation from the angles of the arm joints to the lengths of the arm muscles is important in converting between torques around the joints and the tensions in the muscles. These conversions, which depend on the principle of virtual work, are employed throughout this thesis.

The Principle of Virtual Work

The principle of virtual work states that changing the coordinate frame does not change the total work of a system. The work is always computed from the force multiplied by the displacement in a given coordinate frame. By the principle of virtual work, these products must be equal across all coordinate frames. Thus from the coordinate transformation between the frames, we can find simple relationships between the forces in different coordinate frames. I will demonstrate this concept in a simple system, and then apply it to the arm.

Figure 1-2 shows a water wheel with three connected one-dimensional (one variable) coordinate frames. The three coordinate frames are the height of the paddle (cartesian), the angle of the wheel (polar), and the length of the spring (muscular). One kilogram of water is striking the wheel. The force exerted by the water is one Newton (one kilogram in gravity). The instantaneous cartesian displacement is an infinitesimal, Δy, where y is the height of the water wheel paddle. Work is force times displacement, so the work done by the water in the cartesian coordinate system is 1

Newton Δy Newton-meters. We can also describe this system with the polar coordinate system: namely, the torque about the center of rotation of the water wheel and its angular displacement. The angular displacement is $\Delta\theta$, where θ is the angle of the water wheel. The coordinate transformation between the two systems is $y = R\sin(\theta)$. For more simplicity I will use a small angle approximation to write $y = R\theta$, because I have chosen $\theta = 0^{o}$ when the paddle is perpendicular to the flow of water.

Force to Torque

We can use the polar-to-cartesian coordinate transformation to translate between forces and torques. By the principle of virtual work, the work done by the water must be the same no mater which coordinate system we use,

$$\text{torque}\Delta\theta = 1\text{Newton}\Delta\text{y} = \Delta\text{y(in Newton-meters)}$$

or

$$\text{torque} = \frac{\Delta\text{y}}{\Delta\theta} \tag{1.1}$$

Equation 1.1 is as simple a demonstration of the relationship between coordinate transformations and force conversions as one could hope to find. According to this equation, the torque in the water wheel is given by the derivative of the function relating the height of the paddle to the angle of the wheel. That function is a coordinate transformation between the two systems. It is clear that the derivative of y with respect to θ is R, so the torque in the water is R Newton-meters per degree. We have computed this torque from the cartesian force and from the derivative of the cartesian system's variable with respect to the polar system's variable. The principle of virtual work lead directly to our computing the force conversion from the derivative of the coordinate transformation.

Torque to Tension

I have drawn the water wheel in figure 1-2 with a spring attached to it, because the net system of water force, wheel torque, and spring tension is a one-dimensional analogy

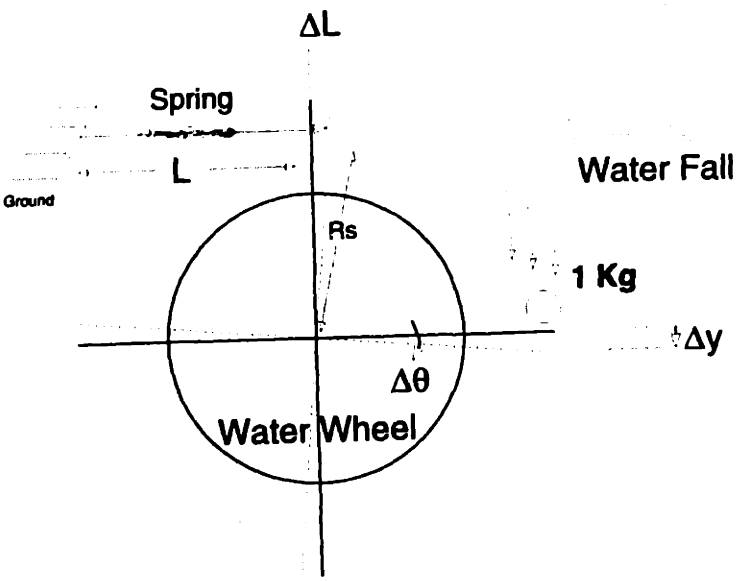

Work = Force * Displacement = Constant

Tension * ΔL = Torque * Δθ = 1 Newton * Δy

So

Torque = 1 Newton * $\Delta y / \Delta \theta$

Derivative of a Coordinate Transformation

$y(\theta) = R \sin(\theta)$

Figure 1-2: A Simple System with Coordinate Transformations In this figure a waterfall strikes a water wheel that has a spring attached to one of its spokes. The height of the paddle, y, is one coordinate system. Y is zero when the paddle is perpendicular to the flow of the waterfall. The angle of the water wheel, θ is another coordinate system. θ is 0° when the paddle is perpendicular to the flow of the waterfall. The length of the spring, L, is the third coordinate system. The length of the spring is L0 when $y = \theta = 0$. A 1 Kg (1 liter) drop of water is hitting the wheel at a radius of R. The radius of the attachment of the spring to the water wheel is R_s. The spring is attached so that it is perpendicular to the spoke of the water wheel when $y = \theta = 0$.

to the multi-dimensional system of gravitational forces, joint torques, and muscle tensions that define many problems in limb control. The waterfall is like the force of gravity, the torque in the wheel is like the torque around your elbow or shoulder, and the tension in the spring is like the tension in your muscles.

Again using the principle of virtual work, I will derive the tension in the spring. We use the principle of virtual work to equate the work in the two coordinate systems:

$$\text{tension}\Delta\text{L} = \text{torque}\Delta\theta$$

so that

$$\text{tension} = \text{torque}\frac{\Delta\theta}{\Delta\text{L}}$$

Once again we need to compute the derivative of a coordinate transformation in order to convert between the forces in those two systems. In this case, we want to know $\frac{\Delta\theta}{\Delta\text{L}}$, the derivative of wheel angle as a function of spring length. The length of the spring, L, is given by

$$\text{L} = \text{L0} + \text{R}_s \sin\theta approx \text{L0} + \text{R}_s\theta, \text{ for small } \theta$$

so that

$$\theta = \frac{\text{L} - \text{L0}}{\text{R}_s}$$

In these equations, R_s is the radius of the attachment point of the spring on the spoke of the water wheel. Again, from the derivative of the coordinate transformation we can compute the tension in the spring:

$$\text{tension} = \text{torque(Newton-meters/degree)}\frac{1}{\text{R}_s}\text{(degrees/meter)}$$

Knowledge of the coordinate transformations between the length of the spring, the angle of the wheel, and the height of the paddle allows us to convert freely between the force on the paddle, the torque about the center of rotation of the wheel, and the tension in the spring.

Coordinate Transformations and the Skeletal-Muscular System of the Arm

The preceding arguments can be applied almost exactly to the analysis of the skeletal-muscular system of the arm. The only difference is that there are many positions, many angles, and many spring-like muscles in the arm. This does not change the arguments tremendously: we simply need to be careful to multiply the forces and displacements in such a way as to produce a single scalar value for the coordinate-invariant work. For example, if forces are written as a row vector, then displacements should be written as a column vector and they should post-multiply the forces. This is because one multiplies vectors by going *across* the first one and *down* the second one:

$$[\overrightarrow{a, b, c}] \begin{bmatrix} x \\ y \\ z \end{bmatrix} \Downarrow = ax + by + cz$$

When we divide two vectors, each element of one gets divided by each element of the other, producing a matrix. For example, a $\vec{\Delta x}$ vector divided by a $\vec{\Delta\theta}$ vector produces a matrix, called the Jacobian of $\vec{x}(\vec{\theta})$. The components of the Jacobian are simply the individual division terms of the components of the two vectors: $\frac{\Delta x_i}{\Delta \theta_j}$.

Force to Torque

Let us now apply the principle of virtual work to the analysis of the skeletal system. Figure 1-3 diagrams two gravitational force vectors being exerted on the arm of a stick figure person. The gravitational forces are acting on the center of mass of the forearm and the center of mass of the upper arm. We can convert those forces into torques about the shoulder and the elbow. To do this we need to know the transformation from the joint angles to the (x, y) positions of the two centers of mass at which the forces are acting. For the upper arm center of gravity the x location is given by $R\cos(\theta)$ and the y location is given by $R\sin(\theta)$, where θ is the angle of rotation of the shoulder in the plane of the page, and R is the distance from the shoulder to the

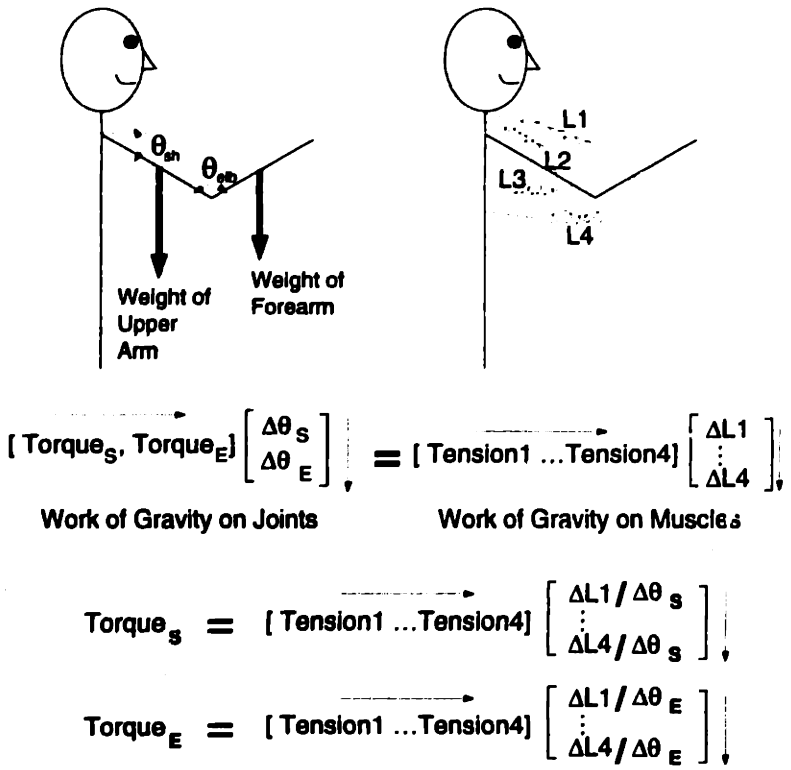

Figure 1-3: A Simple Stick Figure in Gravity In this figure we see a schematic person. The cartoon's arm is held out from its body. The force of gravity acts on the center of mass of each skeletal segment of the arm. One coordinate frame for this system is the (x, y) coordinates of points on the arm. Another coordinate frame is in the angles of the joints. Still another coordinate frame is in the lengths of the muscles that are holding up the arm.

center of mass of the upper arm. Thus, by the derivation we used for the water wheel, the work done by gravity acting on the upper arm is

$$[F_x, F_y] \begin{bmatrix} \Delta \mathrm{x} \\ \Delta \mathrm{y} \end{bmatrix} = \mathrm{torque}_{sh} \Delta\theta$$

Dividing both sides by $\Delta\theta$ we can compute the torque on the shoulder due to gravity acting on the upper arm

$$\mathrm{torque}_{sh} = [F_x, F_y] \begin{bmatrix} \mathrm{R}\cos(\theta) \\ -\mathrm{R}\sin(\theta) \end{bmatrix} \tag{1.2}$$

Once again, knowledge of coordinate transformations has allowed us to convert between the force and torque. We also learn from the coordinate transformation equations that the gravity acting on the upper arm never produces an elbow torque. Since the elbow angle is not needed to compute the (x, y) location of the center of mass of the upper arm, the derivatives corresponding to the elbow torque will be zero.

We can verify with a simple experiment that static forces on the upper arm turn into torques at proximal joints but not at the elbow. Keep your right arm steady in the posture of figure 1-3 while your laboratory assistant pushes down steadily - not suddenly - on your upper right arm. The static force on your upper arm is equivalent to a torque at your shoulder. You should feel your shoulder muscles tensing but not your elbow muscles. The static force is also transmitted through the mechanical linkages of your skeleton into torques in your back, your hips, and your leg joints. As your assistant pushes harder on your upper arm, you should feel your muscles in all these joints tensing, but your elbow can remain relaxed and easy to move. No thought is required to set up the right counterbalancing contractions in the muscles around the proximal joints. Whatever your body is doing to figure out the magnitudes of the muscle tensions, it has to maintain something functionally equivalent to the coordinate transformations being described here.

We can also compute the shoulder and elbow torques produced by the forearm gravitational force. There is more trigonometry needed for this computation because both joint angles are needed to determine the x and y coordinates of the forearm center of gravity. Nevertheless, these equations can be easily written and solved. Because both joint angles are used in the coordinate transformation from joint angles to the x and y coordinates of the forearm center of gravity, the force on the forearm will produce a torque at the shoulder. The total torque at the shoulder is the sum of the upper arm and forearm gravitational torques.

Torque to Tension

It should be clear now how to convert the gravitational torques in the shoulder and elbow to the gravitational tension in each of the muscles. We begin by equating the

work in the two coordinate frames:

$$[\tau_{sh}, \tau_{elb}] \begin{bmatrix} \Delta\theta_{sh} \\ \Delta\theta_{elb} \end{bmatrix} = [\text{tension}_1, \text{tension}_2, \cdots, \text{tension}_M] \begin{bmatrix} \Delta L_1 \\ \Delta L_2 \\ \vdots \\ \Delta L_M \end{bmatrix} = \sum_{i=1}^{M} \text{tension}_i \Delta L_i$$

In this equation, τ_{sh} is the shoulder torque, τ_{elb} is the elbow torque, θ_{sh} and θ_{elb} are the shoulder and elbow angles. The tension and length of muscle k are given by tension_k and L_i respectively. It is an important fact about biological systems that the number of muscles always exceeds the number of joints, but for now let us just consider how to compute the gravitational tension in a single muscle:

$$\text{tension}_K = [\tau_{sh}, \tau_{elb}] \begin{bmatrix} \frac{\Delta\theta_{sh}}{\Delta L_K} \\ \frac{\Delta\theta_{elb}}{\Delta L_K} \end{bmatrix}$$

In order to compute the gravitational tension in muscle K, we need to know how the joint angles will change in response to small changes in the length of muscle K. This computation would tell us how much muscle K would have to be activated to maintain the arm in the current posture. So, the coordinate transformation from muscle lengths to joint angles is needed.

We can easily figure out the coordinate transformations between cartesian coordinates and joint coordinates from simple trigonometric relations, but how can we find the coordinate transformations between joint coordinates and muscle lengths? By analogy to the water wheel example above, we could examine cadavers to find the exact attachment points of the muscles on the skeleton. In fact, that is what most researchers have done. One of the major contributions of this thesis is to use the ideas of coordinate transformations to bypass the laborious, messy, unpleasant, and inaccurate task of approximating muscle length functions from cadaver measurements. In equation 1.2 the Jacobian of the coordinate transformation for the upper arm is expressed as a function rather than as numbers. At any given posture, θ takes on a particular value, and the Jacobian becomes a particular vector of numbers. In

other words, the Jacobian, is itself a function of joint angles. In the simple stick figure example we can write exact equations for the way the Jacobian changes as the arm moves, but in more realistic problems this is not possible. Rather than attempting to find explicit equations for the coordinate transformations between joint angles and muscle length with joint angles (as is done when researchers measure cadaver muscles), we will instead approximate the Jacobian function using statistical modelling techniques. In particular, we choose a parametric representation of Jacobian functions, and then use data to find the parameter values of the Jacobian function of each muscle. In the example of the Jacobian for the upper arm, we might use as a parametric representation

$$\begin{bmatrix} \mathrm{P1}\cos(\mathrm{P2}\theta_{sh} + \mathrm{P3}\theta_{elb}) \\ \mathrm{P4}\sin(\mathrm{P2}\theta_{sh} + \mathrm{P3}\theta_{elb}) \end{bmatrix}$$

In this example of a parametric representation, P1, P2, P3, and P4 are parameters. θ_{sh} and θ_{elb} are the angles of the shoulder and elbow, respectively. We can use statistical modelling techniques to find values for parameters P1 through P4 from many examples of gravitational shoulder torques at different values θ_{sh} and θ_{elb}. The correct values of P1 through P4 are P1 = R, P2 = 1, P3 = 0, and P4 = -R. Once our statistical modelling program (Becker, et al, 1988) has found these parameter values for the Jacobian function, we can work backwards (integrate) to find the coordinate transformation from joint angles to the (x, y) coordinates of the center of gravity of the upper arm.

I have shown above that there are two distinct reasons that the nervous system must keep track of coordinate transformations. Each patch of skin on the arm resides at a location in space which moves around as the angles of the joints in the arm are changed. In order to be able to scratch a patch of skin, its location in space should be represented somehow. We do not know exactly what coordinate systems are used to do this, but we do know that the ability of people and animals to scratch arbitrary patches of skin on their arms indicates that the coordinate transformations between muscle lengths, joint angles, and skin location are contained in the system. There are

also pressure sensors under each patch of skin. We are able to respond to pressure on the arm with counter-acting tensions in the joints of the arm, back, and legs. This ability again requires that the system somehow represent the Jacobians of the coordinate transformations involving each patch of skin.

Kinematics and Dynamics

The ideas and derivations developed above are encompassed by the concept of kinematics. As defined by Hollerbach (1990), "kinematics is concerned with the geometry of the external world, the geometry of a limb, and the transformations between them." I have extended this definition to include the transformations between the limb geometry and the muscle lengths. The forward kinematics of an arm is defined as the function that maps joint angles to arm positions. The forward kinematics of an arm is well-defined and trivial to compute: given the angles of each of the joints we can compute the position in space of any part of the arm. The inverse kinematics of an arm is a mapping from positions to joint angles. The inverse kinematics mapping of an arm is almost always multi-valued, because there are infinitely many possible configurations for most positions of any particular point on the arm. For example, the position of an elbow can be changed independently from the angle of the elbow. Thus, the inverse kinematics mapping from the position of the elbow to the elbow angle would be ill-defined. Similarly, you can put your finger on an object and leave your finger there approximately motionless while changing the angles of joints in your arm. Given enough positions of points on the arm, however, the mapping from those positions to joint angles is completely specified For example, given the position in space of the elbow and of the wrist, there is at most one vector of shoulder and elbow angles that could bring the wrist and elbow simultaneously in line with those positions.

Kinematics is clearly an important idea in motor control. Understanding the kinematics of the arm and muscles allows us to compute *static* inter-conversions between forces on the arm, torques about the joints, and tensions in the muscles. To fully understand the problems of motor control, however, we must also consider the

dynamics of the muscles, the limb, and the world. Unfortunately, "dynamics" is a general word used to describe two different parts of the motor control problem. The first sense of the word is that the forces, torques, and muscle tensions in the arm are altered by movement of the arm. The second sense of the word is that forces, torques, and muscle tensions produced all have temporal characteristics that must be considered. Ultimately, both senses of the word are united in the common mathematical framework of state space equations (see Craig, 1986).

Dynamics as Movement

A simple experiment demonstrates a role of movement dynamics in motor control. Hold your right arm in front of you in the posture illustrated in figure 1-3. Keep your muscles relaxed (your body will automatically tense them just enough to counter gravity, possibly using the calculations described above). Now use your left hand to push down suddenly enough on your right upper arm to cause it to move. Your upper arm will drop and your elbow will fold. You could keep your elbow from folding by tensing your muscles, but please don't do that. The point is that your elbow *does* fold, even though we have shown above that the force exerted on the upper arm does not produce any torque at the elbow. The question is, why does the elbow angle change when you push on your upper arm? What is the source of the torque causing the elbow angle to change?

The answer is clear: the unexplained torque in the elbow is simply due to the movement of the elbow. Movement results in torques that cannot be understood from the static analysis alone. When the upper arm is moved, the elbow accelerates. The acceleration of the elbow is translated into a force – and a corresponding torque – on the forearm.

Converting the acceleration of the elbow into a force on the forearm requires knowledge of the actual mass of the skeletal segments. In figure 1-3 we did not need to know the mass of the upper arm or the forearm to compute the translation between forces and torques. Computing the effects of movements, however, requires that we know the actual physical parameters (mass and distribution of mass) of the arm.

Another complication that movement brings to the analysis of the arm is that the kinematics keeps changing. In the case of the arm we have already described the Jacobian of the coordinate transformation from shoulder angle to the center of mass of the upper arm. That Jacobian *function* will not change as the arm moves, but at each new position of the arm the *values* of the Jacobian will change.

The dynamics of movement also come in to play when considering the functioning of muscles. Muscles have moving parts in them. Each muscle is attached to the skeleton by a tendon, and each muscle contains 1.26 gazillion actin and myosin fibers. The tendon acts as a separate spring and prevents the muscle from getting damaged by sudden external forces. When the skeleton is moved by a force, the resulting tension in the muscle-tendon system is transmitted to the muscle by the tendon. Conversely, when the muscle contracts, the tension is transmitted from the muscle to the tendon to the skeleton. The problem of movement causing a change in coordinate transformation affects the muscle-tendon system because tendons often wrap around bones that move. For example, the tendon of the triceps (the muscle on the back part of the upper arm) wraps around the bony point of the elbow. As a result, movement affects the translation between the coordinate system representing the length of the tendon and the coordinate system representing the length of the muscle.

By experimental design, I have avoided the problem of the dynamics of movement entirely in my thesis work. I have measured the forces at the ankle produced by the torques at the joints produced by the tensions in the muscles that result from stimulation of the spinal cord. To construct the muscle models I made these measurements while stimulating individual muscles rather than the spinal cord. In the final chapter I describe how I made these measurements while stimulating supra-spinal structures. In no case have I measured torques or forces in moving limbs. I also have not modelled how the muscle torques might act on the limb in motion. I have avoided the problem of motion within the muscles by using the peak forces generated by the musculo-tendon system to represent muscular contractions. At the peak force, the tendon and muscle have presumably equilibrated so that they are not moving with respect to each other.

Dynamics as Temporal Properties

The term "dynamics" is also used to describe the temporal variations in forces, torques, and muscle tensions. In figure 1-2 we see a 1 liter drop of water (1 Kg) hitting the spoke of the water wheel. A few moments after the snapshot in figure 1-2, the water will splatter all over the wheel. The function describing the force exerted by the water with respect to time will look quite different from the function describing the force exerted by a 1 Kg bowling ball. The water itself has dynamics in the same time frame as the system of concern.

We are aware of the dynamics of forces in the world whenever we move our arms. For instance, you would be quite clear about the difference between catching a 1 Kg ball as opposed to catching a half-full 2 liter bottle of Diet Pepsi. Although both objects would have approximately the same mass, there would be complicated temporal variations in the magnitudes and orientations of the forces exerted on your hand by the bottle of caustic liquid.

The temporal variations in the joint torques of the arm are mostly due to the relative motion and inertia of the upper arm and the forearm. We described these phenomena in the previous section as the dynamics of movement. There is almost no friction or viscosity in the joints of healthy arms. Consequently, the physical properties of the arm are well approximated by an idealized stick figure with the mass of each limb segment attached. The approximation fails when the joints reach their limits (note, for example, that the elbow locks when it is fully extended). In my work, therefore, I have explicitly excluded those configurations from consideration.

Temporal variations in the properties of muscles arise because muscles are living tissue. A spring is a good approximation of a muscle at any moment in time, but the springiness of muscle is controlled by neural impulses. The tension produced in a muscle by a single impulse is a function of, inter alia, the length of the muscle, its temperature, its fatigue, and its current tension level. These temporal variation in the properties of the muscle occur in the same time frame as the motion of the limb.

Dynamics as temporal properties have played only a small role in my thesis work. I have measured forces by holding the frog's hindlimb fixed in a force sensor. As a

result, the world has exerted forces on the frog equal and opposite to those forces the frog has exerted on the force sensor. I will argue in chapter 2 that our spinal stimulation results add further evidence in favor of the hypothesis that the spinal cord models and inverts (see below) the dynamics of the muscles. In the final chapter, I will describe current efforts to add muscle activation dynamics to the muscle models described in chapter 2.

Representations

There are good reasons to think that the frog's spinal cord contains something functionally equivalent to the mathematics of coordinate transformations. The spinal frog can use a hind limb to wipe a noxious stimulus from any part of its body. The frog whisks the stimulus away by placing its foot to one side of the stimulus and then pushing the stimulus away with the foot. The placement of the foot varies linearly with the position of the stimulus on the back(Giszter, et al, 1989). If the stimulus is on the frog's forelimb, then the spinal frog is able to place its hind foot on the forelimb no matter what posture the forelimb is in (Fukson, et al., 1980). Thus, the spinalized frog is able to translate pain in a patch of forelimb skin into the lengths of the hindlimb muscles needed to bring the foot into contact with the patch of forelimb skin. We have seen that this behavior requires "knowledge" of the forelimb kinematics, the hindlimb inverse kinematics, and the hindlimb inverse dynamics.

Ideally we could relate these observations about coordinate transformation to the spinal circuitry. I think it ultimately will be possible to identify in the operation of spinal circuits the mathematical constraints given in the preceding section, but that achievement will depend on careful consideration of the "what" and the "how" of the data "representations" in the spinal cord. The use of the word representation indicates the needed distinction between the observed features of a computing system and its logical/mathematical purpose. Illustrations of the concept of representation are given below.

The best-known and simplest example of a representation is the use of voltage

levels to represent TRUE and FALSE in computer circuits. The binary values, TRUE and FALSE, are implemented as voltage levels of approximately 5 volts and 0 volts in digital circuits. An important aspect of this representation is that a continuum of voltage values is mapped onto a single logical/symbolic value. Therefore, these many different voltage values have the same functional impact on the computer circuitry. For example, the infinitely-many values between 3.5v and 6v all have the same effect on the circuitry as 5v, and therefore, they all map to TRUE. It is important to understand both what is represented (TRUE, FALSE) and how (high voltages, low voltages) in order to make sense of the computer circuitry. That is, if we were to perform physiology on the computer with an oscilloscope, it would be hard to interpret the circuitry without knowing that 4v and 5v were equivalent.

Figure 1-4 illustrates two levels of representation. In panel A, we start with a hypothetical computer chip which has a single input wire and a single output wire. The ouput voltage is a cleaned-up version of the input voltage. The logic levels of the output voltages are shown for each of eight time points according to the rule indicated above: 3.5+ volts is TRUE and less than 3.5 volts is FALSE. Continuous voltages having discrete logical meanings is a simple example of a representation. In panel B, we have a more complicated computer chip. This chip has two input wires and two output wires, each like that in panel A. The logic levels of the two outputs are again shown in a table at eight time points. In the table shown at the output of the chip, the columns are output values at a given time point and rows are the output for a single output wire. At any given time point, the two outputs are interpreted as a binary number following some conversion rules. The interpretation of the table of outputs is, therefore, a second level of "representation" in this computer chip. Not only are voltages on the output wires interpreted as TRUE and FALSE, but the collection of outputs at each point in time is interpreted as a number. At the bottom of figure 1-4B the interpreted output values are plotted vs. time point in graph 1. Graph 2 shows the plot of the interpreted output values when a *different* conversion table is used to interpret the output data. This demonstrates that there is an element of interpretation in the meaning of "representation". Just as 5v corresponds to TRUE

because the computer circuitry is built to work that way, the numerical values of the chip's output depend on the conversion table being used.

There may be a correlate of the TRUE and FALSE of digital circuits in the action potentials of neurons. Neurons have a voltage across their membranes. The membrane potential is set by pumps that maintain sharp ionic gradients across the membrane. Inputs to the neuron cause non-random fluctuations in the membrane potential. When it reaches a critical level, the conductance to pumped ions increases. As a result, the charged ions fall down their concentration gradients, causing a rapid decrease in the magnitude of the membrane potential. At another critical level, the conductance is shut off and the ions are again pumped out and in to reset the membrane potential (see Keynes & Aidley, 1991). All of these mechanisms operating together allow the neuron to transmit a 1 msec spike of voltage that may in essence be a binary value. In order to determine if the spike acts as a binary value, researchers examine the impact of the spike on the receiving neuron. In other words, by direct analogy to figure 1-4B, we need to know the translation table in order to know how to interpret the output of neurons. The translation tables, however, are embedded in the operation of the pre- and post-synaptic tissue that receives the spike. The *how* of the action potential representation is well understood. *What* spikes represent is one of the central questions of any neuroscientific investigation.

Figure 1-5 illustrates three levels of representation in the motor neurons. In panel A, we show a motor neuron by way of analogy to the chips of figure 1-4. The membrane potential of the neuron is analogous to the voltage in the output wires of the chips. In this figure the membrane potential is being monitored by a cartoon oscilloscope. The membrane potential is being read during three different active states of the motor neuron. In state 1, the membrane potential fluctuates as a result of synaptic inputs on the dendrites (which are analogous to the input wires in figure 1-4). When the membrane potential crosses the threshold (0mV), the cell begins to emit spikes. The spikes are drawn as vertical hash marks on the action potential trace. The frequency of firing is given by the amount that the membrane potential exceeds the threshold (which is in turn dictated by the magnitude of the synaptic currents). In state

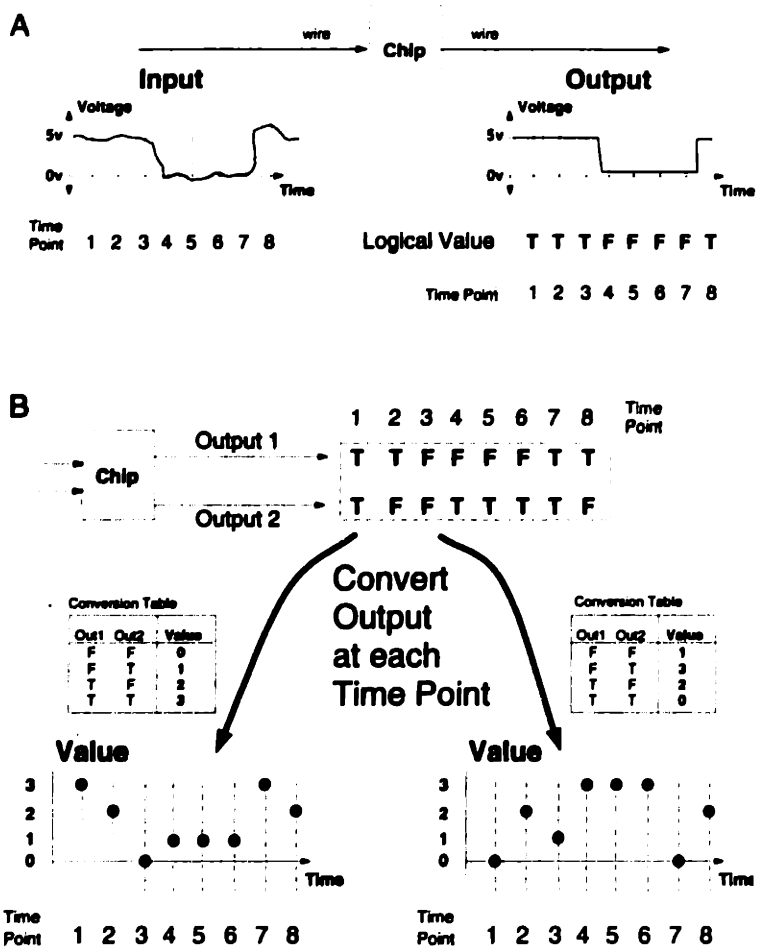

Figure 1-4: Multiple levels of representations in a simple chip This figure illustrates two distinct meanings of "representation" in the context of simple hypothetical computer chip. I take "representation" to indicate the needed distinction between the observed, physical properties of a computational system and the meaning of those properties within the context of the computations being performed. (A) The voltage levels on input and output wires of chips can be measured, but those physical voltage levels also have a meaning that is given by the chip. Most chips use 5 volts to represent a binary TRUE value and 0 volts to represent a binary FALSE value. Not all chips work that way. Five volts is five volts, but the meaning of the voltage level depends on the chip. In this figure the TRUE/FALSE values are shown at 8 time points. (B) Collections of voltage levels can be measured on several wires, but the meanings of those collections depends entirely on the way those wires are hooked into the chips. In this example I have shown two different conversion tables that might be used by a chip receiving the two outputs of the pictured chip. The two different conversion tables lead to two different functions of chip output value vs. time point.

2. the same synaptic inputs cause the same membrane potential fluctuations, but the function relating the rate of firing to the membrane potential has been changed (possibly by serotonin, (Binder, et al, 1993). In state 3, the same synaptic inputs cause similar membrane potential fluctuations, but these fluctuations simply modulate a steady rate of firing (possibly induced by a pulse of afferent activity combined with descending-tract serotonin signals, Hounsgaard, et al, 1987).

The motor neurons perform at least two layers of computations. The spiking behavior of the neuron is an example of the conversion of noisy analogue voltages into binary (TRUE, FALSE) values. The rate of firing of the neuron is an example of the use of binary values to construct a number system. The number system in figure 1-4B was constructed from the vector of all of the chip's (two) outputs. The number system in figure 1-5A is constructed from a single output, [1] but a third level of representation in the biological system, shown in figure 1-5B, uses a vector of outputs. In figure 1-5B we show that each motor neuron in the spinal cord has a state (as shown in figure 1-5A) in addition to a firing rate. The states of the motor neurons are almost certainly controlled by the spinal interneuronal circuitry (just as are the firing rates), so this extra representational power of the motor neurons is an important thing to keep in mind in interpreting our spinal stimulation results. In particular, we do not know if the interneuronal systems we are stimulating reflect inputs to the motor neurons, *per se*, or rather controllers of the states of the motoneuronal systems.

Basis Functions

A central concept to my thesis work is the idea of basis functions. Basis functions are a level of representation like figure 1-4B and figure 1-5B. For example, the spinal cord receives a vector of thousands of numbers (thousands of firing rates of thousands of sensory fibers) for each muscle: what can it do with that information? The idea

[1] Chips are designed to operate at discrete points in time so that there is no timing information in the bits (binary values) it operates on. As a result, the only way to build a numerical representation out of the chip's output is to use several outputs together, as shown. The neuron does not operate at discrete times. The timing of spikes carries information, and so it is possible to build a numerical representation that depends on the intervals between spikes.

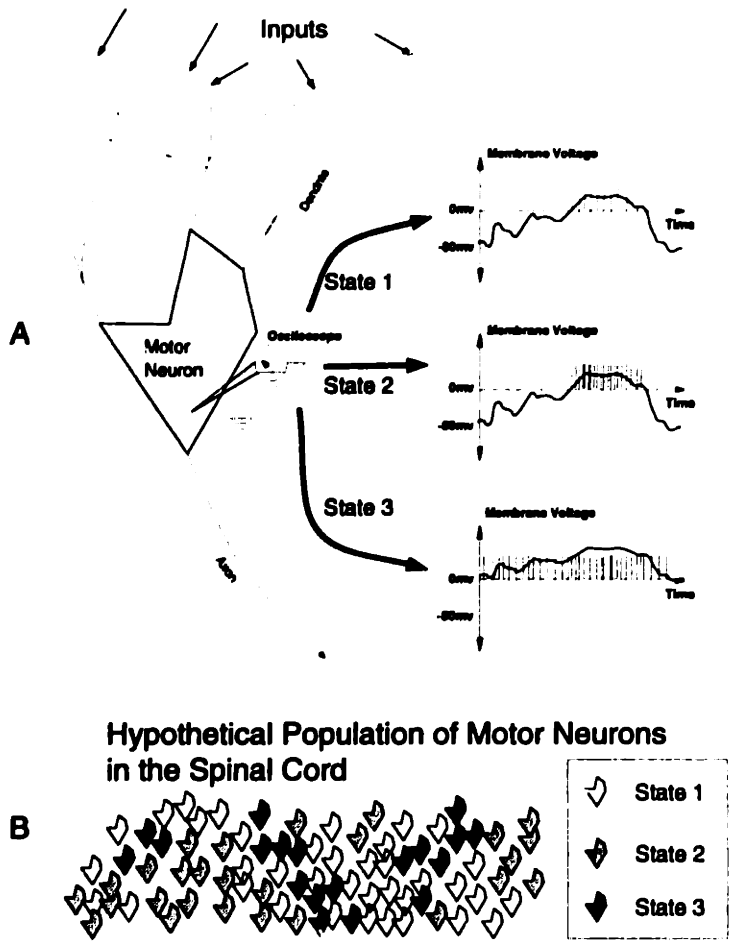

Figure 1-5: Multiple levels of representations in a motor neuron Just as the chips in the previous figure had several different levels of representation to consider, so do neurons. (A) A motorneuron is illustrated. We can measure the potential across the cell membrane, but the meaning of that physical voltage will depend on the state the neuron is in. I have shown three states. In states 1 and 2 the neuron responds to the same variations in its membrane potential with different rates of firing. In state 3, the cell responds to the same inputs with a different membrane potential due to some plateau potential (in a dendritic tree, for example). This example collapses together both (A) and (B) of the chip: the membrane potential is translated into TRUE/FALSE values (spikes) and the conversion is determined by other inputs to the cell (ie, the conversion table can be changed). (B) Because each motor neuron can be switched into a variety of different states, the state of each neuron in a population is itself another physical value that can be measured. The meaning of the physical states depends entirely on the way that the neurons are wired togther.

of the conversion table shown in figure 1-4B comes into play because the meaning of these numbers will depend on their role in the spinal cord's computations. There are two ways the numbers can be used in computations. In the first way, the numbers are information in and of themselves. For instance, each firing rate is itself an estimate of the length of a muscle. In addition, the firing rates of length sensitive fibers from one muscle could all be averaged together to form a reliable estimate of the current length of that muscle. In the second use, the numbers are not answers in and of themselves but rather, are parameters of a basis function. In this scheme, the numbers are informative only in the context of all the other numbers. As a result, the information they convey is implicit in their interpretation. This type of usage is a basis function interpretation of the numbers.

A set of basis functions defines a coordinate system for representing functions (see figure 1-6A for a simple coordinate system of functions). Just as we normally view points according to their (x, y, z) cartesian coordinate representation, we normally view functions according to a standard set of basis functions called delta functions (see below). Recall that there were some added complexities when we moved from the one-variable coordinate systems of the water wheel (figure 1-2) to the two-variable coordinate of the arm (figure 1-3). Here too there are additional complexities to the coordinate systems for functions, because functions have infinitely many dimensions. Instead of Jacobians and matrix multiplication, the coordinate systems of functions are transformed with densities and integrals. The integral of a function with respect to a density is like the inner product of an infinite dimensional vector with one row of a Jacobian. The important point to remember is simply that basis functions are the means by which infinite dimensional coordinate systems can be defined.

In any discussion of basis functions the word "approximation" is necessary. If I told you my elbow was at (x, y, z) = (3, 5, 4) and it turned out on closer examination to be at (3.3, 4.8, 4.1), then the total error of ($\sqrt{(}.3^2+.2^2+.1^2)$) 0.37 would not, presumably, be a tremendous problem. A component-wise error of similar magnitude, however, would really add up over infinite dimensions. In an infinite dimensional problem, the function to approximate is like the finite-dimensional position of the elbow in space

and the basis functions are like the (x,y,z) dimensions. The goodness of a set of basis functions is judged on its ability to reproduce a function of interest with high accuracy. High accuracy alone is not enough, though; we could have represented the location of the wrist with respect to the moon in section 1, but we would have needed 15 significant digits in each of the (x, y, z) coordinates to get reasonable accuracy. Similarly, with enough coordinate values, most sets of basis functions can give high accuracy. Thus, a *really* good set of basis functions will reproduce a function of interest with high accuracy *and* use only a few coordinate values.

My work depends on the concept of basis functions, because the spinal cord may represent (as in instantiate) for the brain the coordinate transformations between muscle lengths, joint angles and skin locations. Those coordinate transformations and their Jacobians are functions. Functions can be represented efficiently with a few numbers (neural activation levels) if the right coordinate system – ie. the right set of basis functions – is used.

Examples of Basis Functions

Figure 1-6 is designed to clarify several different, important points about basis functions. Figure 1-6 shows a cartoon graph (the heaviest line in figure 1-6A, B, C, and E) and several linear (figure 1-6A, B, C) and non-linear (figure 1-6D, E) methods of using basis functions to approximate the graph. Because the cartoon graph could easily be something important for the nervous system, such as the muscle tension vs time needed for a particular task, it is essential that the nervous system be able to represent the graph with the firing levels of a finite number of neurons.

Figure 1-6A shows a series of boxes, each of which approximates the output value of the graph. Each box is a *different* basis function. The basis functions are identical except for their location along the Input dimension. If these boxes were infinitely thin, they would be the standard set of basis functions called delta functions. The heights of the boxes in figure 1-6A are the coordinates of the graph in this box coordinate system. In the coordinate system defined by the box-shaped basis functions, the coordinates of the dark-lined graph in figure 1-6A are (5.1, 5.4, 5.0, 3.0, 2.5, 2.1, 2.3,

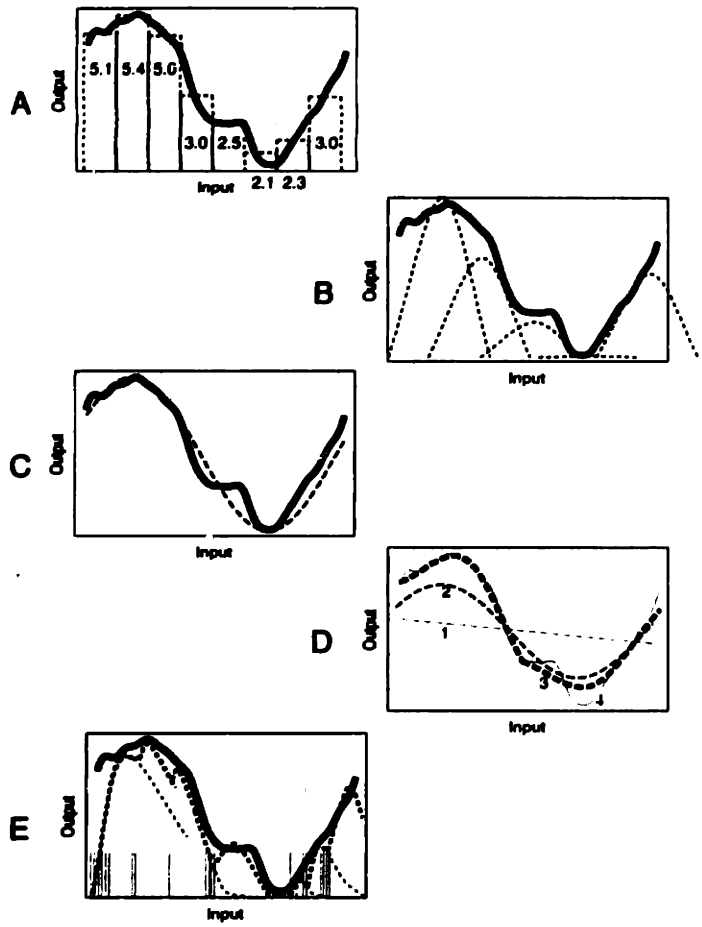

Figure 1-6: Representations of Functions Functions can be thought of as points in a coordinate system. Several examples of coordinate systems for functions are shown. (A) Box coordinate system. Each box is a basis function. The coordinates of the dark-lined graph in the box coordinate system are (5.1, 5.4, 5.0, 3.0, 2.5, 2.1, 2.3, 3.0). (B) Gaussian coordinate system. Each parabolic bump is a basis function. The coordinates of the dark-lined graph would be given by the heights of the bumps. (C) Sinusoidal coordinate system. The dotted line shows the function given by a Fourier approximated to the dark-lined graph. The Fourier decomposition of a function is used to determine the function's coordinates in the Fourier coordinate system. The basis functions of the Fourier coordinate system are sinusoids. (D) Shape-changing coordinate system. The made-up function in this figure changes shape dramatically as the "height" parameter is changed. (E) Muscle tension coordinate system. The firing rate of a motor neuron would give the coordinates of the dark-lined graph in this coordinate system.

3.0).

Figure 1-6B is like figure 1-6A, except the boxes are smeared together. Each of the bumps is again a different basis function, and they again are only distinguished by their location along the Input dimension. This style of basis functions, known as radial basis functions, has been explored extensively in the neural network literature (Poggio & Girosi, 1990). A few heavily overlapping basis functions can form surprisingly accurate approximations. For instance, the models used to produce the force fields of figure 1-7 are constructed from radial basis functions. I believe the spinal force fields are analogous to radial basis functions. The spinal force fields overlap a great deal and a few of them can be added together to produce a surprising range of force fields. In other words, the spinal force fields themselves form a new coordinate system for a representing force fields in the spinal cord.

Another important feature of basis functions is that a good set of basis functions can capture most of the important behavior of a function with only a few numbers. Figure 1-6C shows the approximation given by the first two terms of a discrete Fourier transform of the graph. This approximation is contained in three numbers: the mean value of the graph, the amplitude of the single-cycle sine wave shown in the figure, and the phase (locations of the zero-crossings) of the sine wave. With these three numbers and the sinusoid functions, the dark-lined graph is approximated fairly well.

The basis functions of figure 1-6A,B,and C are used in linear approximations to the graph. This means that the height of all of the basis functions are added together at each Input value to produce the approximation:

$$\text{Output(Input)} = \sum_{i=1}^{N} \text{height}_i * \text{Basis Function}_i\text{(Input)}$$

The linearity of the basis functions is tremendously valuable for use and learning. Because the height of each linear basis function can be easily computed from the graph being approximated, new graphs can be represented, learned, or controlled in a linear basis function coordinate system. For example, in the finite-dimensional coordinate systems, the height of each basis function is the projection of the point to

be represented onto that dimension, so a cartesian coordinate like (3, 4, 5) expresses the fact that the point at (x, y, z) projects onto the x axis as a vector extending out 3 units. The height of the boxes in figure 1-6A are, similarly, the projection of the dark-lined graph onto each box/dimension/basis function.

The key feature of the linear basis function sets is that they do not change shape: 3 * basis = basis + basis + basis. If the output range of the dark-lined graph in figure 1-6 is on the order of 1 million physiologically relevant units, then the bumps in the graph span thousands of units and therefore are probably important. In this case, we want to increase the accuracy of the approximation by the basis functions, because errors in the representation are probably physiologically significant. If, however, the output range of the graph in figure 1-6 is only 1 or 2 relevant units, then the smaller bumps span a negligible number of units and are therefore unimportant. Thus, as the multiplier of the basis function (the coordinate value) increases, the output range of the approximated graph is increased and new, previously negligible, details become more important. For these reasons, it might be desirable to forgo linearity in favor of shape-changing basis functions that change shape as their heights increase.

In figure 1-6D I have illustrated four levels of a single hypothetical non-linear basis function. The panel shows one basis function that changes shape when its multiplier changes from 1 to 4. When the multiplier is 4, the shape of the basis function is exactly the same as the graph being approximated in figures 1-6A,B,C,E. We could not easily find the height coefficients for basis functions like this: it is hard to determine the right values for the coordinates (heights) in the non-linear equation

$$\text{Output(Input)} = \sum_{i=1}^{N} \text{height}_i * \text{Basis Function}_i(\text{height}_i, \text{Input})$$

The non-linear approximation has a benefit, however, in that the complex graph we are trying to approximate has a simple representation in any set of basis functions (coordinate system) that contains the basis function shown in figure 1-6D. For example, if we use a coordinate system comprised of the box basis functions of figure 1-6A and the shape-changing basis function of figure 1-6D, then the boxes would not really

be needed to represent the dark-lined graph. We could set those coordinates to zero and the complex function would have the simple representation (..., 0, 0, 0, 4, 0, 0, ...). This example is like representing the point (3, 4, 5) in a coordinate system made of up (x, y, z) and another vector, Q, that points to (3, 4, 5). The (x, y, z, Q) coordinates of the point (3, 4, 5) are be (0, 0, 0, 1).

In figure 1-6E shows a specific hypothetical example of a basis function representation in the spinal cord. I have explicitly labeled the complex graph as Tension vs Time. The basis functions in this panel are the kind of shape-changing tension responses that muscles produce when activated by action potentials from motor neurons. The vertical hash marks along the bottom of figure 1-6E indicate the timing of hypothetical action potentials from the motor neuron which kick the muscle into action. I have attempted to illustrate the importance of spike timing and frequency on the tension output of the muscle.

The non-linearities of the basis functions in figure 1-6D,E are important to the simulation results of chapter 2, in which I add together the forces produced by many muscles. In other words, I model the muscles as linear basis functions, and the muscle activation levels are the basis function multipliers. It is reasonable to add together the torques produced by the muscles, because the torques sum at the joints. However, the tension output of each muscle is a function of its activation level (see figure 1-6E, or Partridge and Benton (1981)) so that a muscle force field as a basis function should be more like the basis function of figure 1-6D than it is like the radial basis functions of figure 1-6B. For simplicity, I have explicitly assumed that the muscle force fields and the spinal force fields can be treated like the radial basis functions of figure 1-6B. Current work is aimed at quantifying the errors introduced by that assumption (Galagan, et al, 1995).

Computations in the Spinal Cord

The coordinate transformations and their Jacobians are matrices. It is easy and common to think of values of a matrix as synaptic weights. The transformations

and Jacobians change with each change in limb position. Synaptic weights could be modified to reflect these changes in the transformations, but the known mechanisms for rapid changes in synaptic weights involve inputs from other cells. Thus, the coordinate transformations can be represented as matrices of values particular to the current limb position, but the changes in those matrices would require some separate representation of the coordinate transformation *function.* (Windhurst, et al, 1991)

The description of the state of each of the motor neurons is itself another representation. In figure 1-5A we see that each motor neuron's translation from input to output is affected by the operating state. Some inputs change the cell's states and others affect its firing rate. The overwhelming majority of inputs to motorneurons come from spinal interneurons (see Windhurst, et al, 1991). These interneurons can control both the states of the motor neurons and the membrane potentials of the motor neurons. In a sense there are two separate (at least) representations of motorneuronal firing to be expressed in the interneuronal firing (Binder, et al, 1993). We do not know yet if interneuronal stimulation is having its effects by imposing state changes or membrane potential changes or both of these on the motor neurons.

Inverse Dynamics

Yet another aspect of dynamics is the problem of inverse dynamics. I define the inverse dynamics of an arm as a function that maps a desired trajectory of the arm to a sequence of neural impulses to the muscles. Returning to the example of reaching out to touch an object, it is apparent how impossibly difficult the inverse dynamics problem is. In order to get the hand to move along a trajectory from its starting point to the object, a sequence of neural impulses must be sent to the muscles. As the muscles contract they pull on the tendons which induce torques in the arm. As the arm begins to accelerate, new interaction torques arise. Those interaction torques and the changing configuration of the arm impose new conditions on the muscular contractions needed to accelerate the arm along its path to the object. The muscles are also changing length during this process, so the tension produced by impulses going to the muscles are not what they were at the beginning of the problem. Despite

this complexity, we are able to move.

It is not yet clear if the nervous system actually solves the inverse dynamics problem. An alternative possibility is that we are only able to perform a restricted sub-class of trajectories. [refer to representations in sentence here] The only hope for distinguishing these possibilities is to observe regularities in the things the nervous system can not do. Given a theory of how the nervous system represents its solution to the inverse dynamics problem, failures can be interpreted as being consistent with that theory or not. Ultimately, a representation of inverse dynamics that minimally explains the capabilities of a nervous system can be examined with the question, "does this representation restrict the system's performance?" That question can be asked of a mathematical/scientific model. It can not be asked of data. The performance can only be used to build a model. My thesis is centered on testing an equilibrium point theory (see below) of the representation of inverse dynamics.

An Equilibrium Point Theory

The idea behind the equilibrium point theory is that muscle tensions of opposing muscles can be set to counterbalance each other, yielding an equilibrium posture or position. A simple demonstration shows that we are capable of producing such counterbalanced muscle contractions. Hold your arm out from your body with your muscles relaxed. Now tense the muscles of your arm around one or more joints without moving your arm. The fact that you can do this without the arm moving indicates that you can increase the tension of many muscles acting on the arm in such a way that the sum of the increased torque at each joint is zero. In other words, the current position is maintained as an equilibrium point of the system.

As a theory of movement, the equilibrium point theory supposes that moving from the current position involves commanding a new set of muscular contractions that yield an equilibrium at the desired new position. Eventually, the arm will respond to the new muscle tensions by accelerating in the general direction of the desired new position and coming to rest in its general vicinity. To get a sense of this theory, hold your arm out from your body and tense your muscles as before. Your arm is at

equilibrium at position A. Now relax your muscles, move your arm to a new position, B, and tense your muscles. The equilibrium point theory of movement states that you moved from A to B by tensing your muscles as if you were maintaining position B while you were still at A. The result was that your arm moved from A to B.

The equilibrium point theory of movement as expressed above is demonstrably false. We move our wrist or fingers in straight cartesian lines throughout most of our workspace. The equilibrium point theory predicts a circuitous cartesian route for the arm, for several reasons. Setting the muscle tensions to a new level given by the new position will produce torques that are proportional to the difference (between the current and desired positions) in joint angles. All other things being equal, such torques will move the arm in a straight line in joint space, which is quite distinct from a straight line in cartesian space. We have also seen that accelerating the shoulder causes torques at the shoulder from the relative motion of the forearm. In fact, the way to move an arm in a straight line is to produce shoulder torques that look roughly like a full cycle of a sine wave: it is necessary to pull first one way and then the other. Such torques can not be produced by a simple, time-invariant energy well at the desired final position. The dynamics of the arm are not such that the wrist will be made to move easily in a straight line. The fact that we move in straight lines demonstrates that we, somehow and to some level of accuracy, invert the dynamics of the skeletal apparatus. Since, in its original form, the equilibrium point theory was intended as an explanation of how the brain could avoid computing the inverse dynamics of the arm, it cannot be correct.

It appears that most of the pieces of the solution to the inverse dynamics of the arm are available to the brain. The fact that we move in straight lines indicates that we invert the dynamics of the arm. I will present work in chapter 2 that adds support to the notion that the spinal cord inverts the activation dynamics of the muscles. If we can assume for the sake of argument that the spinal cord also inverts the velocity dependence of the muscles, then every piece of the inverse dynamics puzzle is in place. If indeed the brain does compute the inverse dynamics of the arm, then the question becomes, how does the brain represent the solution to the problem?

My thesis supports a more sophisticated version of the equilibrium point theory in which the representation (see below) of the solution to the inverse dynamics of the arm is constructed from simple combinations of equilibrium points. In the equilibrium point theory described above, the muscles act as a source of forces independent from the arm. The fact that the forces are being provided by the muscles does not matter to the arm. We can retain this feature of the original equilibrium point theory. Accordingly, the inverse dynamics problem is divided up into inverse muscle dynamics, inverse arm dynamics, and inverse world dynamics. Each part of the problem requires some neural representation of the computed solution. I provide results that indicate that discrete classes of muscle combinations (that lead to particular equilibrium points) can be found in the spinal cords of decerebrate frogs. I will end with preliminary results indicating that the forces produced by activation of some brain regions can be expressed as combinations of the equilibrium points represented in the spinal cord.

Overview of Previous Results from Spinal Micro-Stimulation of Spinalized Frogs

Spinal stimulation experiments were recently undertaken in an attempt to elucidate the coordinate transformations being performed by the frog spinal cord (Bizzi, et al, 1991; Giszter, et al, 1993; Loeb, et al, 1993; Saltiel & Bizzi 1994). These experiments have demonstrated that the spinal cord of the frog contains a limited number of "modules". That is, we measured the hindlimb forces evoked by spinal interneuronal stimulation, and observed that the evoked forces occurred in a few discrete clusters of orientations (see figure 1-7). This result is unexpected because forces which result from random activation of the frog's hindlimb muscles do not fall into discrete clusters. The structure of the hindlimb musculature does not, therefore, predict the striking regularity we have observed after thousands of microstimulation experiments. The small number of force patterns suggests that the spinal cord preferentially represents a limited number of classes of muscle combinations. We theorize that the limited

number of spinal modules serve as the basic building blocks of posture and movement (Mussa-Ivaldi, 1992). Descending fibers from supra-spinal structures could conceivably activate simple combinations of the spinal modules in order to produce forces that are not directly represented as modules. My thesis is devoted to formulating and preliminarily executing a statistical test of that theory.

Figure 1-7 summarizes several years of spinal stimulation work performed by several people. This section is an extended description of figure 1-7 and will discuss: force fields, the relationship between spinal loci and forces, force field equilibrium, total force vs. active force, and our theory of force field summation. In conclusion, I will discuss our efforts to relate the force fields of figure 1-7 to muscle activations, which leads to the formulation of the statistical test of our theory.

Spinal Force Field Models

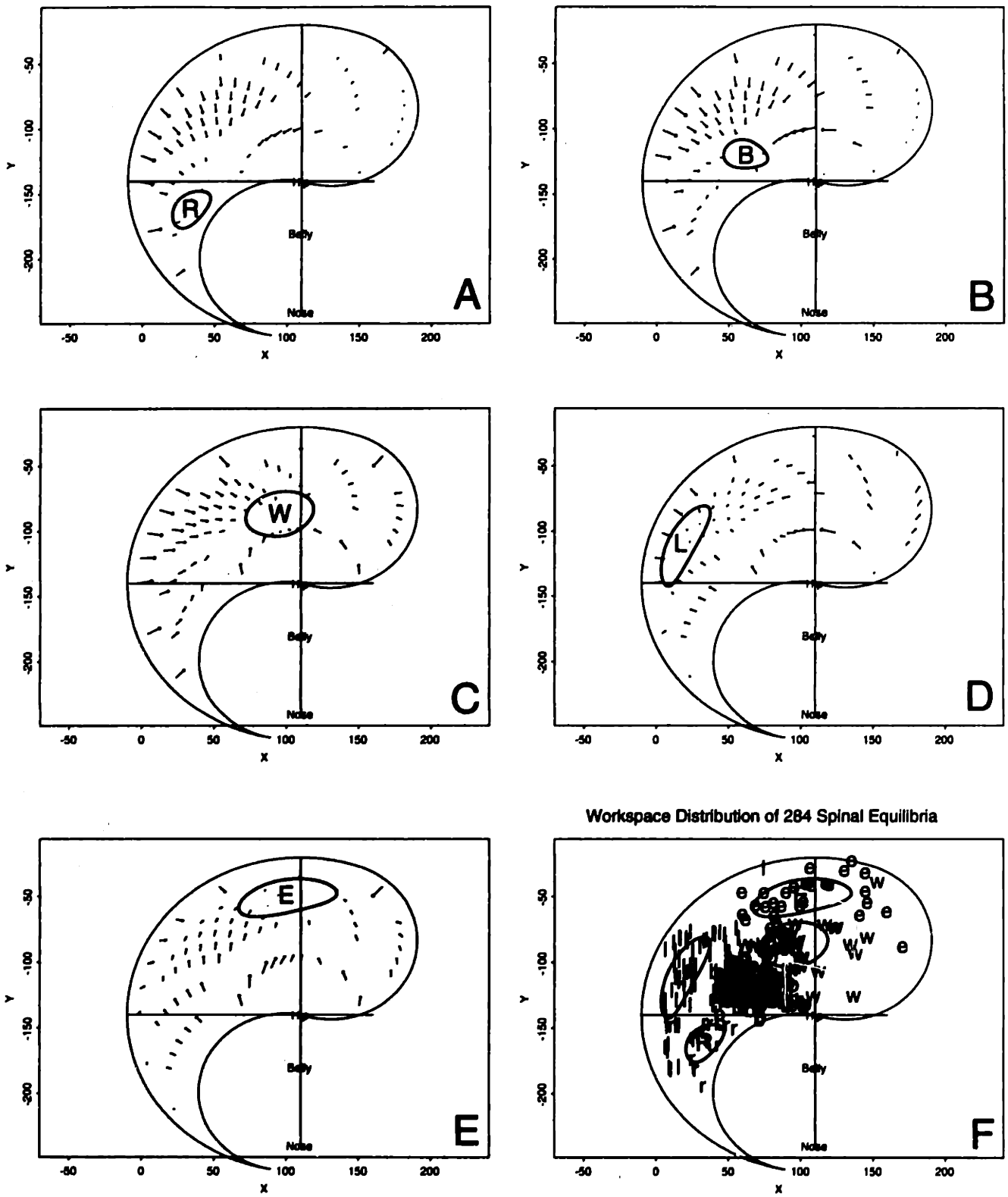

Figure 1-7: The five types of Force Field evoked by Spinal Microstimulation
The five types of Force Field evoked by Spinal Microstimulation We have generally found that spinal microstimulation results in one of a few types of force field. In this figure we see model force fields produced from 284 data force fields evoked by spinal microstimulation (see chapter 2 for details on the construction and interpretation of this figure). The outlined regions are ellipses in joint space, centered at the mean, and one standard deviation wide. The whale-like outlines in each of the plots is the boundary of the workspace of the right hindlimb: it is a square in joint space from hip = -110^o to hip = 80^o and from knee = 0^o to knee = 180^o. "Hip", "Belly", and "Nose" are used to indicate the direction that the frog's body is oriented. The X and Y axes are in units of millimeters. The frog's hip is located at 110, -140, and the link lengths are thigh=60, calf=60. These were the somewhat arbitrarily chosen parameters of a standard frog. Since our force field models were always expressed as torques, we were able to convert them to any link lengths for any frog. (A) Rostral Flexion. There are 21 force fields of this type in the database. (B) Body Flexion. This is the most common type of spinal force field. There are 135 force fields in the database of this type. (C) Wipe. There are 36 force fields of this type in the database. Two of these 36 force fields were evoked by electrically stimulating the ankle of the contralateral hindlimb. Both skin-stimulation force fields "look like" spinally-evoked Wipe force fields, and they correlate best with the Wipe aggregate force field (the force field shown here). The field correlation coefficients are 0.8 and 0.9. (D) Lateral Extension. There are 57 force fields of this type in the database. (E) Caudal Extension. There are 30 force fields of this type in the database. (F) The full distribution of all of the spinal equilibria in our database. Each equilibrium point is marked with the letter of its classification.

Force Fields

Panels A through E in figure 1-7 show force fields. A force field is a vector-valued function relating force to limb position. Each arrow in figure 1-7A-E represents a force at a limb position. We measure force fields by stimulating at a single location with the frog's hindlimb held successively at several different positions by a force sensor. Force fields can be accurately approximated with measurements of hindlimb forces only if the same behavior can be repeatedly evoked with the hindlimb in different positions This generally seems possible: when we have measured forces at large numbers of limb positions, the observed force fields have been smooth – meaning that neighboring limb positions yield nearly identical evoked force measurements (Loeb, et al. 1993).

Spinal Loci of the Force Fields

The force evoked by micro-stimulation depends on the the location of the stimulating electrode. We are investigating the fine structure of the map relating electrode location to evoked force (for lumbar spinal loci: Giszter, et al, in preparation; for cervical spinal: Galagan, unpublished observations; for supra-spinal loci: Loeb, et al, 1995 and chapter 4). We can generally evoke forces in extension by stimulating caudally in the interneuronal grey matter of the lumbar spinal cord. We can evoke flexion forces with rostral lumbar interneuronal electrode placements. Different subtypes of force field (see figure 1-7) are evoked by rostrocaudally oriented stripes in the spinal cord. Our low current stimulation would not be expected to activate an entire strip. By observing the uptake of an activity-dependent dye during stimulation at a single locus, Giszter, et al (1993) found that the activated interneuronal volume appears to correspond to a rostro-caudal strip. This finding underscores our interpretation of the anatomical strips as the neuronal basis of processing modules of some kind.

Force Field Equilibria

Figure 1-7C is a particularly striking example of a force field with an equilibrium point. We can see that this force field has an equilibrium point because all the forces

point toward the same place, the "W". It is important to know the locations of force field equilibria, because an equilibrium point represents the location towards which the ankle would tend to evolve under the influence of the force field.

Resting, Evoked, and Total Forces

In analyzing force fields, we distinguish between total force, resting force, and evoked force. The resting force is the force field measured without any stimulation. The total force is the actual force measurement before and during stimulation. The evoked force = total force − resting force. This definition is reasonable, because at any given limb position the resting force returns to the same baseline level on successive trials (Loeb, et al. 1993). The evoked force field is more reliable measure for quantification than total force field for several reasons. The resting forces include uninteresting variable factors like occasional force exerted by the frog's toes on the experimental apparatus. The resting forces often are not repeatable from trial to trial. The evoked forces are remarkably repeatable. Furthermore, the evoked forces tend to rise and diminish in magnitude along a single orientation, so that the evoked force field at time 1 is proportional to the evoked force field at time 2. As a corollary of that observation, the total forces rotate during a trial: the total force initially points in the direction of the resting force, then rotates toward the peak evoked force, then rotates back to the resting force. Thus, the evoked forces can be more easily summarized than the total forces. Increasing the stimulation strength increases the magnitude of the evoked force but generally does not change its angle. Thus, an evoked force field at one stimulation strength is a multiple of the evoked force field at a different stimulation strength (but same electrode location). Because this is true of the evoked forces it can not be generally true of the total forces. The discrete patterns of forces shown in figure 1-7 are evoked forces.

Force Field Summation

The force fields evoked by focal stimulation of the spinal cord follow a principle of vector summation. If FF1(x) is the evoked force field from spinal site number 1, and

FF2(x) is the evoked force field from spinal site number 2, then the force field evoked by stimulating spinal site 1 and spinal site 2 simultaneously will be highly similar to FF1(x) + FF2(x) (Mussa-Ivaldi, et al, 1994). The sum of force fields is given by the sum of the component forces at each limb position, x. The functional implication of force field summation is that all non-linearities are either eliminated or carefully organized by the spinal modules to preserve linearity. It is easy to concoct examples of plausible non-linearities. For example, if FF1 inhibited some of muscles of FF2, then the forces produced by FF2 under co-activation with FF1 would generally not have the same orientation as the forces of FF2 alone. Thus, inhibition of motorneurons - a common spinal phenomenon - can interfere with force field summation. The fact that we observe summation suggests that the spinal cord is specifically organized to support it.

The surprising fact of linear superposition of spinal force fields leads to the hypothesis that the spinal force fields are the basic elements of posture and movement. According to this hypothesis, the few active force fields represented in the spinal cord are motor primitives which are combined through linear superposition to fashion other postures and complex movements. An important prediction of this hypothesis is that the behaviors of intact frogs should be restricted to actions that can be decomposed into spinal force fields. I have constructed statistical models of the spinal force fields (figure 1-7A-E) that will be helpful in identifying specific aspects of the hindlimb movement "incompetence" that intact frogs should exhibit if our theory is correct. That is, simple simulations can help identify the movements or postures that are theoretically impossible.

Relationship to Behavior

The spinal force fields of spinalized frogs are strikingly similar to the behaviors produced by spinalized frogs. Figure 1-7A summarizes Rostral Flexion force fields. These force fields appear to drive the hindlimb into the preparatory stance that the frog assumes prior to wiping noxious stimuli from its back or head. Figure 1-7B summarizes Body Flexion force fields. These force fields appear to drive the hindlimb into the

neutral posture that spinalized and intact frogs maintain at rest. Figure 1-7C summarizes Wipe force fields. These force fields appear to drive the hindlimb to the position behind the body that both hindlimbs go to when one limb is needed to wipe a noxious stimulus off of the other. Figure 1-7D summarizes Lateral Extension force fields. These force fields appear to drive the hindlimb toward the power portion of its stroke during swimming. Figure 1-7E summarizes Caudal Extension force fields. These force fields appear to drive the hindlimb behind the body in jumping and swimming.

It is not yet clear what conclusions should be drawn from the similarities between spinal force fields and the behaviors of spinalized frogs. I show in chapter 2 that the spinal force fields are also similar to the force fields produced by the muscle combinations that are least altered by changes in the balance of the muscle activations. In other words, there are some combinations of muscles that produce nearly the same force field no matter how much the different muscles in the combination are activated. I suspect that this biomechanical fact is related to the behavioral needs of the animal: the common behaviors that the animal produced became stable points of the co-evolving muscular system. Are the force fields underlying those behaviors also used as building blocks by the rest of the brain? My preliminary results suggest that in fact the spinal force fields *are* used building blocks (chapter 4). The most reasonable alternative is that we are activating behavioral subsystems within the spinal cord.

There is a precedent for a behavioral circuit in the spinal cord being selectively used as a component in a different behavior. The C3-C4 interneuronal circuits for reaching and retrieving have been described in the cat spinal cord by Alstermark and colleagues (Alstermark & Lundberg 1992). The two spinal circuits can be differentially isolated from descending control and differentially lesioned. The authors have shown that one spinal circuit is necessary for the cat to perform a precision reach for food. Significantly, these two circuits have been shown to be distinct from the spinal locomotion generators: when cats walk normally, the C3-C4 interneurons are not active. However, when cats walk on horizontal ladders (a task which requires something like a precision reach at each step) the C3-C4 interneurons are active.

Muscle Force Fields

The force fields of muscles were measured by stimulating the muscles directly (Giszter, et al, 1993). In these experiments, forces were measured at the same 9 limb positions during stimulation of each of 11 muscles in turn. Because the same 9 positions were used, the force fields resulting from random muscle activations could be be computed at those 9 positions. The force fields predicted by these random muscle combinations rarely (8%) converged to equilibrium points within the workspace. I repeated these random simulations (and the muscle stimulations)- with similar results - in chapter 2 using statistical models of the muscle force fields constructed from more data collected over a larger portion of the workspace.

The advantage of using muscle models rather than actual muscle stimulation data is that the models can be sampled at any workspace location. This advantage thus allows more sophisticated questions to be addressed with simulations. It also allows the models themselves to be rigorously tested and improved. For example, it is desirable to know how well a model generalizes. In order to find that out we have to be able to form predictions at new limb positions; otherwise we are simply measuring the repeatability of the underlying data. By measuring the ability of a model to predict new data, I measured the model's success at generalizing from the available data. I subsequently used the types of muscle models that best predicted new data.

The original point of the computer simulations of muscle combinations was to rule out random muscle combinations as a source of the regularity in our spinal stimulation results. A question remains, however: do the biomechanics of the hindlimb dictate our results and to what extent are the results imposed by the neural circuitry. This is a difficult question to address, because the spinal circuitry presumably co-evolved with the hindlimb musculature.

In chapter 2 I present simulation evidence to suggest that the spinal force fields are dictated in part by biomechanical preferences of the skeletal muscular system. I measured the two-dimensional area in the workspace that each possible combination of muscles (each synergy) covered with equilibrium points. The synergies that covered the smallest area covered places in the workspace like those shown in figure 1-7. This

is my favorite result of the thesis. It suggests that the spinal force fields are related to the combinations of muscles that are most robust in the face of noise.

Tests of the Force Field Summation Theory of Supra-Spinal Control

Descending fibers from supra-spinal structures could conceivably activate simple combinations of the spinal modules in order to produce forces that are not directly represented as modules in the spinal cord. One problem for this theory is that the observed spinal modules could be artifacts of spinalization, since our data on spinal modules were collected by stimulating spinal cords that were surgically isolated from the rest of the brain. To address this issue directly, I stimulated the spinal cords of decerebrated, deafferented frogs in order to determine if modules are observed in the presence of supra-spinal descending fibers (chap 3). I found at least one example of each of the force field types shown in figure 1-7, indicating that these modules are not artifacts of spinalization.

Another way to test this theory is to decompose supra-spinal force fields into spinal force fields. The summation theory predicts that much of the variance in supra-spinal evoked force fields should be accounted for by the spinal force fields. In order to determine how much "much of the variance" is, we can compare the decomposition by spinal force fields to a decomposition by *muscle* force fields. This comparison asserts a simple null hypothesis: supra-spinal force fields are the result of the activation of motorneurons. The alternative hypothesis that we wish to test is that supra-spinal force fields can only activate the muscles through a particular intervening structure imposed by the spinal cord. I have performed this test on approximately 30 supra-spinal force fields. These preliminary data indicate that there are some supra-spinal regions that recruit motor neurons and others that operate through the intermediaries of spinal force fields. We can eventually compare these results to the known anatomy as an independent assessment of the validity of this test.

Chapter 2

Muscle Model Force Fields and their Application to the Problem of Understanding Muscle Synergies

Introduction

Recent experiments have shown that the hindlimb endpoint force evoked by micro-stimulation in the interneuronal grey of spinalized frogs vary in predictable ways with the stimulation locus and the hindlimb posture (Bizzi, et al, 1991; Giszter, et al, 1991; Loeb, et al, 1993). The spatial variations in the forces have been summarized as "force fields". A force field is a vector-valued function relating force to limb position. We approximated force field functions by measuring hindlimb endpoint forces evoked at different limb positions through micro-stimulation at a single spinal interneuronal locus. We found that there were a small number of different force fields (FFs) that could be evoked at different spinal loci (summarized in figure 1-7). We have also found that the FFs resulting from micro-stimulation at multiple spinal sites is predicted by the vector sum of the spinal FFs associated with each of the stimulated spinal loci.

These results suggest that supra-spinal circuits could control the limb by activating an appropriate relative balance of spinal FFs (Mussa-Ivaldi, 1992). Indeed, I have found that supra-spinal sites can be stimulated to produce FFs unlike those observed during spinal stimulation, and the FFs evoked by spinal micro-stimulation in deafferented, decerebrate frogs are not altered by spinal transection (see chapter 3). To test the possibility that supra-spinal FFs are produced through simple linear combinations of spinal FFs, I built muscle model force fields (muscle FFs) for each of the frog's hindlimb muscles. If spinal FFs suffice to predict supra-spinal FFs, then a decomposition of any supra-spinal FF into spinal FFs should be statistically indistinguishable from its decomposition into muscle FFs. This chapter describes the muscle model force fields and the uses I made of them.

I used models to obtain simple, analytic functions for each muscle. A muscle model force field is a summary of the position-dependent endpoint forces - the force field - resulting from the activation of a single muscle. Any muscle model that can predict the muscle torques or endpoint forces at arbitrary limb postures can be visualized as a force field. Muscle modelling is typically separated into two problems: modelling muscle moment arm, $\nu(\theta)$ as a function of joint angles, θ, and modelling the magnitude of muscle tension, $M(l, \dot{l}, \alpha, t)$, as a function of the muscle length, l, muscle activation, α, and time, t (Loeb, et al., 1989, Zajac and Winters, 1990). Fitted parametric models of $M(l, \dot{l}, \alpha, t)$ have typically been combined with geometric estimates of $\nu(\theta)$ to estimate net joint torques from EMG signals (Buchanan,et al, 1986; Granata and Marras, 1993; Hof and Ven Den Berg 1977, 1981a-c; Cholewicki and McGill 1994). In this work I have for simplicity used a static model of the muscle tension, $M(l)$, and combined it with a novel fitted parametric model of $\nu(\theta)$. Well-understood dynamic models of the muscle tension can be added to this model (Galagan, et al, 1995). My approach to modelling $\nu(\theta)$ is novel, because parametric techniques have not previously been used to find $\nu(\theta)$, and because the structure of my model mimics the structure of the muscles, yielding an estimate of muscle length as a by-product. Muscle length is generally estimated as a hidden state variable of dynamic muscle models, or else determined experimentally through dissections

(Buchanan,et al, 1986; Granata and Marras, 1993; Palmer 1990; Hof and Van Den Berg 1981). The typical approach of estimating $\nu(\theta)$ from geometric principles and from cadaver measurements of muscle geometric parameters is a potentially large source of noise in many muscle models (Winters and Stark 1988). Because of the complex connective geometries of muscles, the geometric parameters are difficult to measure, and the application of geometric principles is either difficult or inaccurate.

There is a recognized need for more studies of the mechanical effects of muscle synergies and their uses by the spinal cord (Buchanan, et al., 1986; Loeb, 1987). Dynamic optimization is considered to be the best available approach for using muscle models to understand muscle synergies (Zajac and Winters, 1990). Dynamic optimization is an expensive computation, however, that requires researchers to limit the problems they study - by only considering, for example, how to stabilize a single posture (Loeb, et al, 1989). Furthermore, even if a particular optimization provides a good match to available data, it does not necessarily imply anything about the spinal circuitry (Hardt, 1978). A computationally cheaper method of using muscle models to formulate inferences about spinal circuitry would be desirable. In this chapter I describe Monte Carlo simulations (Press, et al, 1992) used infer the range of possible actions that each muscle synergy could perform.

Methods

Data Collection

Surgeries

24 healthy adult bullfrogs (Rana Catesbiana) were anesthetized with 0.5 - 1.5 cc tricaine and spinalized anterior to the first vertebra. The right hind limb was skinned and coated with vaseline to keep the muscles moist. Superficial fascia were cut to allow access to deep muscles and nerves. All large nerves were cut and removed to sever the reflex arcs and to prevent the stimulus applied to one muscle from spreading along the nerves to other muscles.

Pre-experiment Preparation

Spinalized frogs were placed on a moistened molded plastic frame and secured in place by clamps attached to the hip and spinal column. The position of the frog's hip in the apparatus and the length of its right hind limb segments were measured. The right ankle was attached to a movable force sensor (figure 2-1A and 2-2A) by a cuff capable of rotating about the Z axis, or of being secured in place so that it could not rotate. The force sensor is attached immediately above the frog's ankle; the sensor coordinates correspond to ankle positions.

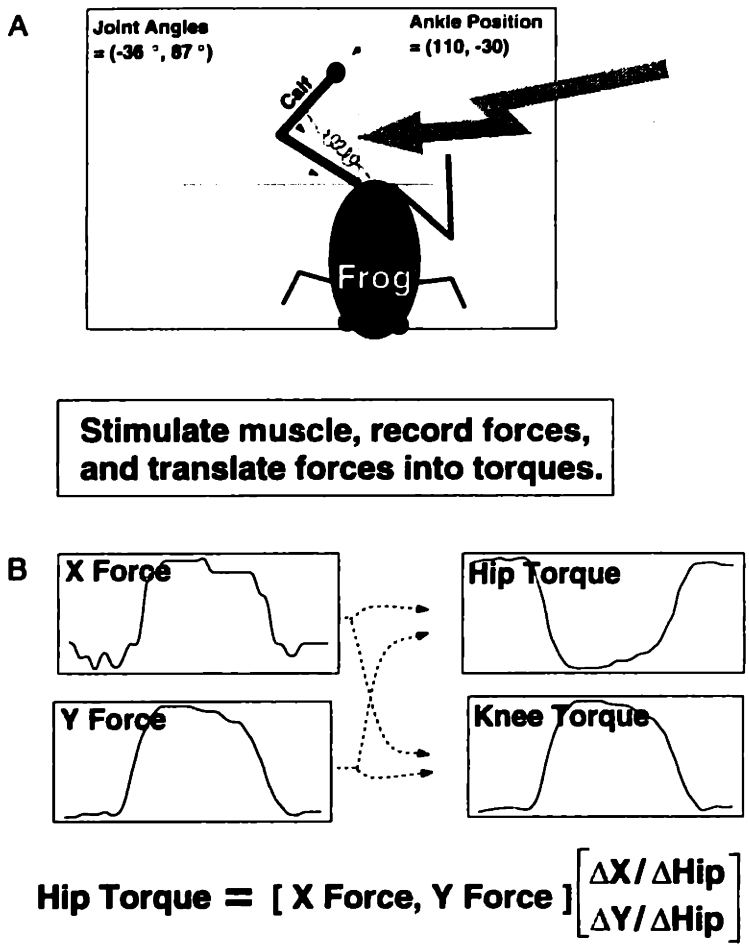

Figure 2-1: Processing Sequence for Force Data

This figure illustrates the processing steps taken to convert the force data from muscle stimulation trials into torque data. (A) A frog is drawn with its hindlimb at a hip angle of $-36°$ and a knee angle of $87°$. A hip angle of $0°$ would cause the thigh to be parallel to the x axis. These joint angles bring the ankle to the location (110, -30) in the workspace. Ankle positions are measured in millimeters relative to the base of the force sensor apparatus. The spring symbol is meant to represent a muscle. The large arrow indicates that the muscle is stimulated. A force sensor attached at the frog's ankle records the translational (x,y,z) forces resulting from the muscle stimulation. (B) The (x, y) force traces recorded during muscle stimulation are displayed. I have not analyzed the z forces in this work. Forces are sampled every ten milliseconds. The force values are translated into hip and knee torques, using the the derivatives of the functions relating the (x, y) location of the ankle (that's (110,-30) in this figure) to the angles of the hip and knee joints (that's $(-36°,87°)$ in this figure).

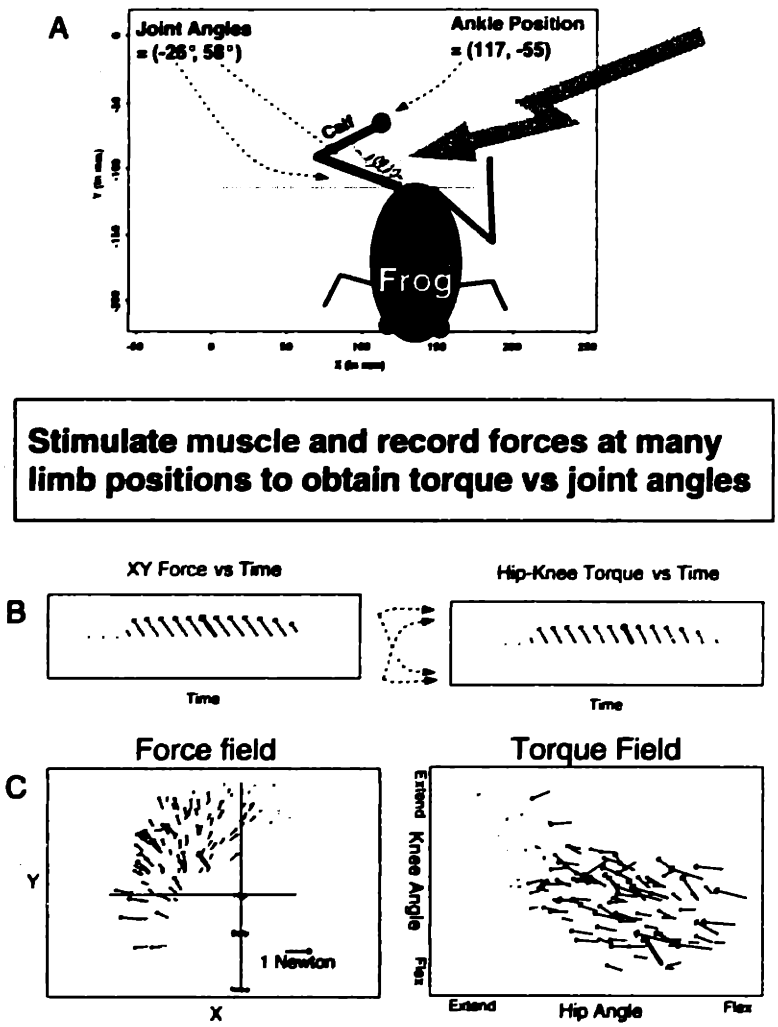

Figure 2-2: Measuring a Torque Field to Fit a Muscle Model

This figure illustrates the processing steps taken to convert the data from muscle stimulation trials into a force/torque field. (A) A frog is drawn with its hindlimb at a hip angle of $-26°$ and a knee angle of $58°$. These joint angles bring the ankle to the location (117, -55) in the workspace. The spring symbol represents the same muscle as shown in figure 2-1. Note that at this new limb position, the length of the spring/muscle has changed from its length in the previous figure. The large arrow indicates that the muscle is again stimulated. A force sensor attached at the frog's ankle records the translational (x,y,z) forces resulting from the muscle stimulation. (B) The recorded (x,y) force traces and corresponding (hip, knee) torque traces are here plotted as sequences of vectors. These vectors are "active" or "evoked" forces and torques, in that their baseline levels prior to the onset of stimulation was subtracted away. The vector with the peak magnitude in each of the two sequences is highlighted. (C) By collecting together the peak force (torque) vector at each limb position (posture), a force (torque) field is constructed. The highlighted peak vector from part (B) is also highlighted in the two fields. The force field (and corresponding torque field) are the actual data measured during Semimembranosus stimulation in eight frogs, also displayed in figure 2-12.

A pair of "fishhook electrodes" (stainless steel wire threaded through a syringe, with exposed wire at the tip bent back to form a hook. (Crago, et al. 1980)) were placed in each muscle under a dissecting microscope. Stimulus voltage was set at the start of the experiment to evoke a visible, sub-maximal muscle contraction without causing contractions in any other muscles: the surgical isolation of the muscles made it possible to verify isolated responses visually. Other stimulation parameters were fixed at 0.6 msec pulses width, 600 msec train duration, and 40Hz.

Recording Force Fields

We measure muscle force fields by stimulating *one* muscle with the hind limb in each of *many* positions. Thus we followed this simple procedure:

1. Secure the ankle cuff in the force sensor.
2. Stimulate the cord while measuring force.
3. Release the ankle cuff for rotation and move the limb to a new posture.
4. Repeat procedure at the next limb posture.

The force sensor was attached immediately above the frog's ankle, so the sensor's (x,y) coordinates correspond to the frog's right ankle position. I did not change the z coordinate of the ankle in this experiment. As the muscle contracts and relaxes in response to stimulation, the force sensor records x, y, and z forces as functions of time. A measured force field consists of 3 force traces per ankle position together with the (x,y) location of the ankle at the time the forces were measured (see figure 2-1A and 2-2A).

Force Filtering

Data from a single trial consisted of three force traces (x, y, and z vs. time) from one muscle at one position as a result of one stimulus train. Every force trace had two parts: "resting" and "active". Because we always begin collecting the force traces before the stimulus onset, the first 50 to 100 milliseconds of the force traces represent

an estimate the resting (baseline) force levels. We compute the active force traces by subtracting the resting force level from the total force evoked by the stimulation of the muscle. For example, the active y-force trace for a muscle was its total y-force trace minus its resting y-force value. Forces were digitized and recorded in units of 0.00125 Newtons.

The (x,y,z) active forces form a time-varying 3-dimensional force vector, the Active Force Vector, AFV(t). The time-varying force vectors sampled at each of the limb positions form a time-varying Force Field, FF(x, y, t). During muscular stimulation, the time-varying forces always rise and fall along a single orientation, so that AFV(t1) $\propto$ AFV(t2). Therefore, FF(x, y, t) can be well-approximated by FF(x, y), a time-invariant force field [1]. At each sampled position, I used the peak of the time-varying force vector at that position, $\max_t \|AFV(t)\|$, as the force vector in the time-invariant force field, FF(x, y) (see figure 2-2C). Although the forces of FF(x, y) are three-dimensional, I only consider the two-dimensional (x, y) forces in this chapter.

Conversion to Torques

In order to compare the results of muscle stimulation across animals, the measured forces were converted to joint torques. Expressing the endpoint forces as joint torques removed the component of variation due to the inter-frog differences in leg lengths. Consider figure 2-3, which displays force fields corresponding to constant joint torques. Variations in the forces in figure 2-3 are strictly due to variations in the position-dependent translation from torques to forces. The forces resulting from hip torques lie along the direction of the calf. The forces resulting from knee torques lie along the line connecting the hip and the endpoint.

[1] We generally find that the latency to peak force is nearly constant across the workspace. Force fields produced by sampling the data at a single latency applied across the workspace (eg, FF(x, y) = FF(x, y, t0)) are similar in most cases to those achived with the peak-force method described here. In other words, FF(x, y, t) may be decomposed as FF(x, y) * G(t).

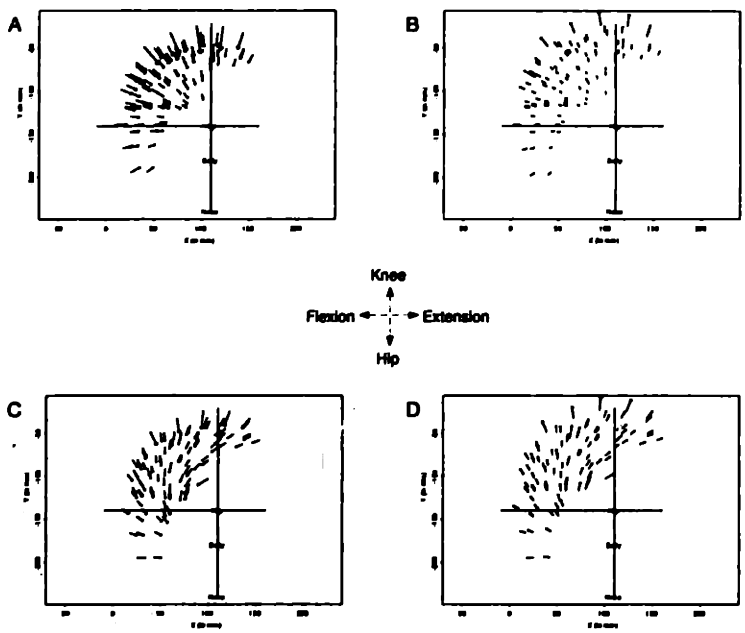

Figure 2-3: Force fields resulting from Constant Torques Four force fields are shown. A force field is a vector-valued function relating force to limb position. Each arrow represents an endpoint force. The base of each arrow is at the workspace location of the vector-valued function. The size of the arrowheads are proportional to the size of the force. Each arrowhead is on the side opposite the base of the arrow – ie these are not pin cusion diagrams. These force fields were generated by (A) constant knee flexion torque, (B) constant knee extension torque, (C) constant hip flexion torque, and (D) constant hip extension torque. Thus, the arrow at each x,y location in these four panels indicates the magnitude and orientation of the force resulting from a given amount of single joint torque, which is constant over the entire plot. Because the torque is constant, and force is the product torque and the Jacobian of the mapping from joint space to cartesian space, the magnitude changes across the workspace are due only to the changes in the determinant of the Jacobian. Note that the forces resulting from hip torques lie along the direction of the calf. The forces resulting from knee torques lie along the line connecting the hip and the endpoint.

Models of the Force Fields Produced by Muscles

The rationale for establishing model muscles rests upon the need to obtain for each muscle simple functions that can be manipulated analytically. In order to find simple, accurate functions, I fit statistical models to the data. There are infinitely many possible parameterized model types one might use, and each model type can have infinitely many different parameter vectors. For a given model type, I found a good parameter vector by adjusting parameters so as to minimize the total error between the model-predicted values and the experimentally-observed values (see figure 2-4b).

Choosing the Right Model Type

I wished to find a model *type* that could produce muscle *models* that would predict the results of muscle stimulation in a new, previously un-observed frogs. To test the generalizability of a model type I used the Jackknife technique (Efron and Tibshirani, 1993), on a data set of force fields observed during Semimembranosus stimulation in 10 frogs. The Jackknife technique involved computing the parameters for a model type under consideration from the force data of 9 of the 10 frogs. Computing the parameters resulted in a muscle model of the Semimembranosus muscle, from which I computed the prediction error on the Semimembranosus force data of the remaining frog. These two steps were performed 10 times (once for each frog in the database) to compute the average prediction error over the dataset.

Table 2 shows the prediction errors for several muscles and model types. The prediction errors are measured as root mean square errors and as correlations. Small root mean square errors and large correlation values indicate that a model generalizes well over new data. The virtual work muscle model is described in detail below. Table 2 shows that the virtual work model can be expected to have the smallest prediction error on new force fields evoked from new frogs.

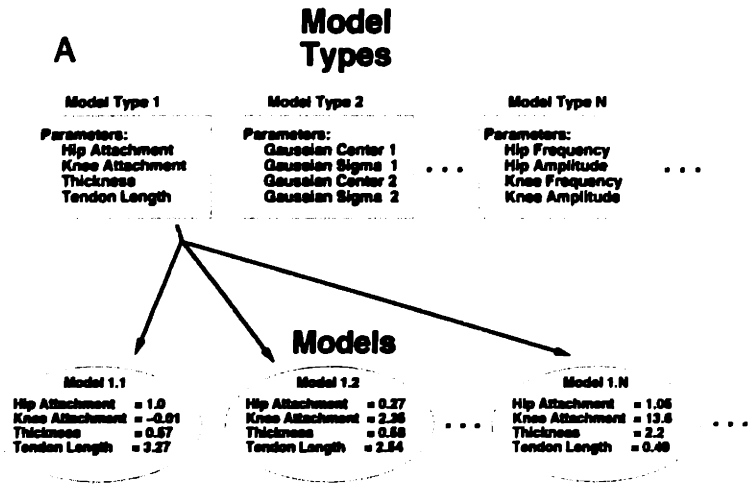

B Finding Good Model Parameters

Observed			Model X.1 (parm = 1)		Model X.7 (parm = 7)	
Hip°	Knee°	Hip Torque	Hip Torque*	Error	Hip Torque*	Error
30	90	150	120	30	170	-20
0	110	25	50	25	10	15
-30	75	15	70	-55	20	-5
-20	130	50	60	-10	20	30
Sum of Squared Error:			4650		1550	

7 is better than 1 as a parameter value for Model Type X

Figure 2-4: Steps involved in statistical modelling (A) There are infinitely many possible model types. Each model type performs a different computation as a function of its inputs and its parameters. Each model type can be used to implement infinitely many different computations, or models, by supplying different sets of parameters. (B) For a given model type, a good set of parameters can be determined by adjusting the parameters so that the input-output behavior of the model most closely approximates some desired input-output behavior. The behavior of a hypothetical model X is displayed at 2 values (1 and 7) of its parameter and at 4 values of the input variables, hip angle and knee angle. The desired behavior of the model is shown in the left-most section of the table. The top line shows that the desired output at Hip angle = 30° and Knee angle = 90° is Hip Torque = 150. When the model parameter is 1, the Hip Torque at (Hip, Knee) = (30°, 90°) is 120, for an error of 30. When the model parameter is 7, the Hip Torque at (Hip, Knee) = (30°, 90°) is 170, for an error of -20. The sum of the square errors over all 4 limb positions is the error criterion that we try to minimize by adjusting the parameters. In the table, 7 is a better parameter than 1, because 1550 < 4650. The next step in the process would be to compare the total error around 7, say at parameter = 4.5 and at parameter = 9.5. By continually moving the parameters in the direction that reduces the total error, we ultimately arrive at a local minimum in the total error.

Muscle	N	Mean Torque FF	Linear Torque FF	9 Gaussians	Gated Experts	Virtual Work
SM	9	4.32 (66%)	3.87 (68%)	4.67 (77%)	2.55 (79%)	2.27 (87%)
SA	9	4.45 (73%)	3.73 (73%)	3.69 (78%)	2.65 (76%)	2.49 (79%)
ST	5	2.22 (72%)	2.85 (83%)	2.41 (87%)	-	1.56 (83%)
AD	7	6.29 (71%)	6.2 (67%)	4.16 (69%)	1.66 (66%)	1.59 (68%)
VI	8	2.88 (59%)	3.36 (52%)	3.5 (65%)	-	2.13 (55%)
IP	6	2.85 (44%)	3.27 (51%)	2.78 (58%)	-	2.71 (57%)
VE	6	3.57 (82%)	3.63 (75%)	2.25 (78%)	2.5 (78%)	2.45 (80%)

Jackknife errors for 5 Model Types: Root mean squared error and mean force field correlation (see below) are displayed for seven hindlimb muscles. The force field correlation of field A and B will be the correlation value for the vectors $(x1_A, x2_A, ...xN_A, y1_A, y2_A, \cdots yN_A)$ and $(x1_B, x2_B, ...xN_B, y1_B, y2_B, \cdots yN_B)$, where xi_A is the x component of the force at position i of field A. The force field correlations are shown in parenthesis. Good generalization is indicated by low squared errors and high force field correlations. For example, the Mean Torque FF model type would be expected to have a root mean square prediction error of 4.32 on new Semimembranosus force field data, whereas the Virtual Work model (described below) would be expected to have an error of 2.27 on the same data. The Mean Torque model predicted joint torques as the mean of the observed joint torques. The Linear Torque model predicted torque as a linear function of the joint angles. The 9 Gaussians model (Mussa-Ivaldi, 1992) and the Gated Experts model (Jacobs, et al, 1991) are described elsewhere.

I approximated muscles as single force fields throughout this work, because I was unable to distinguish functional sub-units in any muscles. I examined the force fields evoked by stimulating different portions of muscles BI, GA, PE, RA, SA, SM, and VE (Biceps Femoris, Gastrocnemius, Peroneus, Rectus Anticus, Sartorius, Semimembranosus, and Vastus Externus, respectively).

The Virtual Work Model Type

I used a virtual work model to compute muscle length as a function of limb position (Mussa-Ivaldi, 1992). A virtual work model finds parameters for a muscle length function so that the spatial gradient of that function best predicts the observed joint torques. The spatial gradient of muscle length is related to joint torques because

torques and forces are locally linearly related by the first derivative of the intervening coordinate transformation. This linear relation can be derived from the invariance of work (force times displacement) with respect to coordinate transformations:

$$\text{muscle work} \;=\; \text{muscle tension } \partial l = \text{skeletal work} = \vec{\tau}^T \vec{\partial\theta} \qquad (2.1)$$

$$\vec{\tau} = (\frac{\partial l}{\partial \vec{\theta}})^T \text{tension} = (\nabla_\theta \text{length}(\theta))^T \text{tension} = J_m(\theta)^T \text{tension} = \nu(\theta) M(l, \dot{l}, \alpha, t) \quad (2.2)$$

In equations 2.1 and 2.2, ∂l is an infinitesimal change in muscle length and $\vec{\partial\theta}$ is an infinitesimal change in the angles of the skeletal joints. $\vec{\tau}$ (and $\vec{\tau}^T$) is the vector of joint torques at the skeletal joints. $J_m(\theta)$, is the 1x2 vector of partial derivatives of the scalar length(θ) function with respect to the vector of joint angles, θ. $J_m(\theta)$ is also written above as the gradient of the length function: $(\nabla_\theta \text{length}(\theta))^T$. As before, $\nu(\theta)$ and $M(l, \dot{l}, \alpha, t)$ are the moment arm and tension magnitude of the muscle, respectively.

The coordinate transformation for a muscle is the function, length(θ), that computes the length of the muscle from the joint angles, θ. The first derivative of the coordinate transformation, $J_m(\theta)$, is the 1x2 vector of partial derivatives of the length(θ) function. $J_m(\theta)$ is a 1x2 vector because length is a one dimensional quantity, and there are two joint angles (hip and knee) in the θ vector in this experiment.

I modeled the muscle length as a function of θ and model parameters, p. I was able to compute $J_m(\theta)$ symbolically at all joint angles, θ, from the values of the parameters of the length model. I also computed a value for the muscle tension from the length function. So, the parameters, p, produced a length function, length($\theta \mid p$) from which I computed $J_m^T(\theta \mid p) * \text{tension}(\text{length}(\theta \mid p))$ at all sampled values of θ. The errors in the equations

$$\vec{\text{torque}} = J_m^T(\theta \mid p) * \text{tension}(\text{length}(\theta \mid p))$$

were then used to update my parameters for the length($\theta \mid p$) function. This general approach could be used with any number of different parameterized length($\theta \mid p$)

functions. I used a sinusoidal length($\theta \mid p$) model (Lieber & Showmaker, 1988a,b):

$$\text{length}(\text{hip angle}, \text{knee angle}) =$$

$$\mathbf{L0} + \mathbf{A_h} * \cos(\mathbf{freq_h} * \text{hip} + \mathbf{phi_h}) + \mathbf{A_k} * \cos(\mathbf{freq_k} * \text{knee} + \mathbf{phi_k})$$

$$\text{tension}(\text{hip angle}, \text{knee angle}) = \mathbf{scale} * \text{sigmoid}(\text{length})$$

There are 8 parameters in this length model: **L0**, $\mathbf{A_h}$, $\mathbf{freq_h}$, $\mathbf{phi_h}$, $\mathbf{A_k}$, $\mathbf{freq_k}$, $\mathbf{phi_k}$, and **scale**. The sigmoid in the tension function approximates the known length-tension properties of muscles (Rack and Westbury, 1969). The parameters with the "h" subscript refer to the part of the length function that depends on the hip angle. The parameters with the "k" subscript refer to the part of the length function that depends on the knee angle. The parameters are adjusted until

$$\text{Torque}_{\text{hip}} = \text{tension} * \frac{\partial \text{length}}{\partial \text{hip}} = -\text{tension} * \mathbf{A_h} * \mathbf{freq_h} * \sin(\mathbf{freq_h} * \text{hip} + \mathbf{phi_h})$$

$$\text{Torque}_{\text{knee}} = \text{tension} * \frac{\partial \text{length}}{\partial \text{knee}} = -\text{tension} * \mathbf{A_k} * \mathbf{freq_k} * \sin(\mathbf{freq_k} * \text{knee} + \mathbf{phi_k})$$

Table 2 shows the fitted values for 17 muscles in the frog hindlimb.

Muscle	L0	A_k	$freq_k$	phi_k	A_h	$freq_h$	phi_h	scale
AD	-0.36	2.71	-0.894	0.826	5.37	0.702	-1.07	1060
ADl	-1330	0.353	1.48	-2.5	1330	0.0234	0.061	2720
BI	2790	3340	0.14	2.14	-160	2.09	3.65	3.47
GA	140	4.87	-1.64	2.62	153	0.0658	2.73	454
IP	24.6	-1.04	1.99	-1.1	10.4	0.634	1.43	969
PE	23.9	7.25	-0.888	2.43	3.86	0.613	2.55	1050
PT	-604	78.2	-0.0286	-0.0912	527	0.042	0.0.046	3540
PY	1380	1570	0.0186	6.16	2950	0.0228	3.2	59.5
QF	-10.1	0.789	-1.06	3.18	-0.486	0.612	4.18	1.73e+08
RA	-4940	0.459	-1.1	-2.94	4930	0.0153	0.03	4.69e+06
RI	394	1.13	-1.13	0.832	403	0.0371	-2.91	5570
RIm	-149	-156	-0.0626	3.22	-7.64	-0.657	-0.908	1100
SA	-5.74	0.149	1.08	-0.591	0.263	0.912	2.07	5.54e+06
SM	656	1.88	1.6	2.45	-841	-0.0146	5.59	1610
ST	1.51	0.956	1.45	-1.06	1.45	0.85	-1.5	4250
VE	-22	32.6	0.272	5.35	2.37	-1.03	-1.98	820
VI	-4180	-4170	-0.00772	3.17	1.61	0.451	2.73	9.64e+06

Virtual Work Muscle Model Parameters for 17 Frog Hindlimb Muscles The muscle abbreviations are AD = Adductor Magnus, ADl = Adductor Longus, BI = Biceps Femoris, EC = Extensor Cruris, GA = Gastrocnemius, IP = Ilio-Psoas, PE = Peroneus, PT = Pectinius, PY = Pyriformis, QF = Quadratus Femoris, RA = Rectus Anticus, RI = Rectus Internus, RIm = Rectus Internus Minor, SA = Sartorius, SM = Semimembranosus, ST = Semitendinosus, VE = Vastus Externus, and VI = Vastus Internus. The subscripts "k" and "h" refer to parameters of the sinusoids in the knee angle and hip angle, respectively.

Muscle Models used to Predict Forces from EMGs Evoked by Spinal Microstimulation

In previous work we have described the forces and force fields measured during spinal micro-stimulation (Bizzi, et al; Giszter, et al; Loeb, et al). The methods used to record the force fields evoked by spinal stimulation are the same as those described above for recording the force fields evoked by muscular stimulation. During spinal microstimulation we also recorded EMG signals from the hindlimb muscles. We have found that spinal micro-stimulation in the interneuronal layers of the frog spinal cord evoke a small number of different force field shapes, shown in figure 1-7. The whale-shaped boundaries in figure 1-7 are squares in joint space indicating the limits of the reachable workspace.

I refer throughout this chapter to two databases of force and EMG data measured during stimulation of spinalized frogs. The Mapping Database, used for validating the muscle models (see below), consists of 3036 stimulation trials evoked at 759 different loci in the interneuronal grey of 4 spinalized frogs with the limb held at a single posture (hip=$-45°$,knee=$70°$). Each spinal locus was stimulated at 1, 2, 4, and 8 μAmps, but I only make use here of the forces and EMG data observed at 8 μAmps. (see Giszter, et al. 1995). The Force Field Database, used to construct models of spinal force fields (see below), consists of 344 force fields (approximately 3100 stimulation trials, at 9 trials per force field) evoked at 93 loci in 27 frogs.

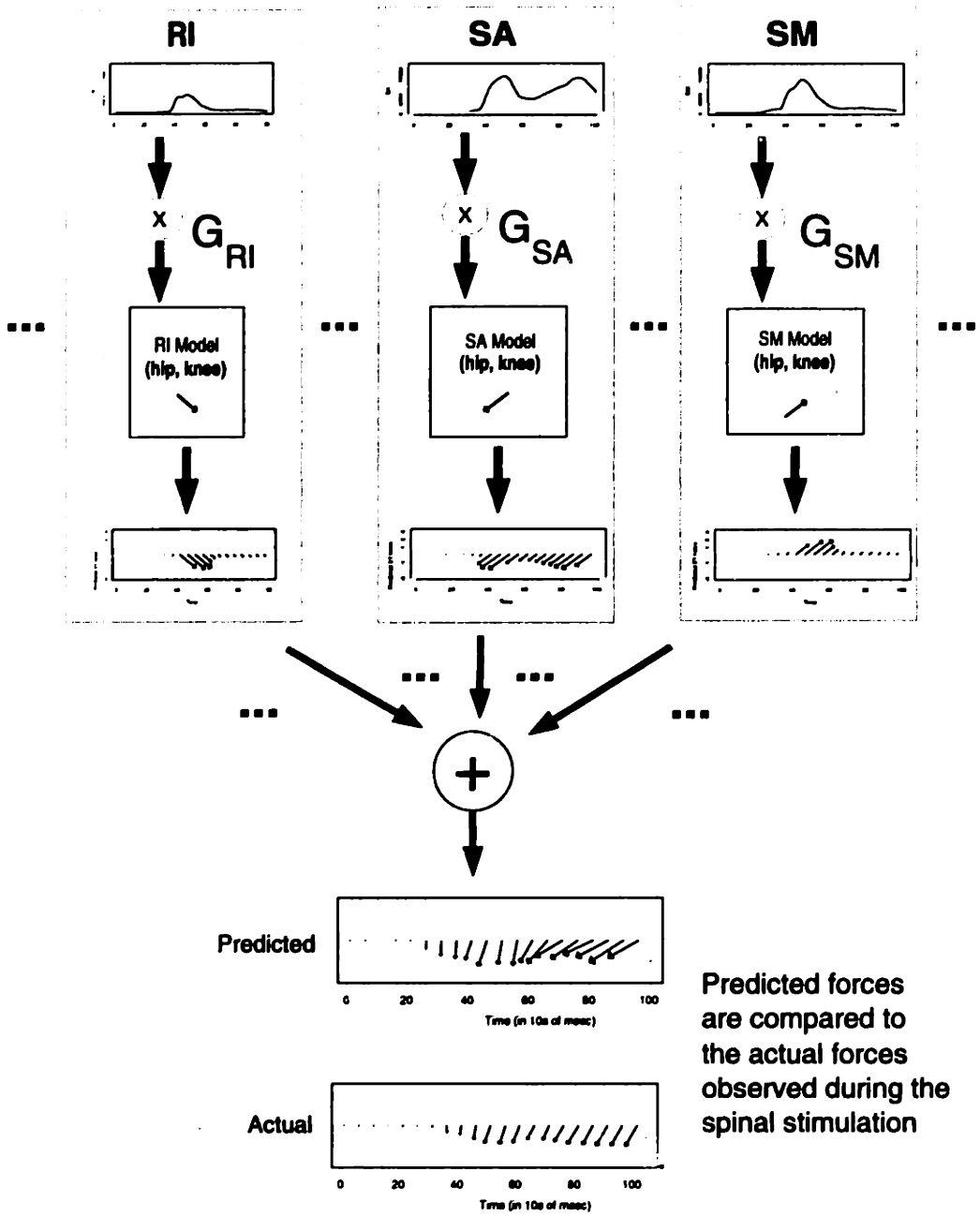

In order to validate the virtual work muscle force field models described in the previous section, I used the models to predict the endpoint forces in the spinal stimulation Mapping Database from their associated EMG signals.. I used these EMG signals that were evoked at a single limb posture during stimulation at many spinal loci to predict the forces. I predicted observed forces in order to quantify the overall accuracy of the force field muscle models. Thus, I made the simplifying assumption

Figure 2-5: Reconstructing Forces from EMGs

Force prediction is almost as simple as multiplying model-predicted force vectors by their respective EMG signals and then adding up all those products. The three boxes in the top part of the figure show for three muscles the steps that we performed for all of the muscles. The rectified and filtered EMG signals for Rectus Internus (RI), Sartorius (SA), and Semimembranosus (SM) are shown in the top part of the boxes. The EMG signals are multiplied by experimentally-determined EMG weighting factors, which are computed by performing the sequence of steps illustrated in this figure many times until the weightings are found that minimize the squared error between the predicted and actual forces (see text). Once weighted, the EMG signals scale the magnitude of the forces of their corresponding models. The three models are shown as separate boxes within their larger boxes. The models take the current hip angle and knee angle as inputs, and return a force vector. The force vectors returned by my models of muscles RI, SA, and SM are shown in their respective boxes. These are the force vectors for the three models at the limb posture (hip=$-45°$,knee=$70°$), which was the limb posture at which the EMG data and the force data in this figure were collected. The products of the weighted EMG signals and the model force vectors are shown in the force time traces at the bottom of the three large boxes. Forces traces such as these from all the muscles are then simply added together to produce the predicted force trace shown at the bottom of the figure. For example, the X component of the predicted force trace at time T is the sum of the X components at time T of each of the muscle force traces. The predicted force appears to capture the orientation and some magnitude variation of the actual force, but the timing of the two traces is not aligned. The predicted force changes direction at the end of the trace, while the actual force does not. The EMG signals for muscles SM and RI also vanish after time 60 (600 msec): my static muscle models do not predict any force from these muscles after time 60, although they were probably still producing force at least until time 80.

that accuracy at one limb posture could be translated into accuracy at another limb posture. Figure 2-5 shows the steps involved in predicting force vectors from a collection of EMG signals. The EMG signals are weighted (see below) and then used to construct a predicted force according to the simple formula (see Hof and Ven Den Berg 1977):

$$\text{force}(t, \text{hip angle}, \text{knee angle}) =$$

$$\sum_{\text{muscles}} \text{Model}(\text{muscle}, \text{hip}, \text{knee}) * \text{weight}(\text{muscle}) * \text{EMG}(\text{muscle}, t) \qquad (2.3)$$

Equation 2.3 is meant to be read as English. The Muscle models (Model(muscle, hip, knee)) are each weighted by a muscle-specific weight factor (weight(muscle), see below) and by the associated EMG signal (EMG(muscle, t)). The weighted muscle models are added together to give a force estimate at each limb posture (force(t, hip, knee)).

Figure 2-6 shows how entire force fields are constructed from either observed EMG signals or hypothetical muscle activations. A force field constructed from observed EMG signals can be compared to the observed force field to assess prediction accuracy. Large numbers of force fields constructed from hypothetical muscle activations can be examined to assess the range of behaviors likely to be subserved by different muscle synergies. This latter computational method is described in more detail below.

EMG Filtering

Rectified EMG signals were filtered with a 50Hz low-pass filter, and downsampled to 100Hz. I low-pass filtered the downsampled signals with a causal filter that introduced a 50ms delay at 25Hz in order to offset the effects of muscle rise-time. Low-pass filtering smoothed the EMG signals and, consequently, the estimated force traces. The processing details were probably not important: in a re-implementation of this system, somewhat different filtering methods were used without altering our prediction accuracy in any appreciable way (Giszter, personal communication).

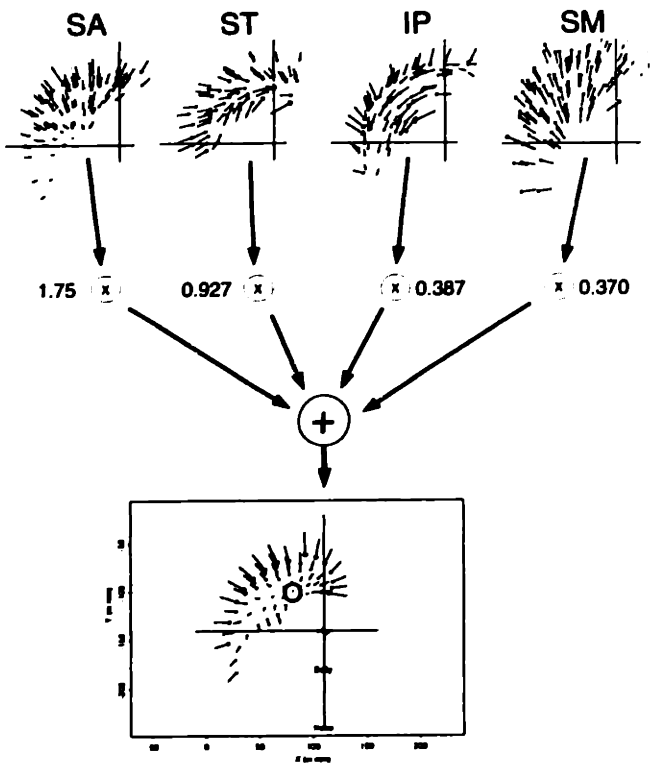

Figure 2-6: Constructing Force Fields from Activation Patterns Force Field construction simply involves multiplying muscle model force fields by their respective activation values and then summing the activation-weighted force fields vectorially. In this figure the activations are (random values) 1.75 for muscle Sartorius (SA), 0.927 for muscle Semitendinosus (ST), and so on. When a force field is multiplied by a value, V, each force vector in the force field gets scaled in magnitude by V. The indicated combination of muscles SA, ST, IP, and SM produce the force field at the bottom of the figure. Note that the force field has an equilibrium point, the location of which can be stored as a point in the workspace that can be stabilized by these four muscles. When the activation values are given by observed EMG signals, the resulting force field is time varying.

Computing EMG Weighting Factors

Several factors effect the translation from an EMG signal to a muscle force - the EMG amplifiers can have different gains, the EMG electrodes can have different transduction efficacies, the muscles can have different balances of fiber types, and so on. I lumped these factors into a single EMG-force weighting factor that I estimated for each muscle of each frog. I used least-squares estimation to find the best collection of weighting factors for a small subset of each frog's trials called the training set. The weighting factors were optimized to give the least square force prediction error over all of the trials in the training set. The weighting factors were constrained to be positive and not too large (max / min $<$ 20 in my objective function) (see Cholewicki and McGill, 1994). Graphically, the steps in figure 2-5 were performed repeatedly, until the eleven weighting factors (one for each muscle) minimized the total squared error between the all predicted and actual force traces in the training set. The trials used to compute the weighting factors - the training set - were removed during subsequent statistical tests.

Statistical Tests

In order to perform numerical comparisons of predicted and actual forces, such as those shown in figure 2-5, I needed to pick two forces to compare. Although one gets a qualitative sense of a good match in figure 2-5, the time mis-alignment of the two force traces makes that qualitative similarity difficult to capture. I used the angle between the Actual Force Vector, AFV(t1), and the Predicted Force Vector, PFV(t2), to quantified goodness of fit. I used two methods of selecting (the time indexes for) these force vectors: the "first predicted peak" method and the "best prediction" method.

For the "first predicted peak" method I used the largest magnitude actual force, AFV(t.max), for comparison with the selected predicted force, PFV(t.fp). The selected time index, t.fp was the time of the largest magnitude predicted force, PFV(t), such that the orientation of PFV(t.fp) was within 45° of the first magnitude peak, PFV(t1). The first predicted magnitude peak, PFV(t1) occurred when

$\|PFV(t1)\| > \|PFV(t1 - 1)\|$ and $\|PFV(t1)\| > \|PFV(t1 + 1)\|$) The first predicted peak method was preferable to simply comparing the orientations of the peaks of the actual and predicted forces, because the predicted forces were often accurate, but then rotated away and became inaccurate during the later portions of the predicted force trace (as can be seen in figure 2-5).

The "best prediction" method selected for comparison the best correlated pair, AFV(tk) and PFV(tk) within 100 msec of the peak magnitude actual force, AFV(t.max). The best prediction method made use of the actual forces in finding the predicted force, and thus, to some extent, made up for the missing information about muscle dynamics that was lost in constructing the static muscle models.

In figure 2-5, the time of the actual peak, t.max, is approximately 55. The time of first predicted peak, t1, is about 42. The next predicted peak occurs at about 65 and then another peak occurs at about 90. The orientation of the predicted force, PFV(65) is within 45° of the orientation of PFV(42), but PFV(90) is more than 45° from PFV(42). Thus, the time of the first predicted peak, t.fp, is 65. The orientations of the actual peak, AFV(55) and pfv(65) would be the values used for statistical comparisons using the first predicted peak method. For the best prediction method, the correlations of AFV(t) and PFV(t) are examined over indexes t.max ± 10. The best correlated pair occur at tk = 46, so the orientations of AFV(46) and PFV(46) would be used for a statistical comparisons using the best prediction method of the predicted and actual traces in figure 2-5.

Force Field Muscle Models and Muscle Synergies

I used the force field muscle models to examine the properties of all muscle synergies. I define a muscle synergy as a binary vector: each muscle is active or not. An activation pattern is a positive real-valued vector. An activation pattern conforms to a synergy if it is zero when the synergy is zero and positive when the synergy is one.

For each muscle synergy of interest, I used Monte Carlo simulation techniques (Press, et al. 1992) to learn about the range of possible equilibrium configurations at which the muscle synergy could stabilize the limb. I generated a large number

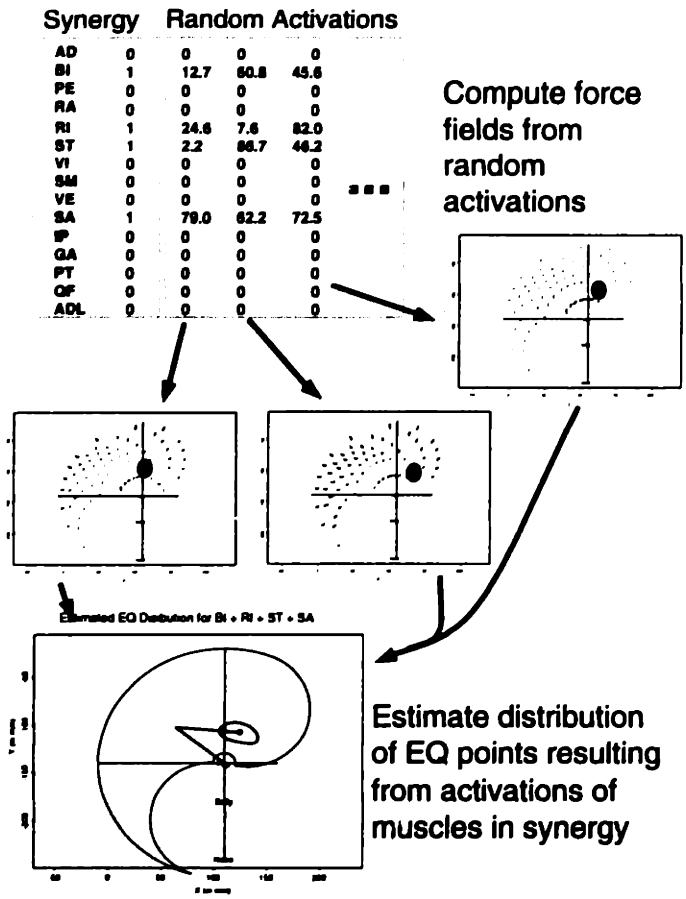

Figure 2-7: Monte Carlo simulation analysis of a muscle synergy A muscle synergy is a binary vector: muscles are active or not. An activation pattern is a positive real-valued vector. An activation pattern conforms to a synergy when muscles have zero activation if and only they are not active in the synergy. Three activation patterns conforming to the BI+RI+ST+SA synergy are shown, along with the force fields resulting from those activation patterns. The displayed force fields "converged", in that the force fields each had some posture towards which all the forces/torques point. 66% of the activation patterns in the BI+RI+ST+SA synergy lead to convergence. 2000 activation patterns in this synergy were sampled, and the XY locations of the equilibrium points of the 1322 convergent force fields were used to compute the distribution shown. The stick-figure leg is shown with its ankle at the centroid of the distribution. The banana-like shape is an ellipse in joint space with major and minor axes given by twice the standard deviation of the hip and knee angles of the 1322 computed equilibria. The outline is a square in joint space from hip $= -110^o$ to hip $= 80^o$ and from knee $= 10^o$ to knee $= 170^o$. Equilibria falling outside these boundaries were discarded.

(thousands to millions) of random activation patterns conforming to the synergy in question. Figure 2-7 sketches the sequence of computations performed in my Monte Carlo simulations. Each synergy-conforming random activation pattern produced a force field, which was the sum of activation-weighted muscle model force fields. I stored each random activation pattern and the equilibrium posture of the resulting force field when it converged (see below). I was thus able to compute the distribution of equilibrium postures that could be produced by each muscle synergy.

Computing Force Field Convergence

A stable posture is a posture towards which all the torques point. I use the terms "convergent" and "stable" interchangeably. I computed an equilibrium (stable) posture of simulated force fields by following the force field gradient from a starting position of 60° hip flexion and 30° knee extension. I considered a force field to be convergent only if the limb reached a stable posture (see below) within pre-determined boundaries: ($-150° <$ hip $< 80°$, $10° <$ knee $< 170°$). A posture was considered stable if the torque magnitude was near zero at that posture and both joint torques reversed sign within five degrees deviation from that posture: $\frac{\tau(\theta+5°)}{\tau(\theta-5°)} < 0$. In other words, once the simulated limb had come to rest at a posture with near zero torques, I sampled the torques at each of four new postures: hip angle $\pm 5°$, and knee angle $\pm 5°$. The hip and knee torques both had to reverse sign across these deviations.

Some equilibrium points lay on saddle points: both torques reversed sign as a result of deviations of one joint from saddle point equilibria, while the torques were nearly zero and approximately unchanged as a result of deviations of the other joint. I ignored the saddle point equilibria in this work, and I do not discuss them any further in this thesis.

Robust Synergies

Some muscle synergies that had the property that no matter how the muscle activations were changed, any equilibrium points of the force fields they produced fell in roughly the same place. I called these synergies "localized". I quantified each

synergy's localization with the two-dimensional area of its distribution of convergent equilibrium points. Some muscle synergies had the property that no matter how the muscle activations were changed, they produced a force field with a convergent equilibrium point somewhere within the workspace. I called these synergies "reliable". I quantified each synergy's reliability with the percentage of random activation patterns that produced convergent equilibrium points. I called the muscle synergies that were both localized and reliable, "robust", because they could produce a convergent equilibrium point in approximately the same workspace location without regard to activation noise in the muscles.

Results

In subsection 2 I describe the force field muscle models (FFMM) used for each of 17 hindlimb muscles. The key points in this section are

1. The FFMM fall into a few easily-recognizable categories.
2. Some muscles produce nearly zero force over large portions of the workspace.
3. No muscle shows a clear reversal of joint torques. This means that no single muscle can stabilize the limb.

In subsection 2 I describe statistical validation of the FFMM. I used EMG signals to weight the muscle models. The EMG-weighted sum of FFMMs predicted the forces and force fields observed during the stimulation trials that produced the EMG signals.

In subsection 2 I describe some uses of force field muscle models. The key points in this section are

1. Random combinations of FFMMs generally have a stable point. Most of the stable points lie in a band within the workspace at approximately 140° knee extension. The continuous distribution of computed stable points does not match the punctate distribution of observed stable points evoked by interneuronal micro-stimulation of spinalized frogs.

2. The punctate distribution of stable points evoked by interneuronal micro-stimulation of spinalized frogs is approximately matched by the workspace locations of the stable point distributions of the muscle synergies that had the most robust and localized stable point distributions.

Force Field Muscle Models

The force fields for most of the frog's hindlimb muscles are shown in figures 2-8-2-13. I have grouped the muscle force fields by eye into six types. Figure 2-8 shows the "Hip Extensor/Knee Flexor" muscle type. This muscle type includes AD, RI, RIm, and ST. The "flexor" muscles (figs. 2-9-2-11) flex the hip and/or the knee: the "Body Flexor" type muscles (BI and SA, fig. 2-9) consist predominantly of knee flexion; the "Rostral Flexor" muscle type (IP and PT, fig. 2-10) flexes both the hip and the knee; and the "Half Flexor" muscle type (ADl, GA, and RA, fig. 2-11) produces no force when the hip is flexed. The "Hip Extensor" type muscles (PY, QF, and SM, fig. 2-12) have explosive-looking force fields. The "Lateral Extension" muscle type (PE, VE, and VI, fig. 2-13) flexes the hip and extends the knee, producing force fields that point laterally away from the body mid-line[2]. To understand the relative proportions of the hip and knee torques of these muscle types , and how they change with limb posture, it is helpful to consider figure 2-3. Forces that point along the line connecting the workspace position to the hip are due to knee torques, and forces components off that line are due to hip torques.

In each muscle group, one or more muscles displays near-zero forces in the part of the workspace towards which its forces point. In these muscles the general flow of the muscle's force field appears to move the ankle to a part of the workspace where the magnitude of the muscle's force becomes negligible. All of the half flexors (ADl, GA, and RA, figure 2-11) have this property, as do RI, RIm, SA, and VI. Clearly, such muscles could be used by the spinal circuitry to selectively modulate force fields in

[2]Muscles EC, TP, and TA are also all knee extensor muscles. I have removed these muscles from further consideration, because they were too small and weak to permit reliable isolation for the stimulation experiments.

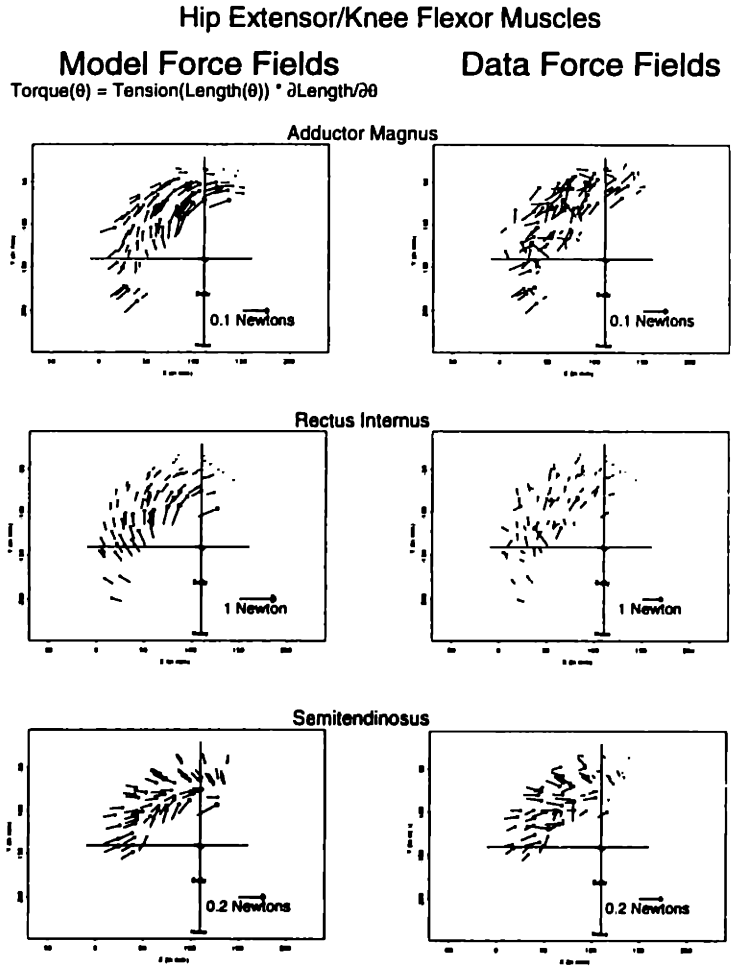

Figure 2-8: The Hip Extensor/Knee Flexor Muscle Type Muscles Adductor Magnus (AD), Rectus Internus (RI), and Semitendinosus (ST) all function as hip extensors and knee flexors. The force fields on the left in each pair is the model force field, while the force fields on the right in each pair is the data from which the model was formed. The model forces are displayed at each sampled workspace point at which there is data in the data force field. The flow of the model force fields in this figure are reminiscent of the wiping behavior of the spinalized frog, but unlike the behavior and the spinal force field, there is no stable point in the muscle force fields. Note muscle RI has a large zero-force region toward which its forces point. The magnitudes of the forces diminish to negligible levels as the ankle move to extension behind the body. Muscles Rectus Internus Minor (RIm) also falls into this class of muscles, but is not shown. The mean force field correlations of the models with the force fields of each contributing frog are 0.76 (AD, 7 frogs)), 0.85 (RI, 6 frogs), 0.87 (ST, 5 frogs), and 0.91 (RIm, 3 frogs).

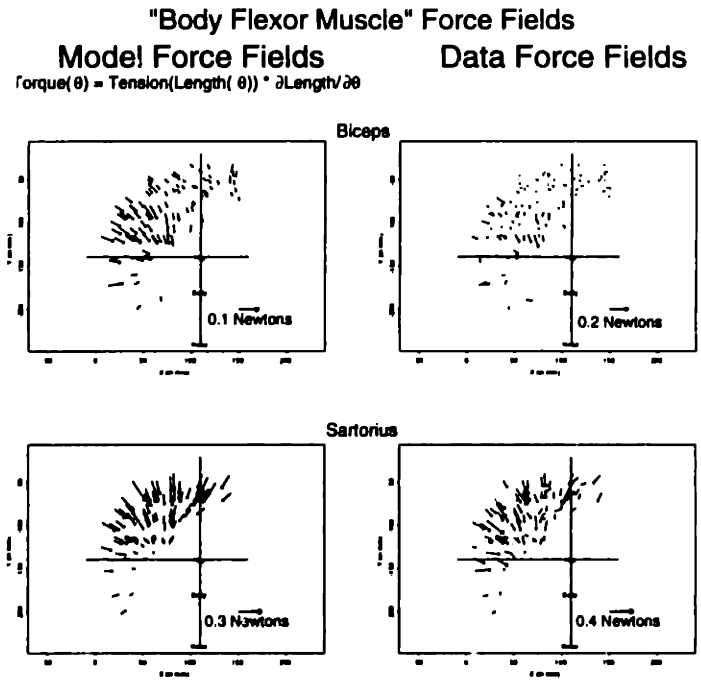

Figure 2-9: The Body Flexor Muscle Type Muscles Biceps (BI) and Sartorius (SA) function predominantly as knee flexors. The relative proportion of hip torques and knee torques varies in these muscles. The hip action of both muscles is more pronounced when the hip is in extension, but the proportion of hip to knee torque at extension is greater in BI than in SA. The relative proportions of the him and knee torques can be inferred by comparing the force fields in this figure to four kinds of pure torque field. Sartorius appears to be predominantly a knee flexor through most of the workspace, with some hip flexion action when the hip is in extension. Biceps appears to have a component of hip extension when the hip is in extension but to be predominantly a knee flexor otherwise. The shapes of these force fields are reminiscent of the flexion withdrawal behavior of the spinalized frog, and thus we term these "body flexor muscles". Displays are as in the previous figure. The mean force field correlations of the models with the force fields of each contributing frog are 0.81 (BI, 8 frogs)) and 0.85 (SA, 9 frogs).

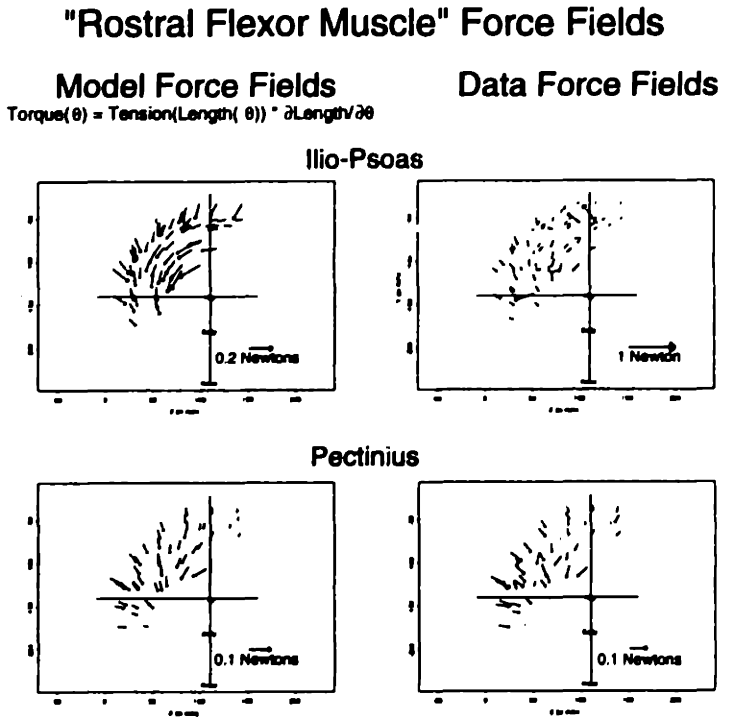

Figure 2-10: The Rostral Flexor Muscle Type Muscles Ilio-Psoas (IP) and Pectinius (PT) function as hip flexors. The shapes of these force fields are reminiscent of the preparatory phase of the back wiping behavior of the spinalized frog, and thus we term these "rostral flexor muscles". The mean force field correlations of the models with the force fields of each contributing frog are 0.78 (IP, 5 frogs)) and 0.90 (PT, 3 frogs).

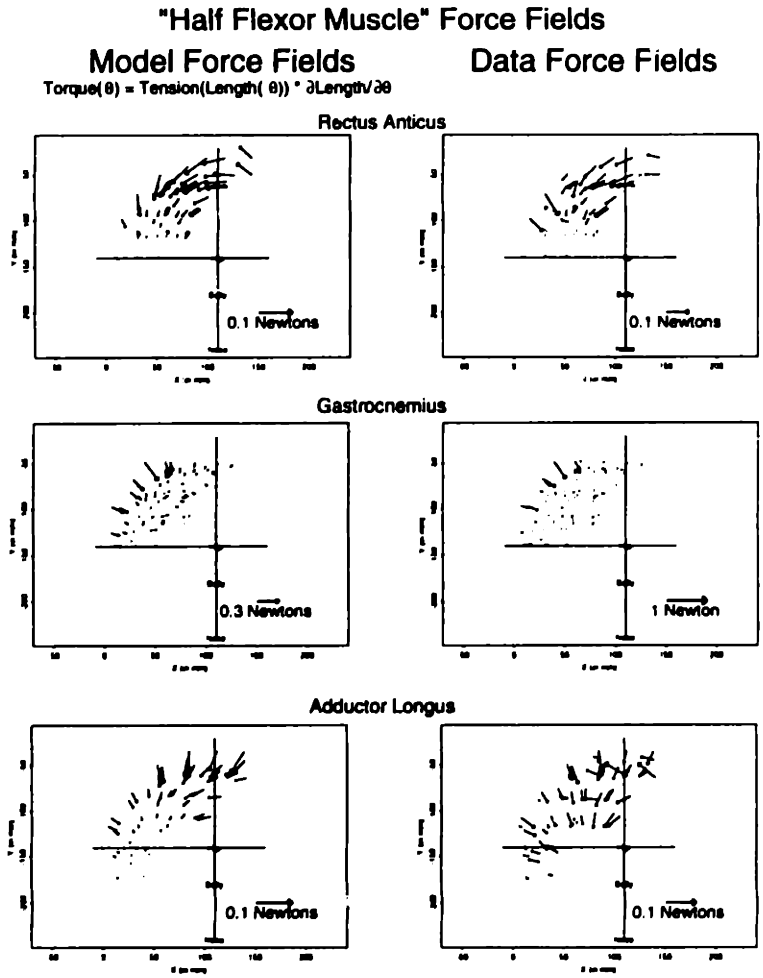

Figure 2-11: The Half Flexor Muscle Type Muscles Rectus Anticus (RA), Gastrocnemius (GA), and Adductor Longus (ADl) all function as hip or knee flexors. All three muscles have vanishing moment (zero forces) when the hip is flexed. The mean force field correlations of the models with the force fields of each contributing frog are 0.90 (RA, 6 frogs)) 0.84 (GA, 8 frogs), and 0.72 (ADl, 4 frogs).

Figure 2-12: The Hip Extensor Muscle Type Muscles Semimembranosus (SM), Pyriformis (PY), and Quadratus Femoris (QF) function as hip extensors. The mean force field correlations of the models with the force fields of each contributing frog are 0.89 (SM, 8 frogs)) 0.93 (PY, 3 frogs), and 0.83 (QF, 4 frogs).

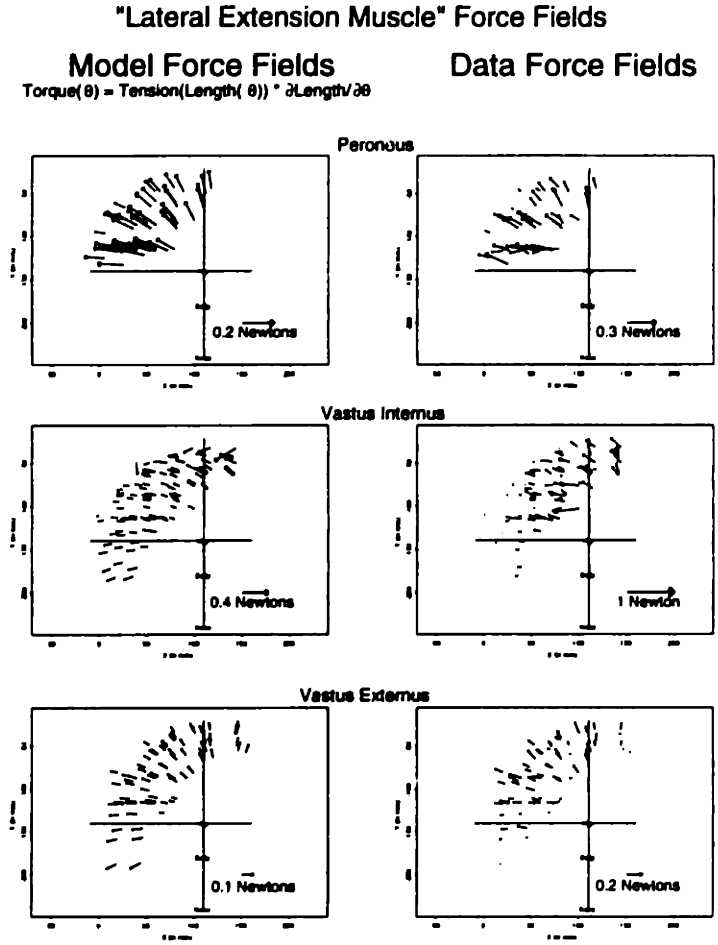

Figure 2-13: The Lateral Extension Muscle Type Muscles Peroneus (PE), Vastus Internus (VI), and Vastus Externus (VE), function as knee extensors. Muscles VE and VI also act as hip flexors. Note in the data force field for muscle VI that it has a large zero-force region toward which its forces point. The model for muscle VI does not capture this feature of the data. Muscles Extensor Cruris (EC), Tibialis Posticus (TP), and Tibialis Anticus (TA) fall into this class but were not used. These muscles were too small and weak to merit further consideration. The mean force field correlations of the models with the force fields of each contributing frog are 0.78 (PE, 5 frogs)) 0.62 (VI, 8 frogs), and 0.90 (VE, 6 frogs).

some parts of the workspace. For example, muscle RA (fig. 2-11) could be activated in a limb-position-independent manner to provide flexion-restoring forces in response to any hip-extending limb perturbations without altering forces in any hip-flexed postures.

In figures 2-8-2-13 we see that no muscle model displays torque reversals around both joints: ie there are no stable muscles. Similarly, none of the measured muscle force fields was stable, in that there were no positions in the workspace surrounded by forces pointing back to that position. Recall that a muscle's torque vector is proportional to the gradient of its length function. Therefore, a stable muscle would have to have a local minimum in its length function at a stable posture. It may be mechanically impossible for a skeletal muscle length function to reach a local minimum in the workspace, in which case no skeletal muscle in any animal of any species is stable.

Muscle Models are used to Predict the Spinal Force Fields Evoked by Spinal Microstimulation

We microstimulated (2 - 10 μAmps) spinal interneurons in spinalized frogs (Bizzi, et al, 1991; Giszter, et al, 1993; Loeb, et al, 1993), while recording endpoint forces and the EMG signals from 11 hindlimb muscles. Spinal microstimulation typically activated 5 - 8 of the recorded hindlimb muscles. I used the EMG signals in a linear predictor of muscle force (see Methods):

$$\text{force}(t, \text{hip}, \text{knee}) = \sum_{\text{muscles}} \text{Model}(\text{muscle}, \text{hip}, \text{knee}) * \text{weight}(\text{muscle}) * \text{EMG}(\text{muscle}, t)$$

Predictions of Force Traces

Figure 2-14 shows four representative examples of observed endpoint forces, EMGs, and predicted endpoint forces. The four sets for force vectors point in different directions. The same EMG weightings were used in all four examples. This figure demonstrates that it is possible to use EMG-weighted muscle models to match the

endpoint force traces evoked by spinal microstimulation. Note that many (but not all) of the same muscles are active in all four examples shown in fig 2-14a-d. The observed force traces result from the co-contraction of several of the muscle types shown in figures 2-8-2-13. There is some activation of at least one muscle of each of the five types of muscles sampled in the experiment. None of the "Rostral Flexion" type muscles (figure 2-10) were sampled in this experiment. The EMG activity of muscles of the same type do not necessarily covary. In fig 2-14c the Biceps (BI) and Sartorius (SA) are active to quite different extents, although both muscles are "Body Flexors" (see fig. 2-9). I appear to have captured the subtle balance that causes the resulting endpoint force to point one way or another. The next step was to quantify the goodness of fit of these models.

Figure 2-15 shows the predicted and actual endpoint force orientations at peak magnitude for 244 spinal stimulation trials from three animals. Both of the plots of predicted orientations vs. actual orientations are statistically significant linear relations (R^2=0.539, F(33, 160)=9.6, p=0. in fig. 2-15a and R^2=0.864, F(33, 160)=36.9, p=0 in in fig. 2-15b). There are 33 free parameters in the F statistics because 11 EMG weightings were computed for each of the three animals in the dataset. 82% of the trials in fig. 2-15a and 95% of the trials in fig. 2-15b have a prediction error strictly less than 45°.

Force Predictions and Muscle Dynamics

The difference between the two plots in fig. 2-15 can serve as a crude estimate of the improved prediction accuracy that could be achieved by including muscle dynamics in the muscle models. In figure 2-15a I am using the "first predicted peak method" (see methods and figure inset) to compare predicted and actual peak forces directly. In figure 2-15b I am compare the peak actual force to the best matching predicted force within 100m (the "best prediction" method)s. I infer from the differences in the R^2 values that another $\frac{1}{3}$ of the variance in the force orientations could be accounted for by models which also represent muscles' dynamics. If our models of the muscles' contraction dynamics were accurate then there should not be a systematic

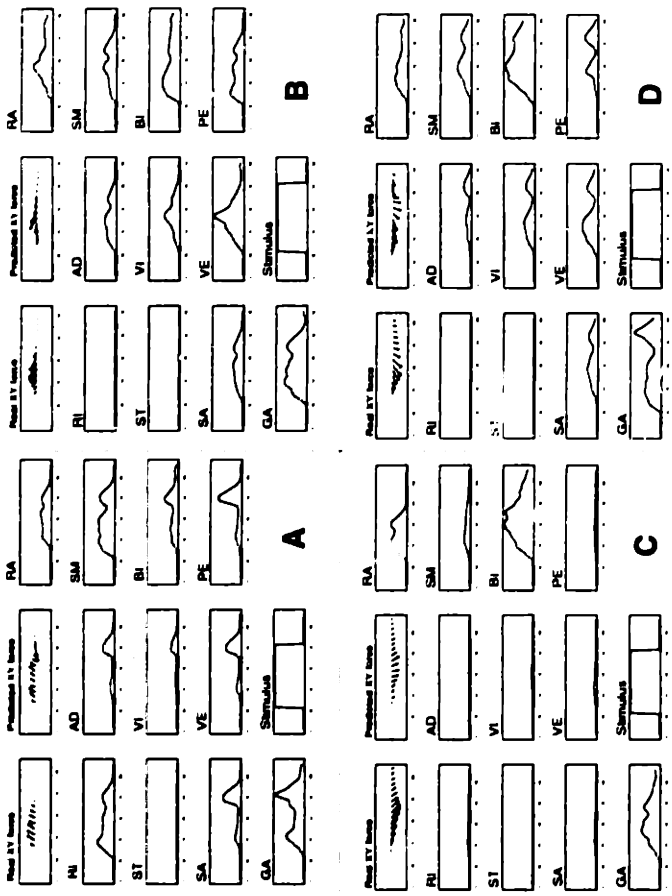

Figure 2-14: Four Spinal Stimulation Trials with Predicted Forces Four spinal stimulation trials from a single frog and the predicted forces are shown. In (A) - (D) the traces along the top row are (from left to right) the observed XY forces, the predicted XY forces, and the filtered, weighted EMG signal from muscle Rectus Anticus (RA). The remaining traces in (A) - (D) are the other filtered weighted EMG signals and the stimulus trace. The four trials were chosen at random by a program written to find four different directions of force traces. The traces and EMG signals are representative of the database. The EMG signals are all normalized to the same, arbitrary scale for display. The force vectors were normalized to the peak in each trace for display. The time axes are all aligned and measured in 10s of msec. Five of the six muscle classes are sampled in this experiment: Half Flexors (Rectus Anticus (RA), Gastrocnemius (GA)), Wipe muscles (Rectus Internus (RI), Adductor Magnus (AD), Semitendinosus (ST)), Jump muscles (Semimembranosus (SM)), Lateral Extensors (Vastus Internus (VI), Vastus Externus (VE), Peroneus (PE)), and Body Flexors (Biceps Femorus (BI), Sartorius (SA)). The Rostral flexor muscles were not sampled in this experiment. The Semitendinosus (ST) signals were zeroed out due to excessive noise throughout this experiment.

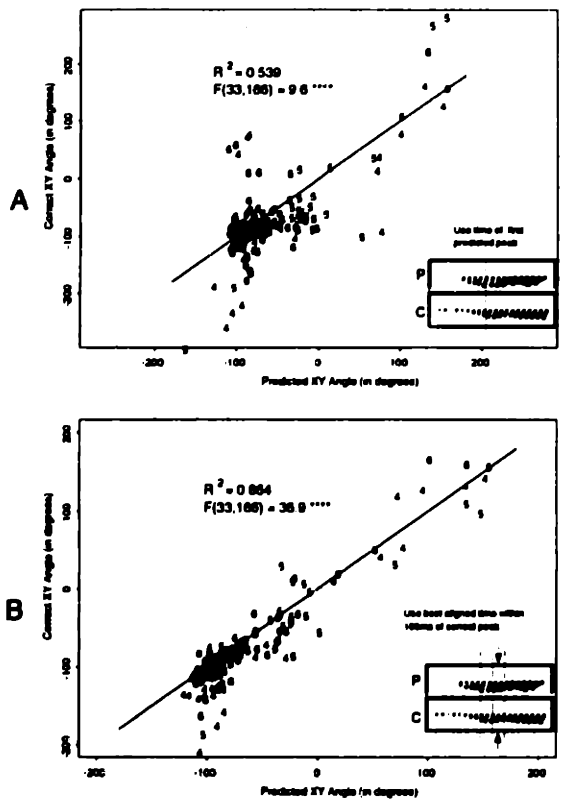

Figure 2-15: Summary Statistics for Force Predictions from a Large Database 244 trials from 3 animals that were thoroughly mapped via spinal μstimulation (Giszter, et al 1994) were used to test the accuracy of force predictions from EMG signals. 15% of the trials from each animal were used to create EMG weighting factors, and the remaining 200 trials were used to test the EMG-weighted muscle model force predictions. The trials are labeled "4", "5", and "6" after their animal labels. (A) Feedforward test. We used the "first predicted peak" method (see Methods) to compare the predicted force orientation to the actual force orientation. This comparison does not rely on any prior knowledge of the correct forces. The individual R^2 values for these animals were 0.443, 0.752, and 0.391 for animals "4", "5", and "6" respectively. (B) Pseudo-dynamics test. We used the "best prediction" method (see Methods) to compare the closest matching pair of actual force orientation and predicted force orientation within a 100 msec window to either side of the actual peak force. The individual R^2 values are 0.863, 0.835, and 0.898 for animals "4", "5", and "6" respectively.

time misalignment between the predicted and actual force traces. Since the best prediction method used in fig. 2-15b is correcting for the time misalignment (without overcorrecting by finding a best overall match), the R^2 value of fig. 2-15b is approximately what one could expect from force field muscle models that included muscle contraction dynamics.

The variations in the EMG signals appear to be produced to counteract the activation dynamics of the muscles. The magnitudes of the actual forces usually rise and fell over a 300 - 500 msec time course, but the orientations of the actual forces remain nearly constant (Loeb, et al 1993, and see fig. 2-14). The predicted force orientations are more variable than those actual force orientations. The spread of the predicted force orientations in the 100 msec surrounding the peak predicted force is an average of 21° greater than the spread of the observed force orientations around their peak ($t = 8.1$, $df=243$, $p=0$). This is important, because the orientation of the actual endpoint force is determined by the muscle-tension-weighted sum of the component muscles endpoint force vectors. We know the muscle tensions must be changing in time because the endpoint force is rising and falling. We can assume that the moment arms (the orientations of endpoint forces) do not change. Therefore, the constancy of the actual endpoint force orientation implies that the relative balance of the rising and falling muscle tensions is nearly constant. The fact that the predicted forces do not have constant orientations, even in the few samples surrounding their peak magnitude, indicates that the proportional constancy of the muscle tensions is not simply due to a proportional constancy of the EMG signals. In other words, the fluctuations in the EMG signals that give rise to non-constant predicted orientations appear to be specifically tuned to the activation dynamics of the muscles.

Predictions of Spinal Force Fields

Figure 2-16 shows five force fields evoked by micro-stimulation at five spinal loci of a single animal and the force fields predicted by the corresponding observed EMG signals (see Methods). The overall shape of each spinal force field is captured by the corresponding sum of EMG-weighted muscle models. Some of the subtle features of

the force fields are not captured. For example, in fig. 2-16c the force reversal in the rostral part of the force field is not predicted. To measure the force field reconstruction accuracy we use the correlation of the X and Y components. Specifically, let a force field be (x1, x2, x3), (y1, y2, y3) where x_i is the x component of the force at position i, and y_i is the y component of the force at position i. The field correlation of field A and B will be the correlation value for the vectors ($x1_A$, $x2_A$, $x3_A$, $y1_A$, $y2_A$, $y3_A$) and ($x1_B$, $x2_B$, $x3_B$, $y1_B$, $y2_B$, $y3_B$). The mean correlation value over 68 tested force fields is 66%, and 78% of the correlation values were greater than 50%. Force fields that correlate at 50% and higher appear similar. At correlation values above 80% it becomes difficult to distinguish the two fields. Figure 1-7 shows the five types of force field most commonly evoked by spinal microstimulation in spinalized frogs.

Force Field Muscle Models and Muscle Synergies

Figure 2-17 shows two two-dimensional histograms of the end-point locations of the stable points I found with a simulation of "all possible" activation patterns in all possible muscle synergies. In practice, I stepped through the possible activation patterns at a coarse grain: using activation values of 0, 0.5, and 1.0 for each muscle. The simulation considered a larger portion of the workspace than previous simulations that have been performed of this kind (Giszter, et al., 1993). In the previous work the authors found that only 15% of the simulated EMG patterns led to equilibria within the workspace. My simulation resulted in 90% equilibria within the workspace, but again approximately 15% fell within the portion of the workspace covered by the previous simulation.

The distributions in figure 2-17 do not predict the regularity indicated by figure 1-7. The distributions do not have five peaks, and the peaks do not fall in the equilibrium locations of the spinal force fields (outlined in green). Note also that the most common spinal force field type in figure 1-7, the Body Flexion force field, has its equilibrium region in the least likely region of figure 2-17. There is presumably *some* method of choosing random muscle activations under which the results of figure 1-7 can be reproduced, but I was not able to repeat the result of five peaks (much less

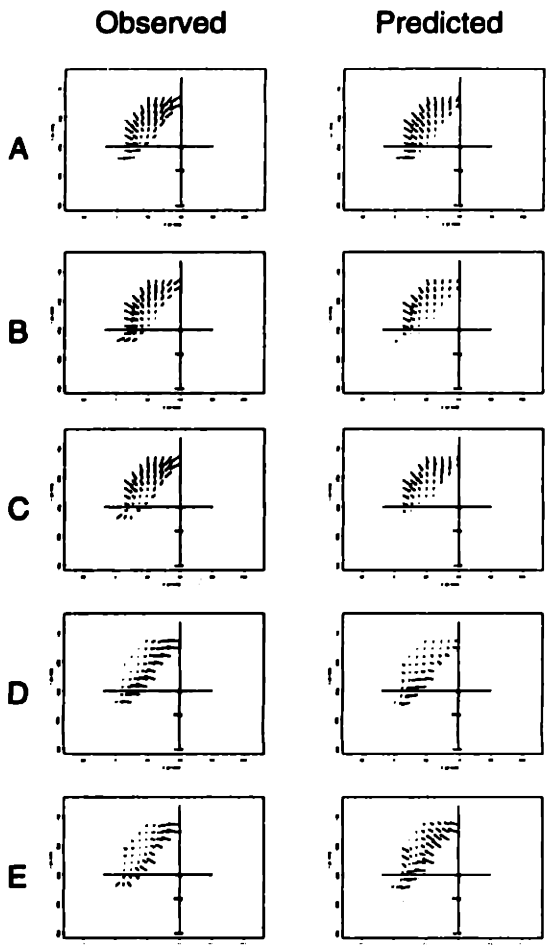

Figure 2-16: Spinal Stimulation Force Fields and Predictions Five spinal stimulation force fields from a single frog and the predicted force fields are shown. In (A) - (E) the vectors shown are the peak forces and peak predicted forces for the trial-by-trial observed forces and forces predicted from the EMGs. The forces are predicted from the EMG-weighted sum of muscle models. The field correlation values in (A) - (E) are 0.932, 0.89, 0.882, 0.727, and 0.814 respectively.

their locations) under any of the reasonable assumptions that I tried[3]. Figure 2-17a was computed with each muscle being stepped through the same [0, 0.5, 1.0] range. In fig. 2-17b I pre-weighted each muscle model with the EMG weightings that were predetermined by my least-squares procedure for animal SGM4 in figure 2-15. By pre-weighting each muscle I warped the activation space that was sampled with the [0, 0.5, 1.0] stepped activation patterns. Thus, figure 1-7 is not predicted by random muscle activations.

[3]In addition to the methods shown here, I tried normalizing the muscles so that they all were equally strong. With the normalized muscles I stepped through the activation levels for 16 muscles as well as the 11 main muscles of fig. 2-17. I also tried choosing random activation levels for each muscle type and then dividing those activations equally across all the muscles of the same type. For example, muscles BI and SA are of the Body Flexor class. If the random level for the Body Flexor class were set at 0.48, then BI and SA would each be activated at 0.24. After each muscle's activation level was chosen in this way, the force field was synthesized, its equilibrium point computed, and the location of the equilibrium point (if any) was stored as one data point for the histogram.

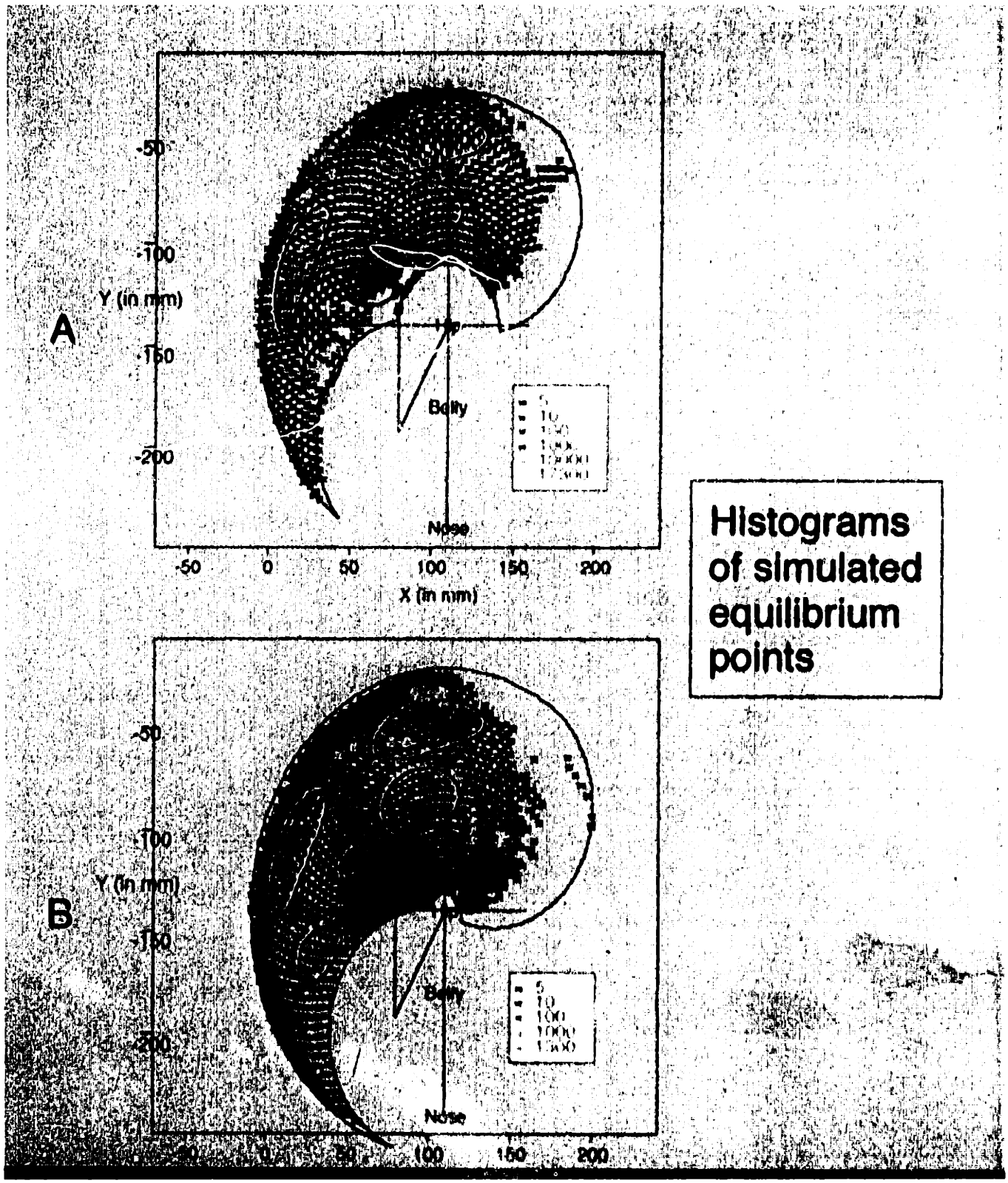

Histograms of simulated equilibrium points

Figure 2-17: Histogram of Simulated Equilibrium Positions

Histogram of Simulated Equilibrium Positions Equilibrium points were found by starting with the limb at the positions shown - 60° hip flexion and 30° knee flexion. The limb then followed a simulated torque gradient until it reached a reversal point in both joint torques. Equilibria outside the boundaries shown were discarded. (A) 4^{11} EMG patterns (4,194,304 = 4 states - 0, .33, .66, 0.99 - for each of 11 muscles - AD, BI, PE, RA, RI, ST, VI, SM, VE, SA, IP) were tested to find their equilibrium points within a large workspace. Each of the 4^{11} patterns corresponded to a simulated torque gradient, given by the pattern-weighted sum of muscle model force fields. The workspace boundaries are drawn at hip = (75°, -110°) and knee = (30°, 150°). These limits were chosen arbitrarily. With these limits we found that 90.86% of the EMG patterns led to equilibria within the workspace boundaries. It was possible to extend the simulation closer to the limb singularity: an outer knee limit of 170° led to 99% within-boundary equilibria. The locations of the equilibria of the five spinal force field types are shown in green superimposed on the histogram. (B) Same simulation, except each muscle was pre-weighted with the EMG weighting factors used for animal SGM4 of the Mapping Database: RA = 1.32, SM = 2.4, BI = 11.7, SA = 2.6, other muscles = 1. The pre-weighting changed the distribution from which the muscle activations were drawn.

As a side effect of the simulations for figure 2-17, I was able to construct lists of activation patterns giving rise to stable points at each workspace location. I had originally intended for these lists to assist in the decoding of EMG patterns. However, there were many different patterns (hundreds to over 100,000) that produced each of the spinal force field types. This result indicates that the EMG signals one observes could well be context-dependent. There are thousands of different EMG patterns that have the same functional significance. This multiplicity of muscle activations, known as motor equivalence, is probably an important feature of the skeletal-muscular system for the control of movement.

The locations of the spinal force field equilibria (the ellipses in figure 1-7) were reproduced by the equilibrium points of the muscle synergies that had the property that any equilibrium points they produced fell in roughly the same place. A muscle synergy is a binary vector: each muscle is either active or not. An activation pattern is a positive real-valued vector. An activation pattern for a synergy has nonzero activation on all and only the muscles that are active in the synergy. Some muscle synergies had the property that no matter how the muscle activations were

changed, they produced a convergent equilibrium point somewhere in the workspace. I called these synergies that usually produced equilibrium points "reliable". Some muscle synergies had the property that they could only produce equilibrium points in some small region of the workspace – usually near to a workspace boundary. I called the synergies that produced equilibrium points only in some restricted part of the workspace "localized". Figure 2-18a shows the equilibrium point distributions of the synergies that were most localized and most reliable. Each of the 100 boxes in figure 2-18a represents the range of workspace locations of the simulated equilibrium points for one muscle synergy. The individual boxes are hard to see because these localized equilibrium point distributions (each produced by a different set of muscles) are heavily overlapping. Note that the locations of these localized, reliable distributions resemble the locations of the spinal force field stable points shown in figure 1-7. These plots are not sensitive to the parameters I used: as more distributions were added by plotting less localized or less reliable synergies, the added distributions accumulated at the five workspace locations typical of spinal equilibria. I call the synergies that are both reliable and localized "robust", because they must produce the same equilibrium points despite a broad range of noise in the muscle tensions. The spinal force fields appear to be related to the robust muscle synergies.

The quantification of muscle synergy localization points to a fundamental tradeoff between robustness and modifiability. Figure 2-17b shows four representative distributions from among the least localized synergies. There are many non-localized distributions like those shown in figure 2-17b, and every muscle contributes to several different non-localized synergies. Figure 2-17b demonstrates that it is possible to construct a tiling or covering of much of the workspace with only a few muscles. Non-localized synergies have the desirable property that small modulations of muscle activations can produce large changes in forces. For example, at the center of any one of the distributions in figure 2-17b the forces must change orientation by about 180° as modulations in the muscle activations of the muscles in the synergy shift the equilibrium point from one end of the distribution to the other. Because these synergies are non-localized, they can not be robust in the face of activation noise. Fluctuations

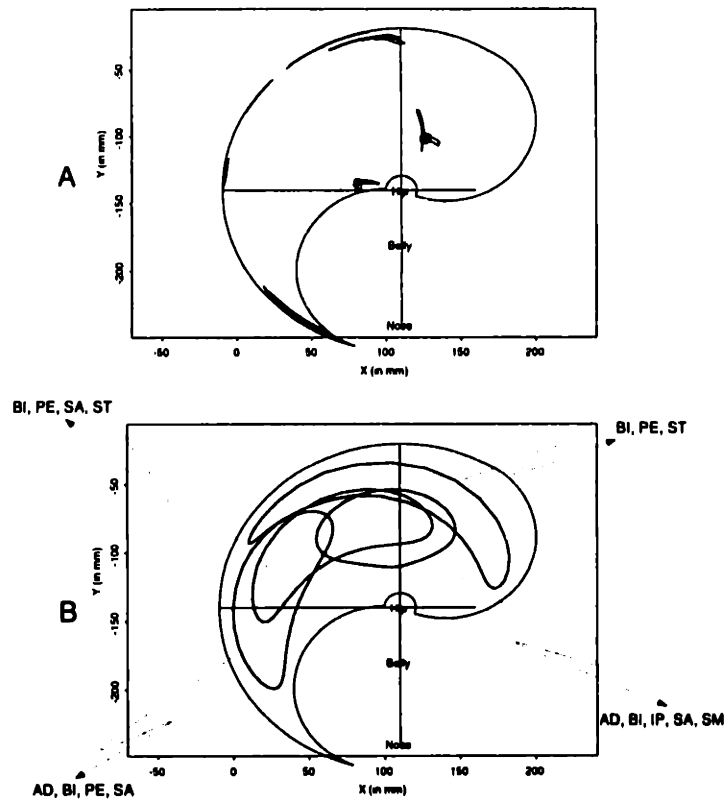

Figure 2-18: Localized and Reliable Distributions of Equilibrium Points The convergent equilibrium point distributions of the most "reliable" muscle synergies are shown. I define a muscle synergy as a binary vector: each muscle is active or not. An activation pattern is a positive real-valued vector. An activation pattern conforms to a synergy if it is zero when the synergy is zero and positive when the synergy is one. Synergies were reliable if a high percentage of random muscle activation patterns conforming to the synergy produced force fields with convergent equilibrium points within the workspace. Synergies were localized if their equilibrium point distributions covered a small area of the workspace. (A) The equilibrium point distributions of the most localized and reliable synergies from a large-scale simulation. Each joint-space box represents the minimum and maximum hip and knee angles observed in 50 random activation patterns for one muscle synergy of all 2^{16} =65535 synergies of 16 muscles (I did not use muscle Pyriformis in this simulation). I plot here the boxes of the 100 most reliable (> 10% in this simulation) and maximum localization (box area <100 square degrees) amongst all 65535 synergies simulated. (B) Four of the least localized distributions from a fine-grain simulation. Each joint-space ellipse represents one standard deviation of the hip and knee angles observed in 500 - 1000 random activation patterns for one muscle synergy of 2^{12} =4096 synergies of the 12 most powerful muscles. I plot here four of the most reliable (> 90% in this simulation) and minimum localization (ellipse area >1000 square degrees) amongst all 4096 synergies examined. The muscles producing each of the distributions is shown to the side.

in the tension output of the component muscles of a non-localized synergy will lead to changes in the endpoint forces, while the robust synergies pictured in figure 2-17a will produce the same endpoint forces despite fluctuations in the component muscles' tensions. It will be interesting to find out how the synergies actually represented in the spinal cord make use of this design tradeoff between synergies that are non-localized and modifiable versus synergies that are localized and robust.

Summary

I have shown force field muscle models for most of the frog's hindlimb muscles. The force field muscle models fall into a few easily-recognizable categories, but no muscle shows a reversal of joint torques. Thus, no single muscle can stabilize the limb. I used EMG signals to weight the muscle models. The EMG-weighted sum of muscle model force fields predicted the time course and orientation of observed forces and force fields with surprising accuracy. Finally, random combinations of muscle model force fields were used to estimate the distribution of workspace stable point available to the frog. Most of the stable points lie in a band within the workspace at approximately 140° knee entension. The continuous distribution of computed stable points does not match the punctate distribution of observed stable points evoked by stimulation of spinalized frogs. The punctate distribution of stable points is approximately matched by the locations of the equilibrium point distributions of the most robust muscle synergies.

Discussion

I first discuss my force field muscle models, which were computed as the spatial gradients of hidden models of muscle length. I note that none of the muscle force fields were mechanically stable, while spinal force fields typically are. I then discuss the validation of my force field muscle models through prediction of observed endpoint forces from observed EMG signals. The observed EMG fluctuations appear to be tuned to the dynamics of the corresponding muscles. Finally, I describe some of the

possible uses of force field muscle models. I found that the punctate distribution of equilibrium points observed during spinal micro-stimulation was not matched by simple random combinations of muscles, but it was matched by the model muscle combinations that produced the most reliable and localized scatters of equilibrium points under random activation. This suggests that robustness under activation noise may be an important criterion by which muscle synergies are chosen for spinal representation. I conclude by describing how force field muscle models can be used in statistical tests of hypothesized descending recruitment of interneuronal systems.

Force Field Muscle Models

I have demonstrated a novel technique for constructing muscle models, whereby I construct a hidden parameterized function, a length(θ) function, relating joint angles to muscle length. Length(θ) is used to compute the joint torques resulting from muscle activation. This technique works because torques and forces are locally linearly related by a Jacobian, which is the first derivative of the coordinate transformation, length(θ). The muscle Jacobian, $J_m(\theta)$, is the 1x2 vector of partial derivatives of the length(θ) function of muscle m. Muscle tension = $J_m(\theta) *$ joint torques, joint torques = $J_m^T(\theta) *$ muscle tension, and endpoint force = $J_e(\theta) *$ joint torques. $J_e(\theta)$ is the 2x2 matrix of the partial derivatives of the functions relating endpoint X and Y coordinates to the joint angles, θ (see section 1). I have used these equations by measuring the endpoint forces, converting those forces to joint torques (using $J_e(\theta)$, which I can compute from observable quantities). I used the joint torques as target values to be matched by the parameterized models of $J_m^T(\theta) *$ muscle tension. I was able to compute $J_m(\theta)$, the partial derivatives of my model of length(θ), at all joint angles, θ, because I chose an easy-to-differentiate parameterization of length(θ). I also computed the muscle tension as a function of the estimated muscle length in a straight-forward way based on known physiological relations (Rack & Westbury, 1969). In summary, the model parameters produced a length(θ) function from which I computed $J_m^T(\theta) *$ muscle tension at all sampled values of θ. The errors in the equations "torque = $J_m^T(\theta) *$ muscle tension" were then used to update the parameters for

the length(θ) function.

An advantage to modelling observed muscle torques with the spatial gradient of estimated muscle length is that an estimation of muscle length is needed by dynamic muscle models to compute the linear tension exerted by the muscle (Loeb, et al, 1989, Zajac and Winters, 1990). If the parameters of muscle geometry do not generalize across subjects (Buchanan, et al., 1986; Winters and Stark, 1988; Zajac and Winters, 1990; Wickland, et al., 1991), then accurate modelling work will require length(θ) functions to be computed or measured for each muscle of each subject. It would certainly be much easier to infer length(θ) from muscle stimulation data in a new subject (and to correct those estimates for the effects of reaction torques) than it would be to measure all the muscle geometric parameters for each of the subject's muscles. Any muscle model that can predict the muscle moment arm at arbitrary limb postures can be visualized as a force field, however, so my method of determining the moment arm from length functions is distinct from the use of force fields.

Length function estimation isolates the Biomechanics Problem

I have modelled the muscle moment arm, $\nu(\theta)$, with the spatial gradient of an estimated length function rather than with the typical approach of computing $\nu(\theta)$ directly from the combination of cadaver data and simplifying assumptions about the muscle geometry. I have thus avoided the difficult problem of understanding how the complex muscle geometry relates to the observed joint torques. Other groups have constructed their estimates of $\nu(\theta)$ from measurements in cadavers of features such as muscle volume and attachment points (Loeb, et al., 1989; Wickland, et al., 1991) *without verifying the estimated moment arm.* I have instead measured $\nu(\theta)$ almost directly by recording the endpoint forces, and hence the joint torques, resulting from the stimulation of individual muscles at many joint angles, θ. It will ultimately be important to understand how the complex geometry of muscles is related to joint torques. Our empirical estimates of $\nu(\theta)$ can be used both to refine the understanding of subtle muscle geometric factors, and to build accurate joint torque models of muscles. In other words, empirical estimates of $\nu(\theta)$ divide the problem domain into

two distinct components, rather than allowing the intricacies of muscle geometry to act as a source of error in joint torque muscle models.

Stability

None of the muscles in the frog hindlimb appear to be stable, but the force fields evoked by spinal micro-stimulation are almost always stable. Because the torques produced by a muscle always points down the gradient of the muscle's length(θ) function, contraction of a muscle could only produce a stable equilibrium at a local minimum of the muscle's length function. At a local minimum of length(θ) the spatial gradient of length(θ) will be zero, and the gradient of length(θ) will point back towards the local minimum at nearby values of θ. I do not know if it is mechanically possible for a skeletal muscle to be stable. Such a muscle would have to be attached to the skeleton so that any movement of the skeleton in any direction away from the stable point would cause the muscle to lengthen. It is difficult to imagine how such a muscle could exist, so it is difficult to imagine how any skeletal muscle's length function could reach a local minimum in the workspace. Thus, it may not be surprising that all of the muscles I observed were unstable. However, we usually observed stable force fields as a result of interneuronal spinal micro-stimulation. One function of the spinal cord may be to insure that the collection of muscles currently active is stable (Loeb, et al., 1989). From the simulations of random activation patterns, I estimate that 75 - 90% of all multiple muscle activations are stable, so insuring stability may not be a difficult constraint for the spinal cord to achieve.

Muscle Models are used to Predict the Spinal Force Fields Evoked by Spinal Microstimulation

We micro-stimulated (2 - 10 μAmps) spinal interneurons in spinalized frogs, while recording endpoint translational forces and the EMG signals from 11 hindlimb muscles (Bizzi, et al, 1991; Giszter, et al, 1993; Loeb, et al, 1993). Except for the additional recording of EMG signals, the methods used to record the force fields evoked by spinal

micro-stimulation are the same as those described above for recording the force fields evoked by muscular stimulation. We have found that spinal micro-stimulation in the interneuronal layers of the frog spinal cord evoke a small number of different force field shapes. The force fields evoked by spinal micro-stimulation also follow a principle of vector summation: simultaneous stimulation of two spinal loci results in a force field which is the vector sum of the force fields produced by independent stimulation of the two loci.

I used a EMG-weighted linear sums of muscle models to predict the forces evoked by spinal micro-stimulation with high accuracy. Other groups have also successfully estimated endpoint forces or muscle tensions from muscle models and EMG signals, using a wide variety of linear (Hof and Ven Den Berg 1977, 1981a-c), and non-linear (Cholewicki and McGill 1994; Olney and Winter, 1985; Loeb, et al., 1989; Buchanan,et al 1986), static and dynamic techniques. The force predictions validate and quantify the accuracy of the muscle models.

Force Predictions and Muscle Dynamics

It appears that the dynamics of the activated muscles are accounted for by the neuromuscular control signals generated by the spinal cord. Orientation constancy in spite of magnitude changes is a ubiquitous feature of the forces in our spinal micro-stimulation studies (Giszter, et al. 1993), both before and after acute deafferentation (Loeb, et al, 1993). The magnitudes of the forces evoked by spinal micro-stimulation rise and fall while the orientations remain within a 20° arc of their mean orientation. One possible explanation for the constancy of evoked forces could be a counter-balancing of muscle types: for example, increases in the EMG signals of muscle RA might be matched by decreases in the GA, because both muscles produce roughly the same forces. I can begin to rule out this simple explanation, because and if counter-balancing had occurred then the EMG-predicted forces should have reproduced the orientation constancy of the actual forces. It is also possible that the orientation constancy is due to counter-balancing activity in unobserved muscles. I can not rule this out, but if the unobserved muscles were covarying with the observed muscles in such a

straightforward way, then one would also expect to see evidence of counter-balancing within the observed muscles. Again, counter-balancing among the observed muscles does not seem to be taking place. The only other reasonable explanation for the observed orientation constancy is that the differences in the dynamics of the activated muscles does not matter for some reason. The dynamics obviously do matter to some extent, because my models, which lack dynamics, are not perfect predictors of the results of multiple muscle activations. Thus, I suspect that the apparent unimportance of the muscle dynamics in the orientations of the forces produced by multiple muscle activations is in fact due to compensation for the differences in the muscle dynamics by the spinal cord.

The constancy of the endpoint force orientations implies that the muscle tensions were "proportionally constant". That is, the magnitude of the torque produced by each muscle is a constant percentage of the total torque. My models ignored the activation dynamics of the muscles, and thus converted variations in the EMG signals directly into variations in the muscle tensions. As a result, the modelled muscle tensions were not proportionally constant. For example, if the magnitude of the predicted endpoint force for muscle RA shifts from 10% to 20% of the total predicted force magnitude (because of an increase in the EMG signal for muscle RA relative to the other EMG signals), then the orientation of the predicted endpoint force will swerve towards the orientation of my model of muscle RA. Thus, we can see that the magnitude of the predicted endpoint force for muscle RA must remain at some fixed percentage of the total magnitude: the actual forces do not swerve one way or another [4]. So, the constancy of the observed orientation of the net torque

$$\text{net torque} = \sum_{\text{muscle } m} \nu_m(\theta) * M_m(\theta, \dot{\theta}, \text{EMG}_m, t)$$

where $\nu_m(\theta)$ and $M_m(\theta, \dot{\theta}, \text{EMG}_m, t)$ are respectively the moment arm and tension magnitude of muscle m, requires that the ratio $\frac{M_{m1}}{M_{m2}}$ is approximately constant for

[4] We can presume that the actual muscle moment arms, $\nu(\theta)$ are all constant. The muscle moment arm ultimately depends on the geometry of the attachments of the muscle to the skeleton, and the attachments do not change over the course of these experiments if at all.

any two muscles m1 and m2 throughout the multiple muscle activation of a trial. In my experiments θ is constant because $\dot{\theta}$ is zero. Thus, $M_m(\theta, \dot{\theta}, \mathrm{EMG}_m, t) = M_m(\mathrm{EMG}_m, t)$. One way for a constant ratio $\frac{M_{m1}}{M_{m2}}$ to occur is for the activation dynamics ($M_m(t)$) for all of the muscles to be the same AND for all muscles have the same EMG pattern. The muscles obviously do have different activation patterns. So, the alternative way to keep $\frac{M_{m1}}{M_{m2}}$ constant is for the different EMG patterns of the two muscles to explicitly counter differences in their activation dynamics. $\frac{M_{m1}}{M_{m2}}$ is constant for every pair of activated muscles and the EMG patterns of pairs of muscles are not the same, so it follows that the observed variations in the EMG signals during stimulation trials are explicitly created by the spinal circuitry to account for the different nonlinearities of the activation dynamics of the muscles. The constant orientations and changing magnitudes imply that the magnitude of each component of the net torque – each muscle's contribution – is a constant proportion of the total magnitude.

It has long been thought that the spinal cord compensates for the dynamics of individual muscles (Nichols and Houk, 1976; Smith and Zernicke, 1987; Loeb, et al., 1989; Loeb, et al. 1993), but the arguments in the preceding paragraph further suggest that the spinal cord also compensates for the dynamics of collections of muscles. When two muscles are activated at varying extents, there must come a point at which one muscle switches to a new fiber type before the other one does, and at that point the dynamics of the muscles are different. If keeping a constant orientation at any magnitude is important, then the system will need to compensate for those switch-over points. For example, suppose an endpoint force at 45° is being produced by a muscle that can exert forces at 50° and a muscle that exerts forces at 20°. Most of the endpoint force will come from the muscle at 50°. At some high force magnitudes, the 45° force will require strong, fast fibers for the 50° muscle while weak, slow fibers are recruited for the 20° muscle. The slow fibers can not be made faster, so the only way to keep the 50° and 20° muscle forces proportional during changes in the 45° force magnitude is to slow down the faster 50° fibers. Since it would not be a good general strategy to slow down the fast fibers at all times, it seems plausible that the

dynamics of the motor pools might be adjusted in a synergy-dependent way.

Force Field Muscle Models and Muscle Synergies

I found that the locations of the equilibrium points of the spinal force fields were qualitatively matched by the locations of the most localized and reliable equilibrium point distributions amongst all the muscle synergies. This finding suggests that an important criterion for muscle synergy selection is the robustness of those muscle synergies in the face of the unpredictable effects of fatigue, muscle length, muscle velocity, and inputs to the motor neurons from afferents and descending fibers. The many factors that can influence the magnitude of force generated in response to motoneuronal discharges make the apparent spinal compensation for muscle dynamics a challenging problem. Spinal representations of robust muscle synergies might serve as a redundant mechanism for producing said compensation. In other words, full compensation for muscle dynamics would require accurate estimates of the activation and length states of the muscles. If the spinal cord uses robust synergies, then errors in those state estimates will not translate into errors in output forces. Thus, the locations of the spinal equilibria in figure 1-7 may indicate a a mechanism for inverting the dynamics of the muscles as well as a mechanism for inverting the dynamics of the limb.

There is a fundamental tradeoff between the robustness of a muscle synergy and its modifiability. Obviously, if a synergy always produces a force field with a convergent equilibrium point in a restricted region of the workspace, then that synergy can not be used to produce force fields with a wide range of workspace locations of equilibria. Modifiable muscle synergies can probably be more quickly switched from producing one direction of force to another. It is easy to imagine, for example, how the synergies pictured in figure 2-18b could be modulated to produce a cyclic motion of the limb. Thus, modifiable synergies might allow more movements and postures to be represented with fewer muscles. It is not clear what behavioral constraints would lead one style of muscle use to be preferable to the other or where the optimal tradeoff point between robustness and modifiability might lie. Combinations of the two kinds

of synergies could be used to produce synergies with robust and modifiable portions sub-regions.

I disagree with the prevalent view that dynamic optimization is the best available approach to studying the effects and uses of muscle synergies (Zajac and Winters, 1990). Dynamic optimization is an expensive computation that requires researchers to limit the problems they study. I have shown above that a thorough exploration of the range of possible actions of muscle synergies was a fruitful approach that did not use optimization. Relatively little use has been made of muscle models in the analysis of spinal circuitry (Zajac and Winters, 1990), and so there is a need further studies of the effects and uses of muscle synergies (Buchanan, et al., 1986). By avoiding optimization, I have been able to examine the properties of approximately 20 million random activation patterns per week using a SPARC workstation. Thus, I believe that the long-standing reliance on optimization as the tool of choice for exploring EMGs and muscle usage (see Hardt, 1978) may have hindered progress to some extent.

Test of Spinal Basis Functions

The original purpose of the muscle modelling work described in this paper work was to enable a statistical test of our theory that supra-spinal centers make use of interneuronally organized spinal force fields as building blocks for motor patterns. We can test this theory by using it to describe observed supra-spinal force fields (explained below) and then comparing that description to the null hypothesis: that supra-spinal force fields are constructed by simply recruiting arbitrary combinations muscles without the hierarchical organization imposed by the spinal force fields. A supra-spinal force field is a force field evoked in the same way as a muscle force field or a spinal force field, but with a stimulating electrode at some supra-spinal locus. I choose as a null hypothesis the possibility that supra-spinal force fields are the result of descending activation of motorneurons. The alternative hypothesis is that supra-spinal force fields can only activate the muscles through a particular intervening structure imposed by the spinal cord. There are many possible intervening structures that one could hypothesize for the spinal cord, and indeed the general

method I propose here could be used to test almost any imaginable hypothesized spinal circuitry. To test the possibility that the spinal cord provides the rest of the brain with the five spinal force field types described earlier (see figure 1-7), we can:

1. Step 1: Evoke a supra-spinal force field, SPFF.

2. Step 2: Estimate the non-negative muscle and spinal force field coefficients to reproduce SSFF:

$$\widehat{\mathrm{SSFF}}_{Sp} = \sum_{i=1}^{5} a_i \mathrm{SpFF}_i = \text{spinal fit}$$

$$\widehat{\mathrm{SSFF}}_{Mu} = \sum_{i=1}^{17} b_i \mathrm{MuFF}_i = \text{muscle fit}$$

   where 5 is the number of spinal force fields and 17 is the number of muscle models.

3. Step 3: If the supra-spinal force field is produced by co-activation of spinal force fields, then there should not be a significant difference in the quality of the spinal and muscle fits:

$$\frac{\sum(\widehat{\mathrm{SSFF}}_{Sp} - \mathrm{SSFF})^2}{\sum(\widehat{\mathrm{SSFF}}_{Mu} - \mathrm{SSFF})^2} \sim F(N, N)$$

   where N is the number of data points used to form the muscle and spinal estimates. With x and y force vectors to be matched by the fits, N will be twice the number of limb positions sampled. If the x, y, and z forces are matched, then N will be 3 times the number of limb positions.

If the F statistic is not significant, it will indicate that the ratio of the errors is indistinguishable from 1.0. In that case we can not rule out simple linear recruitment of spinal interneuronal force fields by supra-spinal fibers. Conversely, a significant F statistic will indicate that the supra-spinal force field is not implemented by the hypothesized spinal circuitry.

Summary

I have built statistical models of each of the muscles in the frog hindlimb. I avoided the biomechanical problem of predicting each muscle's length(θ) function from limb posture and muscle geometry by instead fitting its length(θ) statistically to the torques observed during direct muscle stimulation. From my muscle stimulation experiments I found that the hindlimb muscles do not provide limb stability. We have previously shown that spinal micro-stimulation does provide limb stability, so one role of the spinal cord may be to provide limb stability by activating stable muscle combinations. I used my statistical muscle models to predict the isometric forces observed during spinal micro-stimulation from the corresponding EMG signals. I also computed the distribution of force fields that should result from random activation of all of the hindlimb muscles, and this distribution was markedly different from that observed during spinal micro-stimulation. I used the same Monte Carlo technique to predict the distribution of force fields that would result from random activation of the hindlimb muscles in each possible muscle synergy. I found that the synergies with the most localized and reliable equilibrium point distributions best approximated with their distributions the equilibrium locations observed during spinal micro-stimulation. This Monte Carlo simulation result suggests that robustness in the face of noise may be an important selection criterion for the muscle synergies represented in the spinal cord. Finally, I showed how the muscle models and spinal force field models could be used in statistical tests of our hypothesized spinal circuit.

Chapter 3

Effects of acute spinal transection on the forces evoked by spinal microstimulation in the deafferented, decerebrate frog

Introduction

Recent experiments (Bizzi, et al, 1991; Giszter, et al, 1993) have demonstrated that the spinal cord of the frog contains a limited number of "modules". That is, we measured the hindlimb forces evoked by spinal interneuronal stimulation, and observed that the evoked forces occurred in a few discrete clusters of orientations (see figure 1-7). This result is not necessarily expected because forces which result from random activation of the frog's hindlimb muscles do not fall into discrete clusters. The arrangement of the hindlimb musculature does not, therefore, readily predict the regularity we have observed after thousands of microstimulation experiments. The small number of force patterns suggests that the spinal cord preferentially represents a limited number of classes of muscle combinations[1].

[1] As I showed in chapter 2, the identity of the classes of muscle combinations represented in the spinal cord may be related to the biomechanical preferences of the musculo-skeletal system. The

We theorize that the limited number of spinal modules serve as the basic building blocks of posture and movement (Mussa-Ivaldi, 1992). Excitation from supra-spinal descending fibers could conceivably activate simple combinations of the spinal modules in order to elicit forces that are not directly represented as modules. A problem for this theory is that the observed spinal modules could be artifacts of spinalization, since the spinal modules were observed during micro-stimulation of spinal cords that were surgically isolated from the rest of the brain. To address this issue directly, I have stimulated the spinal cords of decerebrated, deafferented frogs in order to determine if modules are observed in the presence of supra-spinal descending fibers. I have deafferented the frogs in this experiment, because decerebrated frogs can initiate protracted responces to small movements of their limbs, thus complicating the collection and interpretation of the hindlimb force data.

I have further compared the force evoked at single spinal loci before and after acute spinal transection in order to assess the influence of the descending fibers on the spinal modules.

particular muscle combinations that I have called robust in the previous chapter are not *random* in any reasonable sense of the word. So although the properties of the muscles can be used to derive principles that might underly the patterns of forces, those forces are not determined by the musculature. In particular, the fact that we observe only a few kinds of force fields during spinal stimulation indicates that the spinal cord is somehow imposing structure on the results of the spinal stimulation.

Methods

Data Collection

Surgeries

Decerebrations: Eight healthy adult bullfrogs (Rana Catesbiana) were anesthetized with 0.5 - 1.5 cc tricaine. The frogs were decerebrated anterior to the tegmentum, and the optic tectum was removed. Laminectomies were performed to expose the lumbar spinal cord. In four frogs (F8.19, F8.23, F8.25, F8.28), spinal dorsal roots 7, 8, and 9 were cut during the laminectomy and in the other four frogs, they were cut during the experiment. Otherwise, all surgeries were performed at least one day prior to the experiment.

Acute Spinalization: Acute spinal transections were performed by a method previously used in an acute deafferentation study (Loeb, et a, 1993). In brief, the brainstem anterior to the first vertebra is touched with a copper probe cooled in dry ice. The brainstem is then gently lifted and and cut with fine surgical scissors.

Electrode Implantations

Implantation micro-electrodes were constructed from 1 cm stainless steel "insect pins" and fine silver wire. The pins were wrapped with the wire approximately 0.3 cm from the tip. The pins were coated with glass under a microscope (using standard electrode manufacturing equipment), leaving 10 μm unexposed at the tip. The uncoated part of the pin behind the silver wire was cut off, leaving a glass-insulated implantation electrode approximately 2 - 3 mm in length.

At the start of an experiment the decerebrated frogs were sedated with tricaine, placed in a moistened plaster frame, and secured by clamps. The right ankle was attached to a movable force sensor (see figure 3-1A below) by a cuff capable of rotating about the Z axis, or of being secured in place so that it could not rotate. The spinal cord was exposed for the electrode implantation procedure.

Rings of medical-grade tubing (602-205, Dow Corning, 0.040" inner diameter)

were glued to the exposed surface of the lumbar spinal cord with fast-acting tissue adhesive (Vetbond, product number 1469 3M Animal Care Products). An implantation electrode was lowered with a micromanipulator through the center of one of the rings. Micro-electrode penetrations ran dorsal-ventral at sites between dorsal roots 7 and 9. We typically find a low threshold response zone 400 - 500 μm below the dorsal surface of the lumbar cord, and this response zone generally extends for another 600 μm ventrally. Response stability was assessed by visually comparing the magnitude, sign, and shape of the x, y, and z force traces. Once the stable zone was found, the electrode was moved to the depth at which the response had the lowest stimulus threshold, and the general shape and magnitude of the stimulation response was verified after 5 - 10 minutes. I then glued the electrode to the ring and spinal cord and released it from the micromanipulator. In three frogs (F8.23, F8.28, F9.27) a second electrode was also implanted at another spinal site using the same procedures. Thus, a total of 11 spinal sites were examined in the eight experimental frogs. The implantation procedures took 3 - 13 hours. During the implantation procedures, the frogs were kept under sedation with tricaine in order to minimize their movements. Force data was not gathered until the animal had recovered from the tricaine injections.

To determine the exact placement of the implanted electrode, I made a marking lesion (10 μA DC current for 20 - 30 seconds) at the site of the implanted spinal electrode(s) at the end of the experiment. The animals were sacrificed and perfused with a 10% formalin solution. Their spinal cords were stained with cresyl violet and examined to assess the location of the marking lesion(s). This procedure was complicated by the tissue glue, and for various reasons, I was unable locate the marking lesions in animals F8.25 and F9.23. All of the available marking lesions were in the interneuronal grey regions.

Recording Force Fields

We measure force fields by stimulating *one* spinal locus with the hind limb in each of *many* positions. Thus we follow this simple procedure:

1. Secure the ankle cuff in the force sensor.

2. Stimulate the cord while measuring force at the ankle.

3. Release the ankle cuff for rotation and move the limb to a new x,y position.

4. Repeat procedure at the next limb posture.

The force sensor was attached immediately above the frog's ankle, so the sensor's (x,y) coordinates correspond to the frog's right ankle position. I did not change the z coordinate of the ankle in this experiment. As the limb muscles contract and relax in response to the spinal stimulation, the force sensor records x, y, and z forces as functions of time. A measured force field consists of 3 force traces per ankle position together with the (x,y) location of the ankle at the time the forces were measured (see figure 3-1A below).

Stimulation Parameters

The stimulation parameters were typically between 4 - 15 μA; 0.6 msec pulses width; 400 - 600 msec duration; at 40 - 50 Hz. I never changed the stimulation parameters while collecting a force field.

Animals were monitored carefully for signs of pain (blinking, attempts to jump, vocalization) and were kept moist with periodic applications of tap water to the skin. The animals did not react to the placement of the spinal electrodes, nor did they respond in any unusual way to the spinal stimulation.

Data Analysis

One stimulation trial consists of the data gathered during stimulation of the spinal cord through one electrode with the limb at one particular position. A stimulation trial yields 3 force traces (x force, y force, and z force) over time. (see figure 3-1). One stimulation trial at each of several limb positions is needed to measure a force field. The z forces were dropped from analysis in this experiment.

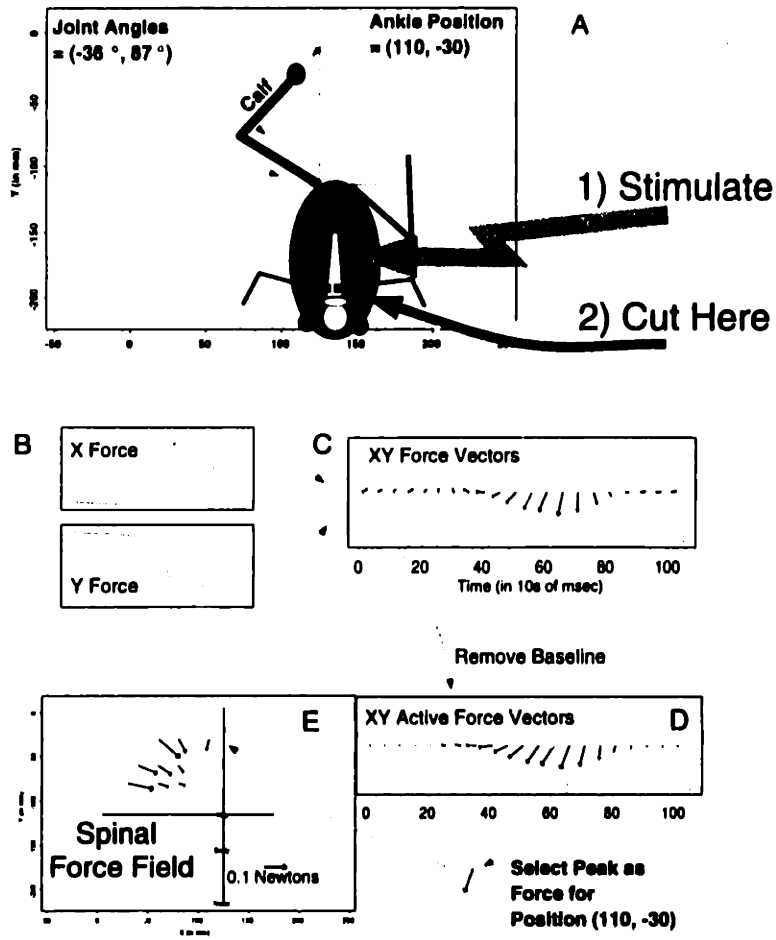

Figure 3-1: Processing Sequence for Force Data This figure illustrates the processing steps taken to convert the data from stimulation trials into a force field. (A) A frog is drawn with its hindlimb at a hip angle of $-36°$ and a knee angle of $87°$. A hip angle of $0°$ would cause the thigh to be parallel to the x axis. The illustrated joint angles ($-36°$, $87°$) bring the ankle to the location (110, -30) in the workspace. Ankle positions are measured in millimeters relative to the base of the force sensor apparatus. (B) Although three data traces (x, y, and z force) are recorded during spinal stimulation, I have displayed only the x and y forces here. Time is measured in tens of milliseconds. The force values are initially non-zero These initial non-zero forces are averaged together to estimate the baseline forces. (C) X and Y force traces are converted into XY force vectors. The non-zero initial forces of (B) are now non-zero initial force vectors. (D) The baseline forces of (B) and (C) are removed from all the force vectors to produce "active" XY force vectors. The initial active forces are not exactly zero, because initial forces in (C) are not exactly equal to average force levels used as the baseline. The force vector with the largest magnitude is the peak force, which is used to summarize the force trial in the time-invariant force field. (E) The time-invariant force field is constructed from the peak forces of several stimulation trials. The peak force from the trial illustrated in (B)-(D) is plotted at ankle position (110, -30). This force vector at (110, -30) and the other force vectors measured with the limb at the other limb positions, together form a force field.

The position of the frog's hip relative to the base of the force sensor apparatus and the length of its right hind limb segments (thigh and calf) were measured at the start of the experiment. These measurements enable the angles of the frog's hip and knee joints to be computed from the (x,y) coordinates of its ankle. From this information one can compute the torques at each joint corresponding to the forces measured during spinal stimulation. The hip angles were negative in extension, positive in flexion, and zero when the thigh was perpendicular to the body. The knee angles were all positive, with 180° being full extension.

Processing

Each force trace has two parts: "baseline and "active". Because we begin collecting the force traces before the stimulus begins, the average of the first 50 to 100 milliseconds of the force traces represents an estimate of the baseline force levels (figure 3-1B and C). We compute the active force traces by subtracting the baseline force levels from the measured forces. For example, the active y-force trace for a trial is the measured y-force trace minus the baseline y-force value (figure 3-1D). The subtracted baseline forces include the effects of kinematic constraints and gravity, which do not change during the course of a stimulation trial.

The (x,y,z) active forces form a time-varying 3-dimensional force vector, the Active Force Vector, AFV(t). These time-varying force vectors measured at each of the limb positions form a time-varying Force Field, FF(x,y,t). During spinal stimulation, we have found that the time-varying forces nearly always rise and fall along a line, so that AFV(t1) $\propto$ AFV(t2). Therefore, FF(x,y,t) can be well-approximated by FF(x,y), a time-invariant force field. At each sampled position, I used the peak magnitude of the time-varying force vectors at that position, $\max_t \|AFV(t)\|$, to select the force vector for the time-invariant force field, FF(x,y) (see figure 3-1E). Although the forces of FF(x,y) are three-dimensional, I only consider the two-dimensional (x,y) forces in this thesis.

Data Overview

I measured a total of 101 force fields under two experimental conditions: Decerebrated (50 force fields) and Spinalized (51 force fields). I examined my database both in terms of force fields and in terms of limb position.

Force Field Correlations

I compared force fields using a correlation measure. The force field correlation of field A and field B is the correlation value for the vectors ($X1_A$, $X2_A$, ... XN_A, $Y1_A$, $Y2_A$, ... YN_A) and ($X1_B$, $X2_B$, ... XN_B, $Y1_B$, $Y2_B$, ... YN_B), where Xi_A is the X component of the force at position i of field A. This measure requires that field A and field B be sampled at the same N positions. I can now correlate measured force fields with the standard force fields shown in figure 1-7, because the models of the standard force fields can be used to predict forces at any limb location. In other words, my spinal force field models allow us to measure forces at arbitrary positions in the workspace, because the models can predict forces (for comparison) at arbitrary positions in the workspace.

The force field correlation is depends on the inner product of the force fields:

$$[FF1_X(x1,y1), FF1_Y(\overrightarrow{x1},y1), FF1_X(x2,y2), \cdots] \begin{bmatrix} FF2_X(x1,y1) \\ FF2_Y(x1,y1) \\ FF2_X(x2,y2) \\ \vdots \end{bmatrix} \Downarrow$$

$$= \sum FF1_X(x_i,y_i) * FF2_X(x_i,y_i) + FF1_Y(x_i,y_i) * FF2_Y(x_i,y_i)$$

where the X and Y subscripts refer to the X force and Y force components of the force vectors of the force fields, FF1 and FF2, at each limb position (x_i, y_i). The scalar computed in this way is the inner product of the two force fields. Because forces from the same limb position are multiplied together, it is critical that the two force fields be measured or computed at the same limb positions. The force field correlation value is this inner product of the two force fields (equation 3.1) divided by the square root

of the product of each force field's inner product with itself. Two force fields that correlate at a value of 0.9 or higher are generally difficult to distinguish. Values of -0.5 and lower come from force fields that look to be direct opposites. Values of 0.5 to 0.8 range in subjective impression from similar to highly similar.

Limb Position-Dependent Force Orientations

Because stimulation trials were performed at each limb position both before and after spinalization, the forces collected during those stimulation trials at a single limb position can be compared directly. At a given limb position (for example (110, -30), see figure 3-1A) in a given frog, I performed 5 to 6 stimulation trials both before and after spinalization. In order to generate statistics of the before/after comparison, I average the before (pre-spinalization) trials together and I average the after (post-spinalization) trials together. Because 98 limb positions were measured in all, a total of 98 before/after comparisons can be made.

I distinguished the orientation and magnitude of the x,y peak forces at each position in order to quantify the effects of spinal transection. The orientation of an x,y force vector is arctan(y force, x force) Radians. The magnitude of an x,y force vector is $\sqrt{((\text{x force})^2+(\text{y force})^2)}$ Newtons. I found that the magnitudes and orientations of the forces evoked by spinal stimulation in the decerebrate (pre-spinalization) animals displayed greater variability than is typical for forces evoked by spinal stimulation in spinalized animals. This variability is an interesting finding for further study (see Discussion), however I wished to exclude the effects of the force variability. I was able to exclude the effects of magnitude variability by simply using the force orientations for comparisons.

I excluded the effects of the orientation variability by comparing only the force orientations that were not "anomolous". I defined a collection of force orientations to contain anomolous orientations if the "true range" of the orientations (see below) was greater than 60°. When a collection of orientations contained anomolous orientations, I used only the orientations that were in the majority. That is, I divided the range of the orientations in two, and then used the orientations in the half that had the

most orientations in it. When each half of the range of force orientations contained an equal number of observations, I chose the half to use at random.

The above procedure for removing anomolous force orientations was applied to the list of (typically five or six) orientations observed during spinal stimulation at a single limb position in a single spinal locus in a single experimental condition. In particular, the pre-spinalization force orientations were culled in this way at each limb position[2]. The non-anomolous orientations at each limb position were averaged together to find the mean orientation (see figure 3-6).

It is necessary to distinguish the true range of orientations from the apparent range. The true range of orientations in the list (-170^o, 170^o, -175^o, 175^o) is 20^o, but the apparent range is 340^o. In order to find the average of a list of orientations such as this, I first added 360^o to the negative angles: (190^o, 170^o, 185^o, 175^o).

[2]The post-spinalization force orientations were subject to the same procedure, but there were few positions at which anomolous spinalized forces were found

Results

Overview: In previous experiments we have found five discrete patterns of forces represented in the spinal cord (figure 1-7). However, these forces were measured in spinalized frogs. I wished to verify that these five patterns of forces are reproducible in more intact animals.

The experiment described here shows that the force fields evoked by lumbar spinal microstimulation in deafferented, decerebrated frogs are substantially the same as those observed previously in spinalized frogs. Furthermore, by comparing the force fields evoked from a single spinal locus before and after spinal transection, I found no qualitative or substantial quantitative difference in the the mapping of spinal locus to force field type.

The spinal force fields are present in decerebrated frogs

In figure 1-7 I display my models of the five types of force fields previously observed during spinal stimulation in spinalized frogs. In the experiment described here I have found examples of each of those five force field types during spinal stimulation in *decerebrated* frogs. Representative examples of my data are shown in figure 3-2. Each of the four force fields in figure 3-2 is highly similar to one of the five types of force fields evoked in spinalized frogs (see figure 1-7). The categorization of the force fields in figure 3-2 was determined by correlation with the model force fields in figure 1-7 (see Methods). Figure 3-2A is a "Body Flexion" type force field; figure 3-2B is a "Wipe" type force field; figure 3-2C is "Rostral Flexion" type force field; figure 3-2D is a "Caudal Extension" type force field. The "Lateral Extension" type force field was also evoked in one animal, as shown below in figure 3-4.

My data cannot rule out the possibility of the decerebrated frogs having other force field types not seen in the spinalized frogs. In general, however, the majority of the force fields I observed in the decerebrated frogs were qualitatively and quantitatively similar to those I have observed in spinalized frogs. The mean field correlation value of each pre-spinalization force field with the best matching spinal force field model

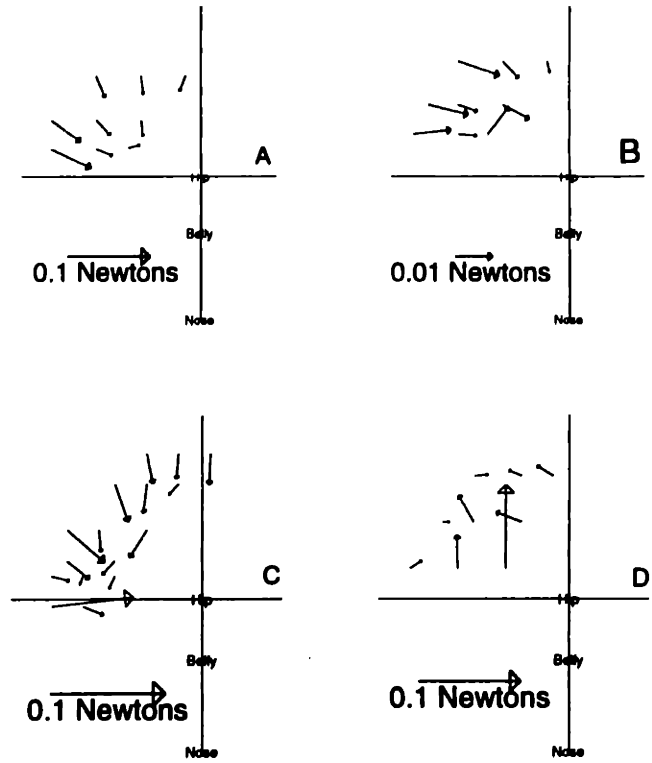

Figure 3-2: Four examples of Spinal Force Fields in Decerebrated Animals Each arrow in is the peak force vector from one stimulation trial. The base of each vector is indicative of the ankle position at the time the stimulation trial was executed. The arrow head points in the direction of the force. (A) Force field from animal F10.28. This force field correlates best with the "Body Flexion" spinal force field, with a correlation value of 0.84. (B) Force field from animal F8.23, electrode B. This force field correlates best with the "Wipe" spinal force field, at 0.916 (C) Force field from animal F9.23. This force field correlates best with the "Rostral Flexion" spinal force field, at, 0.84. (D) Force field from animal F8.25. This force field correlates best with the "Caudal Extension" spinal force field, at 0.79.

was 69%, and $\frac{3}{4}$ of these correlation values were above 55%.

Within-locus comparison of force fields before and after spinalization

Having found each of the five spinal force field types in the spinal cords of decerebrated frogs, I wished to make a closer comparison of the forces evoked before and after spinalization. Figures 3-3 through 3-5 show a comparison of pre- and post-spinalization force fields within individual frogs. The stimulation threshold did not appear to be altered by spinal transection in any of the animals.

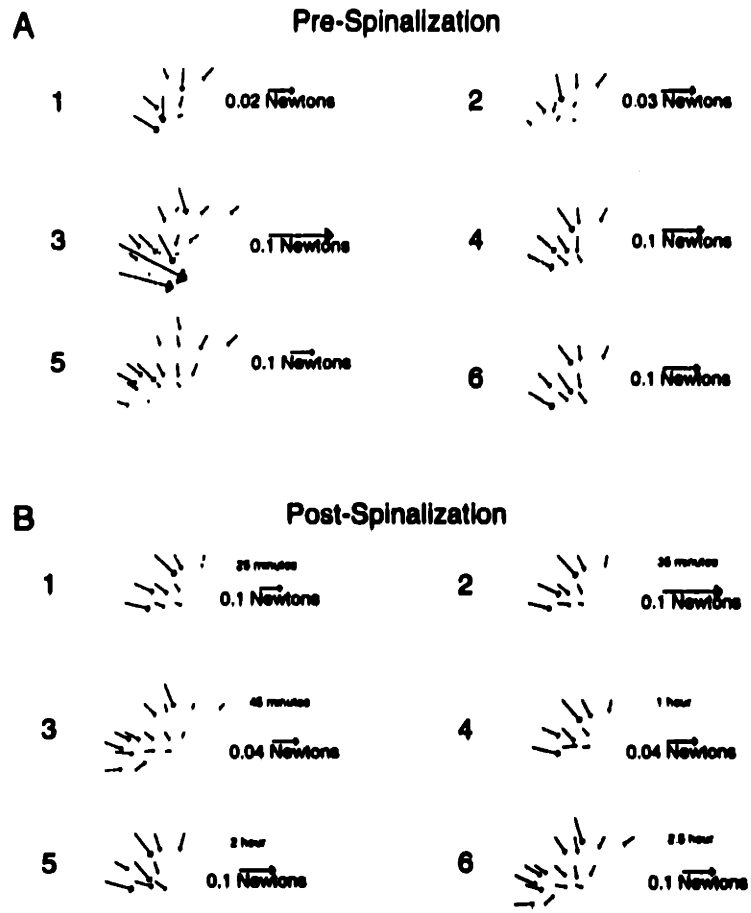

Figure 3-3: Effects of Spinalization on Forces Evoked by Spinal Stimulation
Effects of Spinalization on Forces Evoked by Spinal Stimulation These plots show several "Body Flexion" force fields evoked by spinal microstimulation through a single implanted electrode before and after spinalization of deafferented, decerebrated frog F10.20. Each arrow represents the peak force observed during one stimulation trial. The location of each force vector is indicative of the cartesian position of the ankle at which the limb was held by the force sensor when the stimulation trial was executed. I have dropped the cross-hairs that show the location of the hip. As usual, however, the force field is to the left of the hip, and the frog is oriented with its nose toward the bottom of the page. The numbers indicate the order in which the force fields were measured. There is no pairing implied by the numbers: for example, pre-spinalization force field number 4 is not related to post-spinalization number 4 except in the way that all of these force fields are related (they are all evoked by a single, unmoving, implanted, spinal electrode). The force field correlations of these force fields with each other are shown in table 3. The post-spinalization force fields are correlated at about 0.95. Pre-spinalization force fields (4, 5, 6) are also correlated with each other and with the post-spinalization force fields at above 0.80. There are magnitude fluctuations in pre-spinalization force field number 3. Some orientation fluctuations are evident in force fields number 1 and 2.

Field	D1	D2	D3	D4	D5	D6	X1	X2	X3	X4	X5	X6
D1	1.0	-	-	-	-	-	-	-	-	-	-	-
D2	0.73	1.0	-	-	-	-	-	-	-	-	-	-
D3	0.81	0.71	1.0	-	-	-	-	-	-	-	-	-
D4	0.85	0.77	0.82	1.0	-	-	-	-	-	-	-	-
D5	0.84	0.73	0.79	0.91	1.0	-	-	-	-	-	-	-
D6	0.84	0.70	0.81	0.98	0.89	1.0	-	-	-	-	-	-
X1	0.74	0.71	0.73	0.95	0.81	0.93	1.0	-	-	-	-	-
X2	0.74	0.74	0.75	0.95	0.84	0.91	0.99	1.0	-	-	-	-
X3	0.70	0.66	0.75	0.91	0.83	0.88	0.97	0.98	1.0	-	-	-
X4	0.7[illegible]	0.73	0.71	0.92	0.79	0.91	0.98	0.98	0.97	1.0	-	-
X5	0.76	0.71	0.75	0.95	0.82	0.97	0.96	0.95	0.93	0.96	1.0	-
X6	0.78	0.76	0.77	0.96	0.90	0.95	0.96	0.96	0.96	0.96	0.98	1.0

Field Correlations for Animal F10.20: This table shows the field correlations for the pre- and post-spinalization force fields shown in figure 3-3. Force fields D1-D6 ("D" for Deafferented) correspond to the pre-spinalization force fields. Force fields X1-X6 ("X" for Transected) correspond to the post-transected force fields. The force field correlation of field A and field B is the correlation value for the vectors ($x1_A$, $x2_A$, ... xN_A, $y1_A$, $y2_A$, ... yN_A) and ($x1_B$, $x2_B$, ... xN_B, $y1_B$, $y2_B$, ... yN_B), where xi_A is the x component of the force at position i of field A. Only the bottom half of the matrix of correlations is shown in this table, because the correlation of field A with field B equals the correlation of field B with field A. Each force field is perfectly correlated with itself, as shown by the diagonal in the table, where the correlation values are 1.0. Note that the last force field collected before the spinal transection, force field D6, correlates with all of the post-spinalization force fields at a level 0.88 or better.

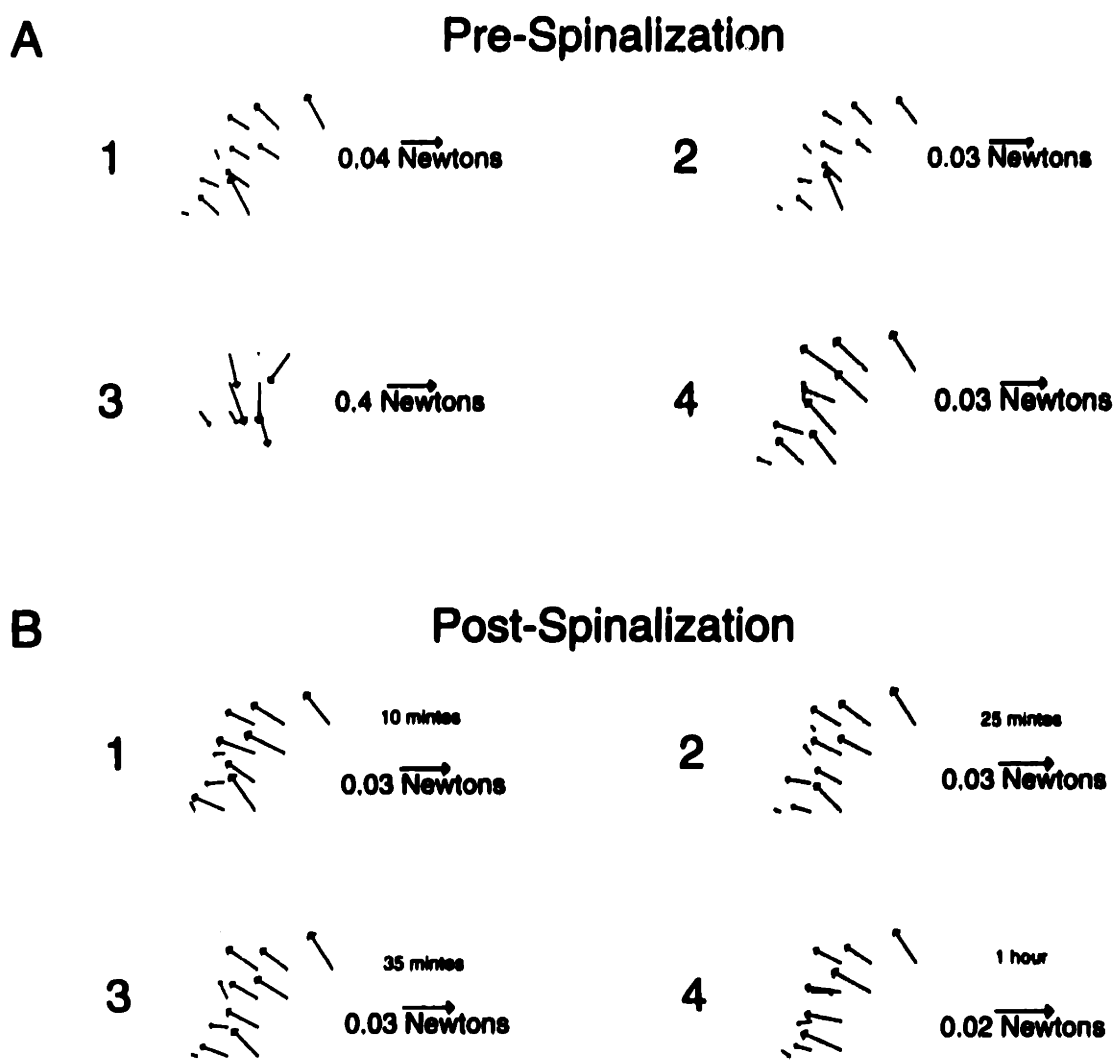

Figure 3-4: Effects of Spinalization on Forces Evoked by Spinal Stimulation
These plots show several "Lateral Extension" force fields evoked by spinal microstimulation through a single implanted electrode before and after spinalization of deafferented, decerebrated frog F8.19. Force fields are displayed as in figure 3-4. There is no pairing implied by the numbers, which merely indicate the order in which the force fields were measured. The matrix of correlations of these force fields are shown in table 3. With the exception of pre-spinalization force field number 3, all of the pre- and post-spinalization force fields are correlated at at least 0.80. The third force field collected before spinal transection was obviously quite different from all of the others. In fact, pre-spinalization force field number 3 correlates with the Rostral Flexion type standard force field (see figure 1-7) at 0.84. The other force fields all correlate best with the Lateral Extension type force field. It is not clear why the type of evoked force field would suddenly switch, but it is interesting that it switched to one of the standard force field types.

Field	D1	D2	D3	D4	X1	X2	X3	X4
D1	1.0	-	-	-	-	-	-	-
D2	0.99	1.0	-	-	-	-	-	-
D3	-0.56	-0.58	1.0	-	-	-	-	-
D4	0.97	0.95	-0.59	1.0	-	-	-	-
X1	0.95	0.95	-0.35	0.94	1.0	-	-	-
X2	0.96	0.94	-0.41	0.96	0.97	1.0	-	-
X3	0.96	0.94	-0.44	0.97	0.96	0.99	1.0	-
X4	0.83	0.80	-0.13	0.85	0.88	0.90	0.90	1.0

Field Correlations for Animal F8.19: This table shows the field correlations for the pre- and post-spinalization force fields shown in figure 3-4. Force fields D1-D4 ("D" for Deafferented) correspond to the pre-spinalization force fields. Force fields X1-X4 ("X" for Transected) correspond to the post-transected force fields. See table 3 for more generic details. Note that the last force field collected before the spinal transection, force field D4, correlates with all of the force fields collected after the spinal transection at a level of 0.85 or better.

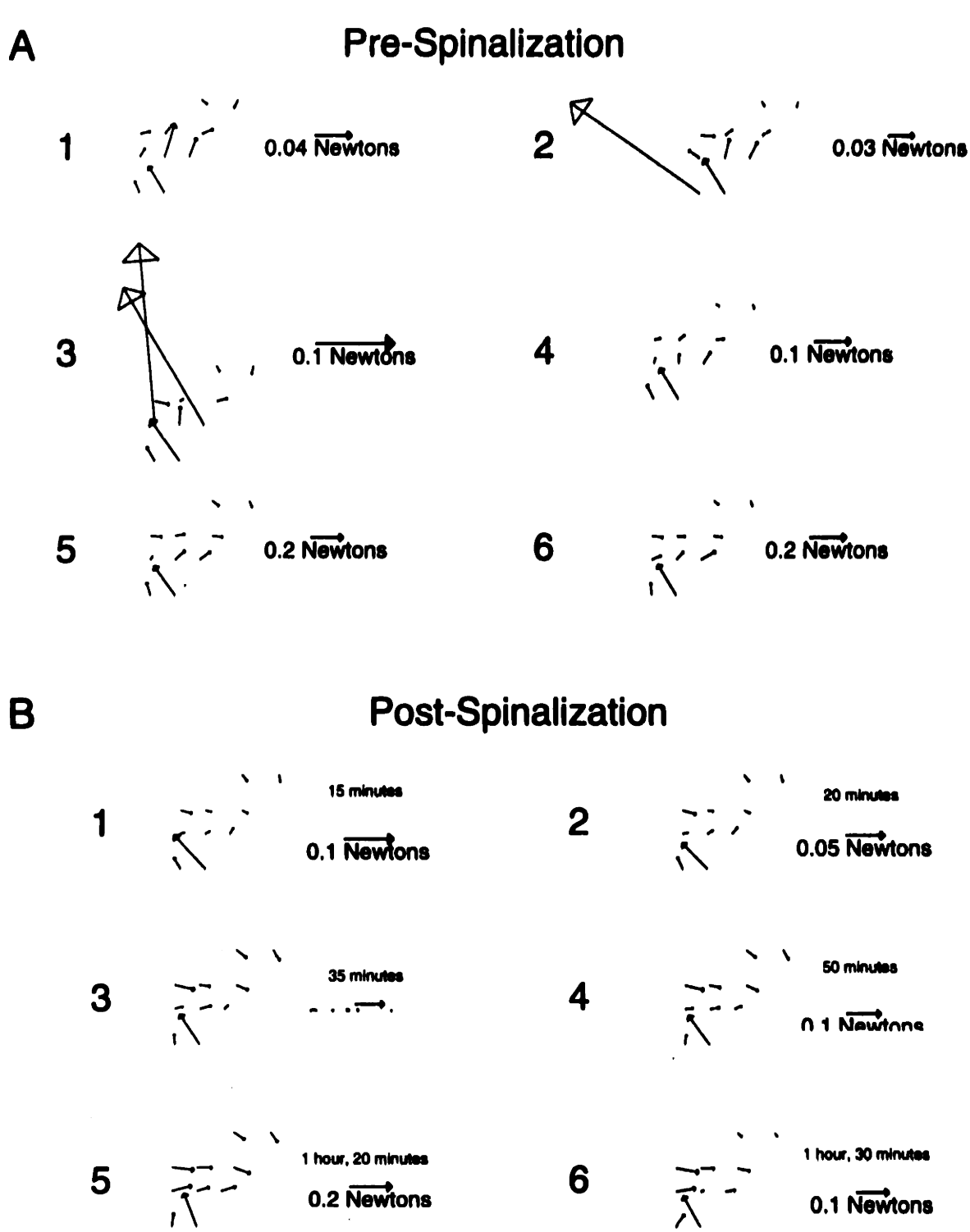

Figure 3-5: Effects of Spinalization on Forces Evoked by Spinal Stimulation
Effects of Spinalization on Forces Evoked by Spinal Stimulation These plots show several "Caudal Extension" force fields evoked by spinal microstimulation through a single implanted electrode before (A) and after (B) spinalization of deafferented, decerebrated frog F8.28. See figure 3-3 for display details. The numbers simply indicate the order in which the force fields were measured. The force field correlation values for these force fields are shown in table 3. Note the tremendous magnitude fluctuations in pre-spinalization force fields 2 and 3. Note that the rest of the fields are correlated above a level of 0.80.

Field	D1	D2	D3	D4	D5	D6	X1	X2	X3	X4	X5	X6
D1	1.0	-	-	-	-	-	-	-	-	-	-	-
D2	0.47	1.0	-	-	-	-	-	-	-	-	-	-
D3	0.45	0.21	1.0	-	-	-	-	-	-	-	-	-
D4	0.85	0.58	0.40	1.0	-	-	-	-	-	-	-	-
D5	0.84	0.50	0.30	0.95	1.0	-	-	-	-	-	-	-
D6	0.81	0.44	0.26	0.94	0.98	1.0	-	-	-	-	-	-
X1	0.71	0.48	0.28	0.92	0.94	0.92	1.0	-	-	-	-	-
X2	0.75	0.50	0.28	0.92	0.96	0.94	0.99	1.0	-	-	-	-
X3	0.69	0.37	0.24	0.84	0.94	0.92	0.92	0.95	1.0	-	-	-
X4	0.68	0.34	0.19	0.84	0.94	0.93	0.92	0.95	0.99	1.0	-	-
X5	0.69	0.33	0.19	0.81	0.90	0.94	0.82	0.87	0.95	0.95	1.0	-
X6	0.63	0.24	0.17	0.79	0.86	0.92	0.83	0.87	0.92	0.93	0.95	1.0

Field Correlations for Animal F8.28: This table shows the field correlations for the pre- and post-spinalization force fields shown in figure 3-5. Force fields D1-D6 ("D" for Deafferented) correspond to the pre-spinalization force fields. Force fields X1-X6 ("X" for Transected) correspond to the post-spinalization force fields. See table 3 for more generic details. Note that the last force field collected before the spinal transection, force field D6, correlates with all of the post-spinalization force fields at a level of 0.92 or better.

In figure 3-3 we see six pre-spinalization and six post-spinalization force fields in frog F10.20. Each force field was evoked by lumbar spinal stimulation through an implanted electrode. The frog was decerebrated and deafferented prior to the experiment. The force fields are numbered in the order in which they were measured: in each column of the figure, force field 1 was evoked before force field 2, and so on. In the post-spinalization forces I also list the time since the spinalization. For example, post-spinalization force field number 3 of figure 3-3 was measured approximately 45 minutes after the spinalization was performed (by stimulating through the same implanted electrode, of course). Although there could be large fluctuations in the magnitudes of the forces evoked in the pre-spinalization case, the pre-spinalization force fields are similar to the post-spinalization force fields. This similarity was measured by force field correlation. The correlation values are given in tables 3 through 3. For example, in figure 3-3, pre-spinalization force field number 6 correlates with post-spinalization force field number 1 at 0.925. The mean of the 36 correlation values between the six pre-spinalization force fields in table 3 and the six post-spinalization force fields is 0.81.

Most of the force fields in figure 3-3 are classified as the "Body Flexion" type, as previously identified by spinal stimulation of spinalized frogs. Figure 3-5 shows the "Caudal Extension" type force fields from frog F8.28, electrode B. Figure 3-4 shows the "Lateral Extension" type force fields evoked in frog F8.19. The forces evoked following spinalization were more repeatable than the pre-spinalization forces (see particularly the exception exemplified by pre-spinalization force field number 3 of figure 3-3 or pre-spinalization force field number 2 of figure 3-5) In spite of a few exceptions, however, these figures emphasize the astonishing point that I could lift and cut the spinal cord at the level of the first vertebra and immediately evoke virtually the same forces as I had prior to the spinal transection.

Because of the magnitude fluctuations evident in figures 3-3 through 3-5, I used orientations of non-anomolous forces to quantify the differences in the pre-spinalization and post-spinalization forces (see section 3). The results of this quantification, are shown in figure 3-6. The distribution of angular differences is approximately normal

with a mean value of 5.3°. This mean angular difference could not be distinguished statistically from 0°. Thus, spinalization did not cause any systematic change in the orientations of the forces evoked by lumbar spinal microstimulation.

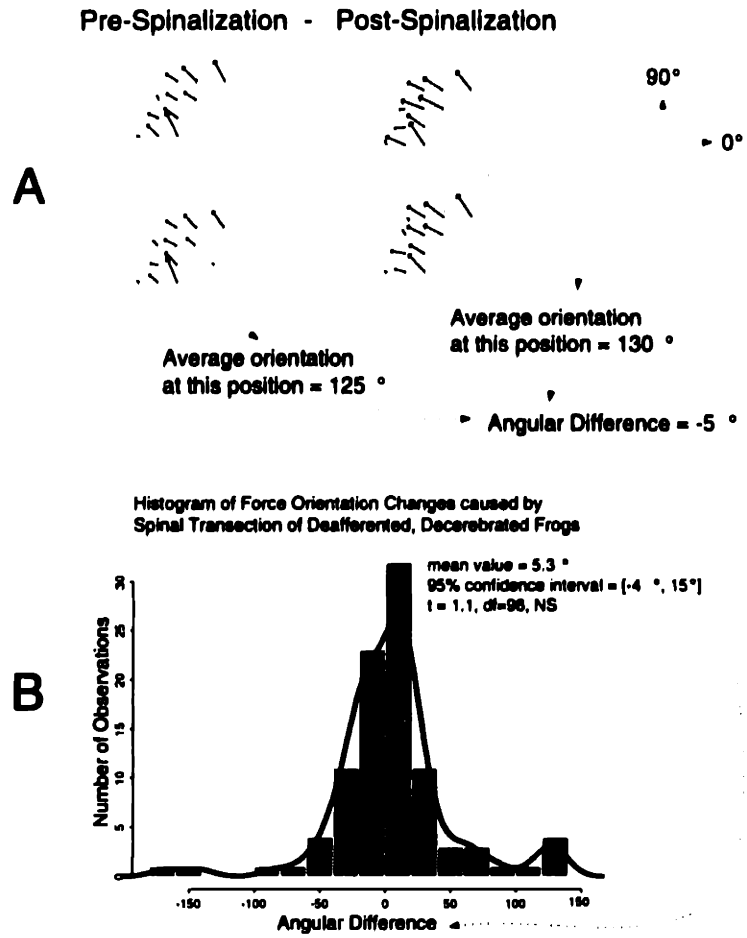

Figure 3-6: Distribution of Peak Force Orientation Differences In this figure I show the distribution of differences in force orientation over all the limb positions, and how that distribution was computed. The distribution is approximately gaussian with a mean value of 5.3°, which is not statistically different from 0°. (A) The computation of angular differences is illustrated on four example pre- and post-spinalization force fields (taken from figure 6). At each limb position, I computed the average orientation of the non-anomalous forces (see section 3). There are no anomalous forces in the displayed force fields. The average orientation of the circled pre-spinalization forces is 125°. The average orientation of the circled post-spinalization forces is about 130°. Therefore, the difference in the orientations at this limb position is $-5°$. The angular difference of $-5°$ is accumulated in the histogram shown part (B). (B) The histogram of angular differences at all 98 limb positions. The height of the histogram for angular differences between 0° and $-15°$ is 25 observations. One of those observations is the $-5°$ computed in (A). Since there are 11 limb positions in each of the force fields of (A), these force fields contribute 11 observations to the histogram of (B).

Discussion

Spinalized frogs are quiescent, and have been shown to give repeatable responses at many limb positions to spinal micro-stimulation at a single locus (Loeb, et al, 1993). These characteristics enabled us to characterize spinal force fields: we repeatedly elicited a single response by microstimulating a single spinal locus while holding the hindlimb at many different positions (Bizzi, et al, 1991; Giszter, et al, 1993; Loeb, et al., 1993). By measuring hindlimb endpoint forces at different limb positions in the frog, we can approximate continuous force field functions from a few samples. It only makes sense to do this, however, if the same behavior can be repeatedly evoked with the hindlimb in different positions.

I wished to examine these force field patterns in frogs which were not spinalized. Specifically, my goal in the study described here was to discover if the five force field types shown in figure 1-7 could be evoked by spinal stimulation in decerebrated frogs. This goal was complicated by the tendency of decerebrated frogs to initiate protracted responses to small movements of their limbs. Thus, I performed our experiment in *deafferented*, decerebrated frogs.

The results, summarized with representative examples in figure 3-2, demonstrate that force fields evoked by lumbar spinal microstimulation in deafferented, decerebrated frogs are substantially the same as those observed in spinalized frogs. In a database comprised of 50 force fields evoked by spinal stimulation of the deafferented, decerebrate frogs, half of the force fields were well correlated to one of the spinalized spinal force field types (median field correlation value of 72%). The observation of the five modelled spinal force field types (see figure 1-7) in decerebrate frogs suggests that it is possible these five spinal force fields serve as building blocks of movement for the descending tracts.

The forebrain and tectal tissue that I removed from these frogs do not contain projections to the spinal cord. Supraspinal projections to the frog's lumbar spinal cord come from the brain stem reticular formation (Corvaja et al 1973, Peterson 1984), the brain stem interstitial nucleus (Ten Donkelaar 1982), the tectum (Rubinson

1968), the cervical spinal cord (Rubinson 1968, Corvaja et al 1973), the tegmentum (Masino and Grobstein 1989b), the vestibular complex (Corvaja et al, 1973), and the deep cerebellar nucleus (Montgomery 1988). There are no forebrain projections to the spinal cord in the frog (Simpson 1976) and the tectospinals descend only to the cervical level of the cord (Masino and Grobstein 1990). Thus, having demonstrated that the spinal force fields types are all present in these decerebrate frogs, it is feasible that the spinal force field types are also present in the fully intact frog.

I also examined the forces evoked at each stimulation locus and limb position before and after acute spinal transection. The forces evoked in the decerebrated animals were more variable in orientation and in magnitude than the corresponding forces in the spinalized animal. I excluded the effect of the magnitude variability by comparing the orientations of the forces. I excluded the effect of the orientation variability, by examining only the most common force orientations at each site. Under this comparison, the forces evoked before and after spinalization had the same mean orientation (as shown in figure 3-6). There were 13 limb positions at which spinalization caused a change in the force orientation of more than 60°. Five of these 13 positions were from force fields of one animal (F9.27, electrode B, medial site near the central canal). Thus, ten of my eleven electrode placements assessed the evoked forces as being the same in decerebrate frogs as in spinalized frogs.

The sole indication in my data of an influence of descending fibers on the spinal cord was the obvious increased variability of the force magnitudes and orientations. It is unlikely that this variability of the pre-spinalization forces was due to the electrode moving from trial to trial. I implanted the electrodes in response zones that were produced the same forces over several hundred microns, and the anomalous pre-spinalization forces were generally preceded and succeeded by forces that were highly similar to the subsequent post-spinalization forces. For these reasons, therefore, it seems likely that the pre-spinalization force variability was due to modulation of spinal excitability by descending fibers.

Future examination of the variability of pre-spinalization forces may help to elucidate how the spinal interneuronal systems of the spinal cord are modulated by the

supra-spinal systems. It appears preliminarily that the anomalous evoked forces may fall into the usual set of discrete clusters. Figure 3-7 shows the distributions of force orientations in a larger version of the experiment than reported here. Note particularly the peaks in figure 3-7a. Each peak in figure 3-7a appears to correspond to the force orientation of one of the five spinal force field types. The motivation for figure 3-7a can be seen in figure 3-4, where pre-spinalization force field number 3 suddenly changes direction. In fact, pre-spinalization force field number 3 of figure 3-4 is a fine example of a rostral flexion force field. In general, although the pre-spinalization forces change orientations occasionally, they nevertheless appear still to be constrained in their orientations by the discrete clusters of forces given by the spinal force fields.

Summary

We theorize that the limited number of spinal modules serve as the basic building blocks of posture and movement (Mussa-Ivaldi, 1992). It would be problematic for our theory if the observed spinal modules were artifacts of spinalization. I have shown in this experiment that the spinal modules are not artifacts of spinalization.

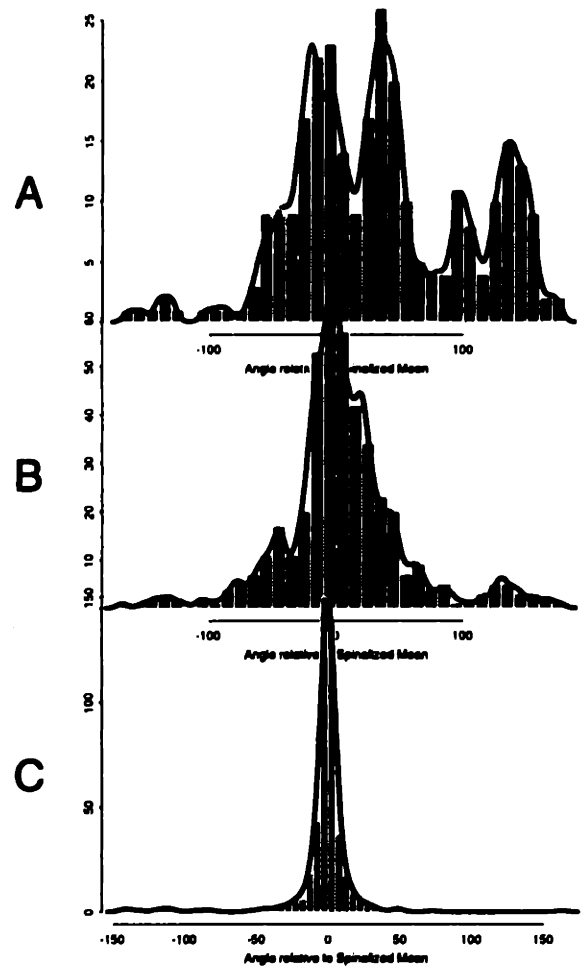

Figure 3-7: Distribution of Peak Force Orientations In this figure I show the distribution of force orientations over all the limb positions. At each limb position, the mean orientation of the non-anomalous spinal forces is computed. That angle then becomes 0^o. The three histograms in this figure show all of the force orientations relative to the new 0^o at each limb position. (A) Spinal force orientations in decerebrate frogs *with the afferents intact.* Although not described in this write-up, I evoked spinal forces in four animals prior to cutting the dorsal roots to deafferent them. Note that the distribution of force orientations is strikingly peaked. (B) The histogram of force orientations in the deafferented, decerebrate frogs. (C) The histogram of force orientations in spinalized frogs. Note that this histogram is quite tight around its mean value. This indicates that the forces evoked by spinal micro-stimulation are highly repeatable in the spinalized frogs.

Chapter 4

Supra-spinal microstimulation in the decerebrate frog

Introduction

Recent experiments (Bizzi, et al, 1991; Giszter, et al, 1993; Loeb, et al 1993) have demonstrated that the spinal cord of the frog contains a limited number of "modules". That is, we measured the hindlimb forces evoked by spinal interneuronal stimulation, and observed that the evoked forces occurred in a few discrete clusters of orientations (see figure 1-7). This result is unexpected because forces which result from random activation of the frog's hindlimb muscles do not fall into discrete clusters. The structure of the hindlimb musculature does not, therefore, readily predict the regularity we have observed after thousands of microstimulation experiments. The small number of force patterns suggests that the spinal cord preferentially represents a limited number of classes of muscle combinations.

We theorize that the limited number of spinal modules serve as the basic building blocks of posture and movement (Mussa-Ivaldi, 1992). Descending fibers from supra-spinal structures could conceivably activate simple combinations of the spinal modules in order to produce forces that are not directly represented by the individual modules. To test this hypothesis, I stimulate supra-spinal structures and measure the evoked forces. I then investigate whether the forces evoked by supra-spinal stimulation can

be accounted for with combinations of the spinal modules or with combinations of the muscles. If the patterns of supra-spinal evoked forces are more compatible with combinations of muscles than with combinations of spinal modules, then the hypothesis of we linear superposition of spinal modules becomes clearly untenable.

A supra-spinal structure of particular interest in the frog is a tegmental cell column identified by Masino and Grobstein (1989a,b). These cells project to the spinal interneuronal grey matter. Lesions of these cells are necessary and sufficient to eliminate the frog's prey orienting response (Masino and Grobstein 1989a,b). The authors found that the lesioned animals would lunge and snap their tongues at prey at the correct distance but at the wrong angle: in other words, the animals did not change orientation. Masino and Grobstein (1989a) hypothesized that the tegmental cells make use of a second subsystem in the spinal cord involved in "selection of a particular motor synergy" to produce changes in body orientation. We can now test whether that hypothesized spinal subsystem is our identified collection of spinal modules.

Methods

Data Collection

Surgeries

Decerebrations: Six healthy adult bullfrogs (Rana Catesbiana) were anesthetized with 0.5 - 1.5 cc tricaine. The frogs were decerebrated anterior to the tegmentum, and the optic tectum was removed. In two frogs (F4.12, F4.21, spinal laminectomies were performed to expose and cut dorsal roots 7, 8, and 9. All surgeries were performed at least one day prior to the experiment.

Electrode Placements

At the start of the experimental session the decerebrated frogs were sedated with tricaine, placed in a moistened plaster frame, and secured by clamps. The right ankle was attached to a movable force sensor (see figure 4-1A below) by a cuff capable of

rotating about the Z axis, or of being secured in place so that it could not rotate.

A stainless steel micro-electrode (0.1 - 2 μm at the tip, with 1 - 10 Mohms impedance in the tissue was lowered with a micromanipulator in the following supra-spinal structures: brainstem, cerebellum, pons, and tegmentum. As the electrode was lowered, response repeatability was assessed by visually comparing the magnitude, sign, and shape of the x, y, and z force traces at different stimulation depths. I searched for repeatable response zones extending dorso-ventrally for 600 μm or more that produced clear and repeatable force fields. Once a repeatable zone was found, the electrode was moved to the depth at which the response had the lowest stimulus threshold. The repeatability of the stimulation response at that depth was verified over a period of 5 - 10 minutes. After a number of force fields were collect (see below) at the chosen stimulation site, the electrode was removed and I repeated the above procedures to find a new site.

To determine the exact placement of electrodes, I made marking lesions (10 μA DC current for 20 - 30 seconds) through the electrode. After all electrode penetrations were completed, the animals then were sacrificed and perfused with a 10% formalin solution. Brain sections were stained with cresyl violet and examined to assess the location of the marking lesion(s).

Recording Force Fields

I measured force fields by stimulating *one* supra-spinal locus with the hind limb held sequentially in each of *many* positions. Thus I followed this simple procedure:

1. Secure the ankle cuff in the force sensor.
2. Stimulate the supra-spinal locus while measuring the force at the ankle.
3. Move the limb to a new posture.
4. Repeat procedure at the next limb posture.

The force sensor was attached immediately above the frog's ankle, so the sensor's (x,y) coordinates correspond to the frog's right ankle position. I did not change the

z coordinate of the ankle in this experiment. As the limb muscles contract and relax in response to the supra-spinal stimulation, the force sensor records x, y, and z forces as functions of time. A measured force field consists of those 3 force traces at each ankle position together with the (x,y) location of the ankle position (see figure 4-1A below).

Stimulation Parameters

I found that higher stimulation parameters were generally required to excite the supra-spinal tissues than was typical for the spinal interneuronal stimulation. Stimulation parameters ranged between 7 - 50μA; 0.3 - 0.8 msec pulses width; 300 - 800 msec duration; at 40 - 300 Hz. Typical stimulation parameters were 10 - 40 μA; 0.6 msec pulses width; 400 msec duration; at 60 Hz. The stimulation parameters were never changed while collecting a force field.

Data Analysis

One stimulation trial consists of the data gathered during stimulation of some supra-spinal locus (through one electrode) with the limb at one particular position. A stimulation trial yields 3 force traces (x force, y force, and z force) over time. (see figure 4-1). One stimulation trial at each of several limb positions is needed to measure a force field. The z forces were dropped from analysis in this experiment, and are not shown in figure 4-1.

The position of the frog's hip relative to the base of the force sensor apparatus and the length of its right hind limb segments (thigh and calf) were measured at the start of the experiment. These measurements allow us to compute the angles of the frog's hip and knee joints from the (x,y) coordinates of its ankle. From this information I was also able to compute the torques at each joint corresponding to the forces measured during spinal stimulation. The hip angles were negative in extension, positive in flexion, and zero when the thigh was perpendicular to the body. The knee angles were all positive, with 180° being full extension.

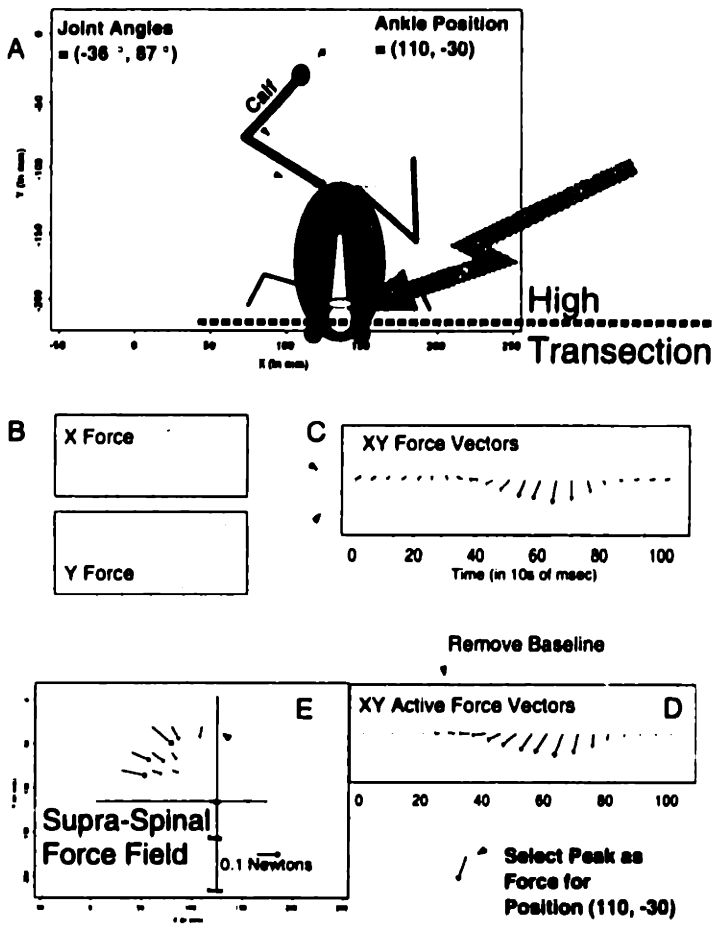

Figure 4-1: Processing Sequence for Force Data

Processing Sequence for Force Data This figure illustrates the processing steps taken to convert the data from supra-spinal stimulation trials into a force field. (A) A frog is drawn with its hindlimb at a hip angle of $-36°$ and a knee angle of $87°$. A hip angle of $0°$ would cause the thigh to be parallel to the x axis. These joint angles bring the ankle to the location (110, -30) in the workspace. Ankle positions are measured in millimeters relative to the base of the force sensor apparatus. (B) Three data traces (x, y, and z force) are recorded during supra-spinal stimulation. We have displayed only the x and y forces here. We have not analyzed the z forces in this work, and they are dropped for the remaining processing description. Time is measured in tens of milliseconds. The force values are initially non-zero (20 units initial X force and 5 units initial Y force). These initial non-zero forces are averaged together to form the baseline forces. (C) X and Y force traces are converted into XY force vectors. The non-zero initial forces of (B) are now non-zero initial force vectors. (D) The baseline forces of (B) and (C) are removed from all the force vectors to produce "active" XY force vectors. The initial active forces are not exactly zero, because initial forces in (C) are not exactly equal to average force levels used as the baseline. The force vector with the largest magnitude is the peak force, chosen to represent this progression of forces. (E) The peak force from the stimulation trial is plotted at ankle position (110, -30). The force vector at (110, -30) and the other force vectors measured with the limb at the other limb positions, together form a force field.

Processing

Each force trace has two parts: "baseline and "active". Because I began collecting the force traces before the stimulus began, the first 50 to 100 milliseconds of the force traces represents an estimate of the baseline force levels (figure 4-1B and C). I computed the active force traces by subtracting the baseline force levels from the measured forces. For example, the active x-force trace for a trial was the measured x-force trace minus the baseline x-force value (figure 4-1D). The subtracted baseline forces include the effects of kinematic constraints, baseline muscular activation, and gravity.

The (x,y,z) active forces form a time-varying 3-dimensional force vector, the Active Force Vector, AFV(t). The time-varying force vectors sampled at each of the limb positions form a time-varying Force Field, FF(x, y, t). During spinal stimulation, we have found that the time-varying forces nearly always rise and fall along a line, so that AFV(t1) $\propto$ AFV(t2). Therefore, for spinal stimulation, FF(x, y, t) can be well-approximated by some time-invariant force field, by FF(x, y)[1]. I construct the time-invariant FF(x, y) by sampling the time-varying force field. In particualr, at each sampled position I used the peak of the time-varying force vector at that position, $\max_t \|AFV(t)\|$, as the force vector in the time-invariant force field, FF(x, y) (see figure 4-1E). Although the forces of FF(x, y) are three-dimensional, I only consider the two-dimensional (x, y) forces in this paper.

Statistical Analysis

I have measured a total of 43 force fields from 24 supra-spinal sites in 6 frogs. I have used these 43 force fields to test the hypothesis that supra-spinal force fields result from the recruitment of combinations of spinal force fields. The null hypothesis for this test is the possibility that supra-spinal force fields activate the muscles through the particular intervening organization imposed by the spinal cord; in particular, through the spinal force fields (shown in figure 1-7). The alternative hypothesis,

[1]The validity of summarizing supra-spinal force fields with time-invariant FF(x, y) remains to be tested.

which we accept if the statistics are significant, is that the muscles provide a better explanation for the supra-spinal force fields than the spinal force fields do.

This statistical test involves a few simple steps:

1. Step 1: Evoke a supra-spinal force field, SPFF.

2. Step 2: Estimate the non-negative (zero or positive) muscle and spinal force field coefficients (the 5 values a_i and the 17 values b_i) to reproduce SSFF:

$$\widehat{\mathrm{SSFF}}_{Sp} = \sum_{i=1}^{5} a_i \mathrm{SpFF}_i = \text{spinal fit}$$

$$\widehat{\mathrm{SSFF}}_{Mu} = \sum_{i=1}^{17} b_i \mathrm{MuFF}_i = \text{muscle fit}$$

   Where 5 is the number of spinal force fields, and 17 is the number of muscle force fields.

3. Step 3: If the supra-spinal force field is produced by co-activation of spinal force fields, then there should not be a significant difference in the errors of these fits:

$$\frac{\sum(\widehat{\mathrm{SSFF}}_{Sp} - \mathrm{SSFF})^2}{\sum(\widehat{\mathrm{SSFF}}_{Mu} - \mathrm{SSFF})^2} \sim F(N-1, N-1)$$

   Where N is the number of data values used to create these estimates. If I sample L leg positions, then N will be 2*L, because there are two error terms at each leg position: the error in the X force and the error in the Y force.

The F statistic will indicate whether he ratio of the errors is distinguishable from 1.0. If the supra-spinal force field is determined by a significant contribution of direct muscle activations or by any mechanism other than the activation of spinal modules, then there should be a significant difference in the errors. Thus, if the F statistic is significant, we will have evidence that the supra-spinal force field is not implemented by the hypothesized spinal circuitry. If the ratio of errors is not significant, then linear recruitment of spinal interneuronal force fields by supra-spinal fibers is a possible explanation of the results.

Power Analysis of the Test

An unusual aspect of the statistical test described above is that I am using it to accept the *null* hypothesis that there is *no* difference in the errors. If the statistical test is not significant, then I will begin to accept that the null hypothesis, which we interpret as indicating that supra-spinal fibers recruit only spinal force fields. It is not entirely clear how likely I am to be wrong in accepting the null hypothesis. If I were using the statistical test in the usual way, then a significance level of 0.05 would indicate that there is a 5% chance of being wrong in accepting the test. It would be desirable to know the same information – how likely I am to be wrong – for this test. In particular, I am interested in detecting differences in spinal vs muscle recruitment by supra-spinal fibers. The differences of interest lead to different error distributions that will cause me to accept the null hypothesis (no difference in the error distributions) with some probability. To find out that probability, I performed a statistical power analysis.

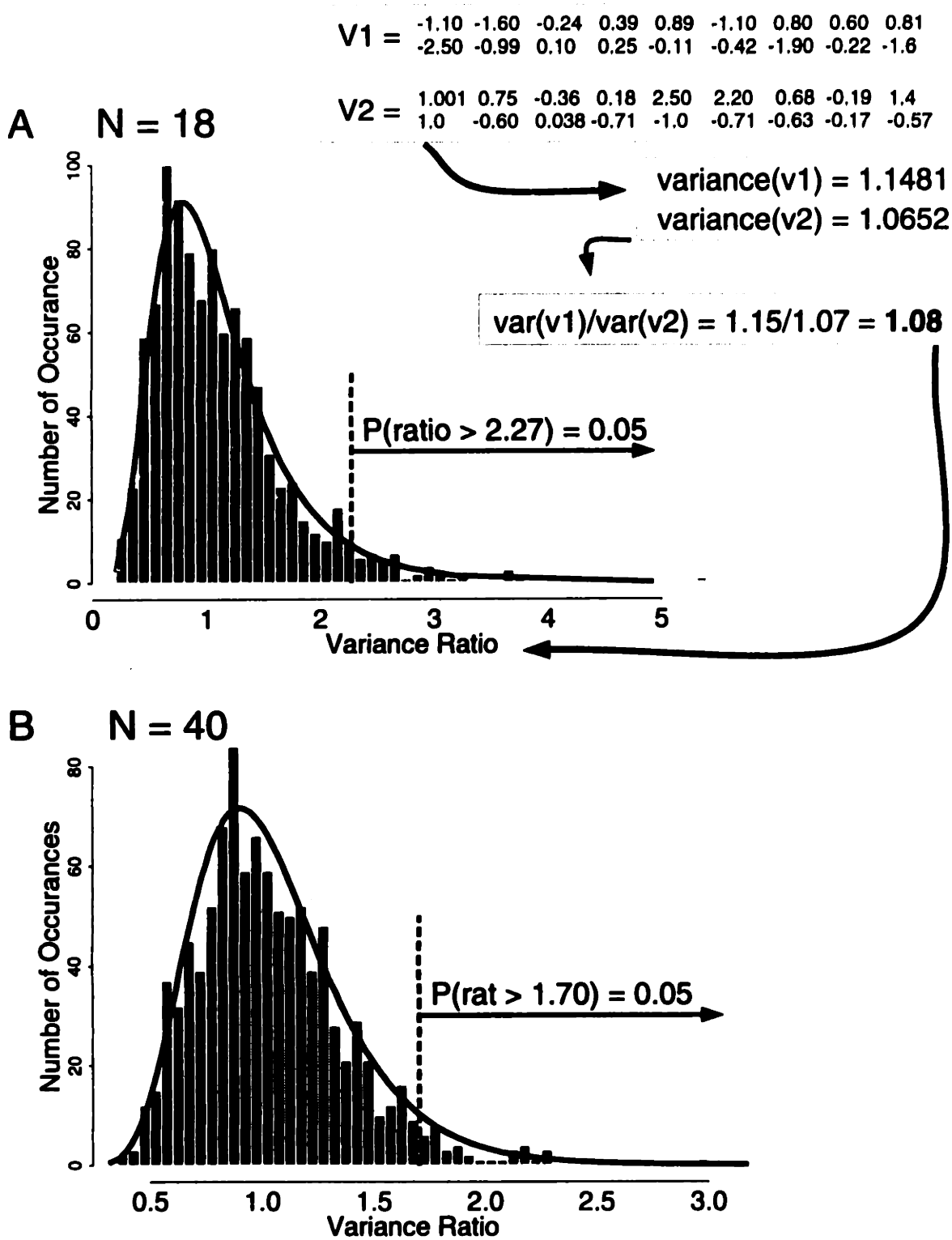
V1 = -1.10 -1.60 -0.24 0.39 0.89 -1.10 0.80 0.60 0.81
-2.50 -0.99 0.10 0.25 -0.11 -0.42 -1.90 -0.22 -1.6
V2 = 1.001 0.75 -0.36 0.18 2.50 2.20 0.68 -0.19 1.4
1.0 -0.60 0.038 -0.71 -1.0 -0.71 -0.63 -0.17 -0.57
A N = 18
variance(v1) = 1.1481
variance(v2) = 1.0652
var(v1)/var(v2) = 1.15/1.07 = 1.08
P(ratio > 2.27) = 0.05
Number of Occurance
Variance Ratio
B N = 40
P(rat > 1.70) = 0.05
Number of Occurances
Variance Ratio

Figure 4-2: Two F distributions under the Null Hypothesis
In this figure two F distributions are pictured. Random numbers that are generated from the sample variances of two Normal random variables will follow the F distribution. In particular, the boxed numbers called V1 and V2 (to the right of distribution (A)) are two random variables. Both V1 and V2 have 18 values associated with them. The 18 values were drawn from a Normal distribution with a variance of 1. The sample variance of each set of 18 numbers is another pair of random numbers (from a Chi Square distribution). The sample variances of the two variables V1 and V2 is 1.1481 and 1.0652, respectively. The ratio of these two variances is 1.07775. This ratio of variances is one random value drawn from an F distribution. (A) The theoretical F distribution for the sample variances of 18 Normal random numbers. The histogram in this figure is an empirical F distribution created from 1000 ratios of the kind just described. The fact that there are 18 numbers used to generate the sample variances is important to the shape of the histogram and also the shape of the theoretical distribution (dark line). The histogram and distribution both depend on the assumption that V1 and V2 have equal variances. That is, the two sample variances should be estimates of the same number. Under that assumption, it would be surprising to observe values of an F statistic greater than 2.27. The integral of the F distribution from 2.27 to infinity is 5% of the integral from 0 to infinity. (B) An empirical distribution and the theoretical F distribution for N = 40 samples. The histogram in this panel was constructed as in part (A), but variables V1 and V2 had 40 samples each from Normal distributions with equal variances. The 5% surprising value of the F statistic has now dropped to 1.7.

The point of the power analysis is to find out how likely it is that no difference in the errors will be found when in fact there is a difference. Figures 4-2 and 4-3 illustrate the mathematics underlying the statistical power analysis. The F test is used to test for a difference in sample variances. The F test compares the ratios of sample variances to the value at which the ratio is surprisingly large. If we use a 5% test level, and there is no difference in the two sample variances, the test will accidentally wrongly indicate there is a significant difference 5% of the times the test is used (on average). If we use a 5% test level and there is a 30% difference in two samples of 18 values each, then the test will wrongly indicate that there is *no* difference approximately 88% of the times the test is used (on average). We can gain more statistical power by sampling more numbers. If we use a 5% test level and there is a 30% difference in two samples of 40 values each, then the test will wrongly indicate there is *no* difference 80% of the times the test is used (on average). The point of the power analysis is to examine integrals (the shaded regions in figure 4-3) in order to find out how likely my test is to wrongly indicate that force fields are a

combination of spinal force fields when they are in fact produced by a combination of muscle force fields.

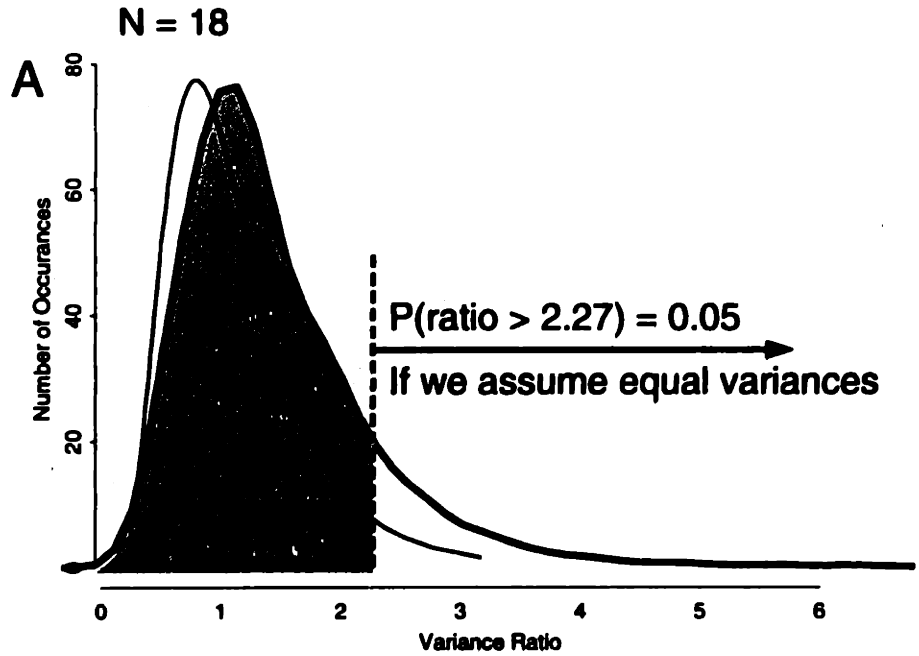

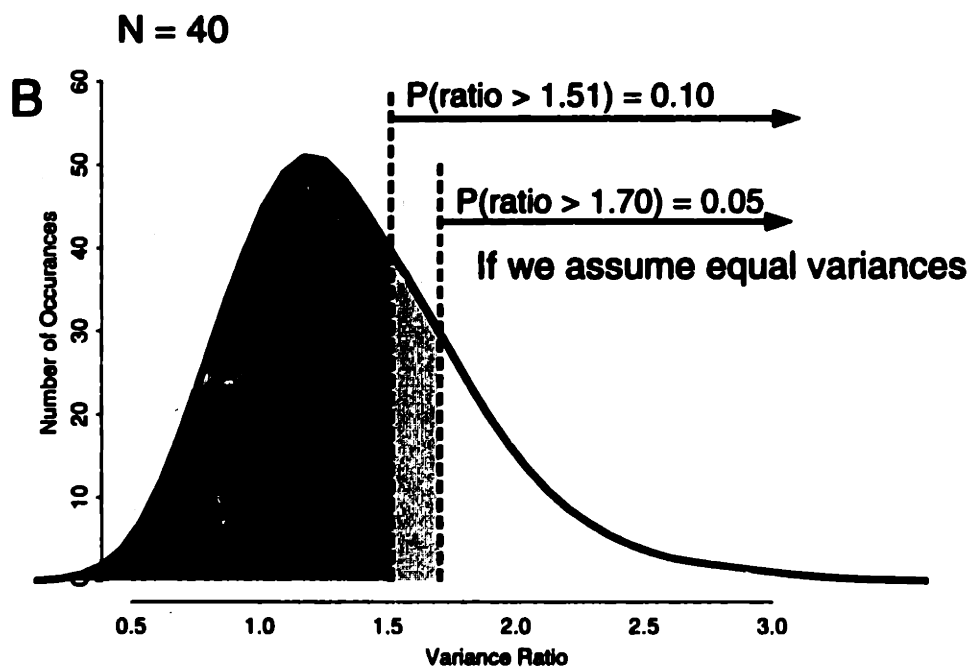

Performing the power analysis for the test of supra-spinal recruitment of spinal force fields requires that errors be generated somehow. Errors must be generated because the power analysis requires a distributional assumption: what differences do we want to be sure to detect? For example, in figure 4-3 the shaded distributions were generated from numerator and denominator Normal populations that had variances of 1.3 and 1.0 respectively. Having generated figure 4-3 I was able to compute the probable outcomes of an F test on the numerator and denominator sample variances. The errors of the spinal force field and muscle force field fits to supra-spinal force fields are also like sample variances: the errors have a mean value of zero, and the errors are computed from sum of squared differences. In order to find out the probable outcome of an F test on a ratio of fit errors, I need to make some kind of assumption about the distribution of spinal and muscle fit errors. Once I have assumed something about the underlying distributions, then I can generate error statistics according to those assumptions and use the generated statistics to compute the power of the spinal recruitment test.

The obvious distribution to consider is that of force fields constructed from random combinations of muscle models. Force fields generated from combinations of muscle force fields should produce significant spinal recruitment F statistics, just as the shaded distributions in figure 4-3 "should" produce significant variance ratio F statistics. I constructed 1000 force fields from uniform [0,1] random activations of muscle models (as in figure 2-6). I produced hypothetical supra-spinal force fields by sampling the random muscle combination force fields at a few (between 7 and 40) limb positions, and by adding Normal noise (zero mean, variance = 100 units) to the hip and knee torques. The hip and knee torques typically ranged from 10 to 10,000 units, so the signal to noise ratio ranged from approximately 10% to 99%, depending on the limb position. I then performed the statistical test on the sampled random force fields: I fit them with the muscle models and also with the spinal force field models. The ratio of the errors in the fits was compared to an F distribution for the corresponding number of samples, and the likelihood that the generated supra-spinal force field was produced from muscle activations was returned. In no case did

Figure 4-3: Two F distributions under H1

In this figure two F distributions are pictured. Random numbers that are generated from the sample variances of two Normal random variables will follow the F distribution. I have created the two shaded distributions in this figure precisely as in the previous figure, except that the sample variance of V1, the numerator variable, is 1.3 instead of 1.0. (A) The likelihood of accepting the null hypothesis for two sample variances with an expected ratio of 1.3. The light line is the theoretical F distribution for two samples of N=18 values drawn from equal-variance Normal distributions. The darker like is the empirical density observed in 1000 random values, each created from the ratio of sample variances. The sample variances used to create these numbers were not equal, so the F test would ideally indicate that the variances were not equal. This panel shows a dashed line at 2.27 (from figure 4-2), above which only 5% of the F values should fall under the null hypothesis. Note that the empirical (dark-lined) distribution is more likely than the null hypothesis distribution to produce numbers above 2.27. The shaded region under the dark-lined distribution is the value to be computed in order to gauge the power of the F test for a true variance ration of 1.3 and 18 samples from each population. The shaded region is (proportional to) the probability that the F test will nevertheless indicate that the sample variances are not different. The probability that a value from the dark-lined F distribution will fall in the shaded region is 88% Thus, the F test will indicate that there is no difference in the variances of the two sampled populations in 88% of all such experiments. (B) An empirical F distribution produced from 40 samples from Normal distributions with a true ratio of variances of 1.3. The null hypothesis distribution is not shown in this figure, because it is only used to produce the value over which we expect only 5% of the F statistics to fall. The shaded region is (proportional to) the probability that an F test performed on sample variances of 40 samples each will indicate that the two underlying populations have the same variances even though they really have different variances (1.3 for the numerator and 1.0 for the denominator). The dark grey illustrates the integral needed to compute the probability of a false negative when the F test is performed at an 0.1 level of confidence (68%), while the dark grey plus the lighter grey indicate the power of the statistical test when the F test is performed at the 0.05 level (80%).

the F test fail: random muscle activations plus noise were always identified as being produced from muscle combinations rather than from spinal force field combinations.

Preliminary Results

I first show preliminary results from animals with intact afferents. There is a methodological problem with afferent-intact experiments that I will describe. Two points can be made from the afferent-intact results: there are evoked force fields that are better fit by the muscles than by the spinal force fields, and there is preliminary indication that topographic maps of equilibrium point locations can be demonstrated by supra-spinal micro-stimulation. I next show several examples of force fields evoked by tegmental stimulation in deafferented frogs. These force fields are fit by the spinal force fields as well as by the muscle force fields.

Stimulation with Afferents Intact

My first experiments were performed with the afferents intact. When the afferents are intact, the afferents allow control strategies in which completely different muscles and/or spinal regions are recruited at different limb positions. The test that I use assumes that a single set of limb-position-independent coefficients can fit the supra-spinal force field with muscle force fields. Another set of limb-position-independent coefficients is used to fit the supra-spinal force field in terms of spinal force fields. The negative results, in which the supra-spinal force fields are shown to be possibly composed of spinal force fields, is not valid when the afferents are intact because the alternative hypothesis of feedforward recruitment of muscles is a straw man. The positive results, in which the supra-spinal force fields are shown to be composed of muscle force fields, does not really rule out supra-spinal recruitment of the spinal modules, because the afferents allow limb-position-dependent recruitment to which the test is not sensitive. Thus, the first set of 27 force fields measured in afferent-intact animals are only helpful as a demonstration of concept.

Figure 4-4 shows that it is possible to evoke a supra-spinal force field that is better fit by the muscle models than by the spinal models. In figure 4-4 we see data measured during brainstem stimulation, two reproductions of that data by spinal and muscle models, and the coefficients of those reproductions/fits/decompositions. Note

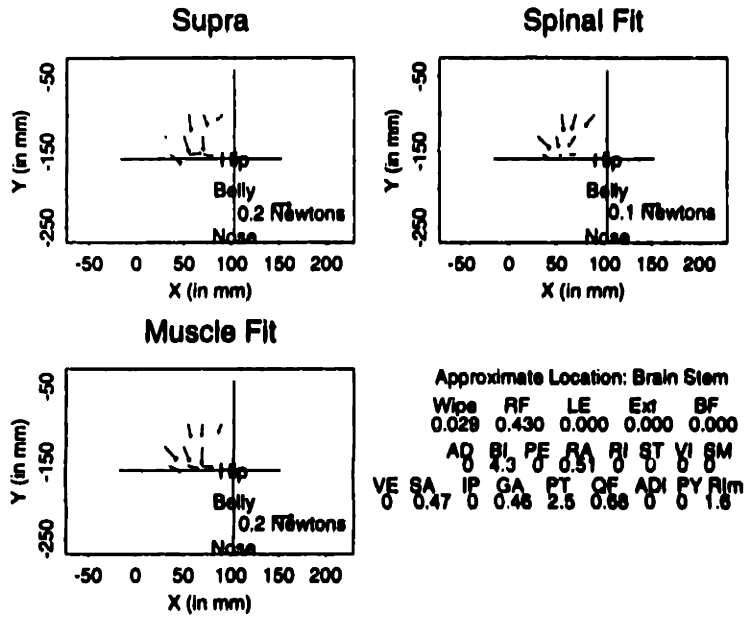

Figure 4-4: A fit of muscle models and spinal models to a brainstem force field The three panels in this figure show a force field evoked during brainstem stimulation and the two fits to that data by the muscle and spinal force field models. Each arrow in the three panels is a peak force vector. The x,y location of the base each arrow indicates the limb position at which the force was measured or computed. The hip, belly, and nose of the animal are indicated in each plot. The brainstem stimulation (300 msec burst at 200 Hz, 0.5 msec pulse width, 40 μA) produced forces pointing straight towards the hip when the limb was in flexion. The muscle fit was able to reproduce those forces but the spinal fit was not. The best fit of the spinal force fields to the brainstem force field was (0.029 * Wipe + 0.43 * Rostral Flexion). The best fit of the muscle force fields to the brainstem force field used 7 muscles: Biceps (BI), Rectus Anticus (RA), Sartorius (SA), Gastrocnemius (GA), Pectinius (PT), Quadratus Femoris (QF), and Rectus Internus Minor (RIm). Muscles QF and RIm are two different kinds of extensor (see chapter 2) and the other muscles are flexors.

that there is a near-zero force at the lateral edge of the data force field. Neither the muscle models nor the spinal models are able to reproduce that near-zero force. The fit by the muscle models appears to be more accurate overall than the fit by the spinal models. Because the afferents were intact during this experiment, the statistical test can not be interpreted in the way it was intended. Nevertheless, the test results were significant, so muscle models can be shown to fit a supra-spinal force field better than spinal models. Examination of the muscles used in the fit show that the fitting procedure predicts co-contractions of the different types of muscles defined in chapter 2.

Figure 4-5 demonstrates the potential of force fields for quantifying the complex feedback modulation generally hypothesized as the role of the cerebellum. Figure 4-5 is suggestive of a topographic map of force field equilibrium points. The apparent equilibrium posture of force fields in figure 4-5A-C becomes progressively more rostral as the electrode is moved laterally. There was no significant difference in the spinal and muscle fits to the force fields in figure 4-5. If topographic maps of cerebellar force fields that are fit by spinal force fields can be found in deafferented animals, then it will suggest that the cerebellar cortex (which does not project to the spinal cord) produces outputs in the spinal force field coordinate system. If stimulation and recording techniques can be used simultaneously in the cerebellum, then force fields and receptive fields could potentially serve as a powerful pair of tools in understanding cerebellar modulation of (medial in fig 4-5E and lateral in fig 4-5A,B,C,D) descending systems.

Stimulation with Afferents Cut

I have measured 16 force fields in 3 deafferented animals, and 14 of these show no significant difference between the spinal fit and the muscle fit. I measured eight force fields from three sites in the tegmentum in one deafferented frog, and none of these force fields showed a significant difference between the muscle fits and the spinal fits despite a large number of sampled limb positions. These eight force fields are densely sampled, in that I measured forces at many workspace locations. I show three of these force fields (one from each site) in figures 4-6 through 4-8.

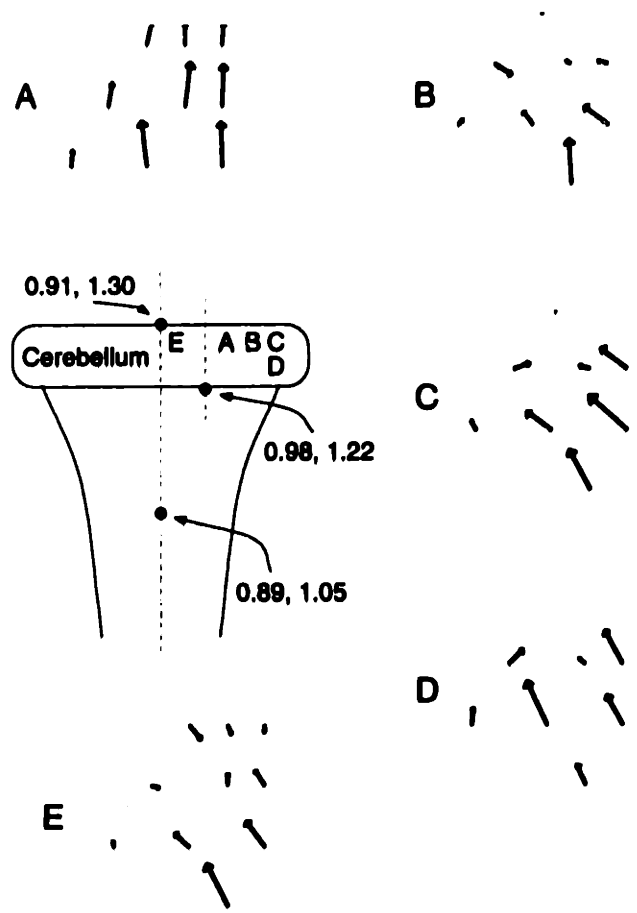

Figure 4-5: Five Cerebellar Force Fields The five data force fields in this figure were measured during cerebellar stimulation at the sites indicated. The cartoon shows the cerebellum and three sites on the surface of the brain that were measured with the vernier coordinate frame on the electrode holder. The electrode coordinates are in millimeters. The stimulus parameters were set at each locus (except E) by examining the strongest response at different frequencies, pulse width (chronaxie/rheobase measurements), and train duration. The electrode depth and best pulse width suggest that cell bodies in the cerebellar cortex were being stimulated. (A) Electrode coordinates (0.95, 1.28), depth = 0.500 mm. 400 msec train at 300 Hz, 40 μA pulses of width 0.6 msec. (B) Electrode coordinates (0.98, 1.28), depth = 0.35 mm. 400 msec train at 200 Hz, 40 μA pulses of width 0.6 msec. (C) Electrode coordinates (1.0, 1.28), depth = 0.6 mm. 400 msec train at 200 Hz, 30 μA pulses of width 0.6 msec. (D) Electrode coordinates (1.0, 1.25), depth = 0.45 mm. 400 msec train at 200 Hz, 20 μA pulses of width 0.8 msec. (E) Electrode coordinates (0.92, 1.28), depth = 0.5 mm. 400 msec train at 200 Hz, 80 μA pulses of width 0.8 msec.

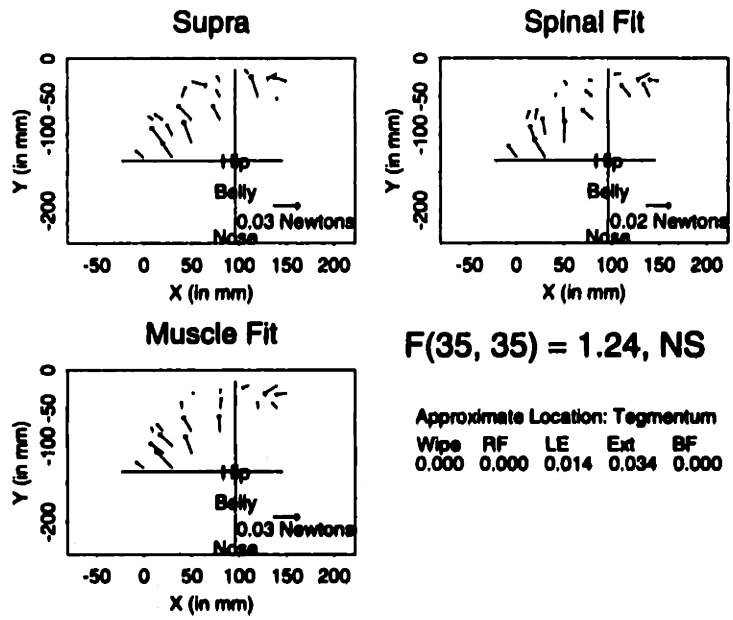

Figure 4-6: Tegmentum Site One Data and fits for a tegmental force field measured at 18 limb positions. The Spinal fit and the Muscle fit both reconstruct the data "pretty well". The F statistic has 35 degrees of freedom, because the errors are measured in two dimensions, hip and knee torque (2*18 positions minus one is 35). The F statistic is not significant, so we can apparently accept the null hypothesis, that there is no difference between the muscle and spinal errors. The tegmental force field is constructed from spinal force fields as (0.014 Lateral Extension + 0.034 Extension). Note that there is a hint of the lateral extension and extension equilibria in the data. Electrode depth = 1.3 mm. 500 msec train at 50 Hz, 15 μA pulses of width 0.6 msec.

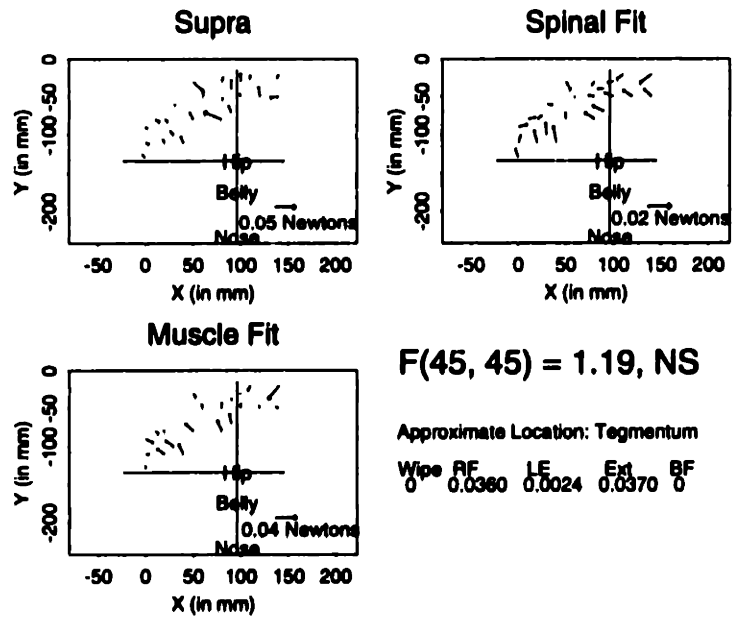

Figure 4-7: Tegmentum Site Two Data and fits for a tegmental force field measured at 23 limb positions. The Spinal fit and the Muscle fit both reconstruct the data "pretty well". The F statistic (F(45, 45) = 1.19) is not significant, so we can apparently accept the null hypothesis, that there is no difference between the muscle and spinal errors. The tegmental force field is constructed from spinal force fields as (0.036 Rostral Flexion + 0.0024 Lateral Extension + 0.037 Extension). Note that the lateral extension and extension equilibria can be seen in the data as reversals of forces. I have previously found non-linearities in the magnitudes of spinal force fields following deafferentation (Loeb, et al., 1993) that could explain why the underlying spinal force fields might be visible in their superposition. Electrode depth = 1.1 mm. 400 msec train at 50 Hz, 35 μA pulses of width 0.8 msec.

Summary

It is clearly possible to measure force fields in decerebrate frogs and decompose those force fields into linear combinations of spinal and muscle force field models. I have measured 43 supra-spinal force fields in six decerebrate frogs, and for 16 of these the frogs had beed deafferented. The force fields evoked during tegmental stimulation may indeed be composed of spinal force fields, in that the statistical test of the model errors were not significant. Thus, I have demonstrated in this chapter the feasibility of the new experimental method designed in this thesis.

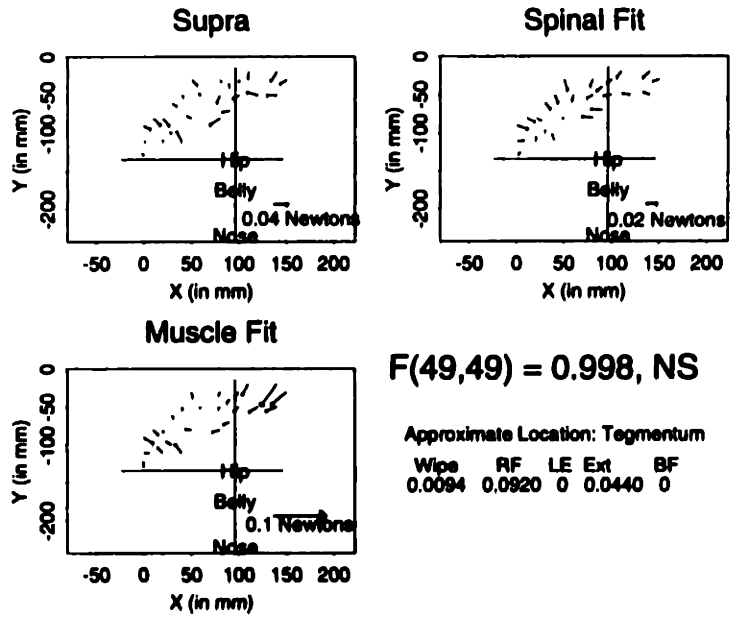

Figure 4-8: Tegmentum Site Three Data and fits for a tegmental force field measured at 25 limb positions. The Spinal fit and the Muscle fit both reconstruct the data "pretty well". The F statistic (F(49, 49) = 0.99) is not significant, so we can apparently accept the null hypothesis, that there is no difference between the muscle and spinal errors. The tegmental force field is constructed from spinal force fields as (0.0094 Wipe + 0.092 Rostral Flexion + 0.044 Extension). Note that the extension equilibrium can be seen in the data, as a reversal of forces in the most caudal extended limb positions. Electrode depth = 2.0 mm. 800 msec train at 60 Hz, 20 μA pulses of width 0.6 msec.

Appendix A

Bibliography

Alstermark, B. and Lundberg, A. (1992), "The C3-C4 Propriospinal System: Target-Reaching and Food-Taking", in Muscle Afferents and Spinal Control of Movement; Pergamon Press, Oxford, New York. IBRO Symposium (1991: Paris, France)

Asanuma H (1981) Microstimulation Techniques. In: Electrical stimulation research techniques (Patterson MM, Kesner RP eds), pp 61-69. New York: Academic Press.

Becker, R.A, Chambers, J.M, Wilks, A.R (1988), "The New S Language: A Programming Environment for Data Analysis and Graphics", Wadsworth and Brooks/Cole Computer Science Series, Pacific Grove, California, ISBN 0-534-09192-X

Binder, M.D, Heckman, C.J, Powers, R.K, (1993), "How different afferent inputs control motoneuron discharge and the output of the motoneuron pool", Current Opinion in Neurobiology, v. 3, pp. 1028 - 1034.

Bizzi E, Mussa-Ivaldi FA, Giszter SF (1991) Computations underlying the execution of movement: a novel biological perspective. Science 253: 287-291.

Buchanan, T.S, Almdale, D.P, Lewis, J.L, and Rymer, W.Z (1986), "Characteristics of Synergic Relations During Isometric Contractions of Human Elbow Muscles", *Journal of Neurophysiology*, v. 56, pp. 1225 - 1241.

Buchanan, T.S, Moniz, M.J, Dewald, J.P.A, and Rymer, W.Z. (1993), "Estimation of Muscle Forces About the Wrist During Isometric Tasks Using an EMG Coefficient Method.", J. Biomechanics, v. 26, pp. 547 - 560.

Chanaud, C.M., Pratt, C.A, Loeb, G.E (1991), "Functionally Complex Muscles of the Cat Hindlimb. V. The roles of histochemical fiber-type regionalization and mechanical heterogeneity in differential muscle activation", *Experimental Brain Research*, v. 85, pp. 300 - 313.

Cholewicki, J. and McGill, S.M., (1994) "EMG Assisted Optimization: A Hybrid Approach for Estimating Muscle Forces in an Indeterminate Biomechanical Model", J.Biomechanics, v.27, pp.1287 - 1289.

Corvaja, N, Grofova, I, and Pompeiano, O. (1973) "The Origin, Course, and Termination of Vestibulospinal Fibers in the Toad" Brain Behav. Evol. v 7, pp 401 - 423.

Crago, P.E, Peckham, P.H, Thrope, G.B. (1980), "Modulation of Muscle Force by Recruitment During Intramuscular Stimulation", IEEE Transactions on Biomedical Engineering v. BME-27, number 12, pp. 679 - 684.

Craig, J.J (1986) Introduction to Robotics, Addison-Wesley, ISBN 0-201-10326-5, Reading, Massachusetts.

Efron, B. (1982). *The Jackknife, the Bootstrap, and Other Resampling Plans.* Society for Inductrial and Applied Mathematics.

Favilla, M; Hening, W.; Ghez, C. (1989), "Trajectory Control in Targeted Force Impulses", Brain Research, v. 75, pp. 280 - 294.

Fukson, O.I., Berkinblit, M.B, Feldman, A.G (1980), "The spinal frog takes into account the scheme of its body during the wiping reflex" Science, v. 209, pp. 1261 - 1263.

Galagan, J.E.; Loeb, E.P.; Bizzi, E.*; "A Dynamic Model of the Frog Hindlimb Musculature"
Abstracts for the Society for Neuroscience 1995 Annual Meeting

Giszter SF, McIntyre J, Bizzi E (1989) Kinematic strategies and sensorimotor transformations in the wiping movements of frogs. J Neurophysiol 62: 750-767.

Giszter, S.F (1994) "Movement organization in the frog spinal cord: pre-rational intelligence?", in *Proceedings of the Conference on Emergence of Prerational intelligence in biology: from sensorimotor intelligence to collective behavior. Part 2.*,

pp25-36.

Giszter SF, Mussa-Ivaldi FA, Bizzi E (1993) Convergent Force Fields Organized in the Frog Spinal Cord. Journal of Neuroscience, v. 13, pp. 467 - 491.

Granata, K.P and Marras, W.S (1993), "An EMG-Assisted Model of Loads on the Lumbar Spine During Asymmetric Trunk Extensions", J. Biomechanics, v. 26, pp. 1429 - 1438

Hardt, D.E (1978), "Determining Muscle Forces in the Leg During Normal Human Walking – An Application and Evaluation of Optimization Methods" J. Biomechanical Engineering, v. 100, pp. 72 - 78.

Hof, A.L. and Van Den Berg, Jw. (1977), "Linearity Between the Weighted Sum of the EMGs of the Human Triceps Surae and the Total Torque", J. Biomechanics v. 10, pp. 529 - 539.

Hof, A.L. and Van Den Berg, Jw. (1981a), "EMG to Force Processing I: An Electrical Analogue of the Hill Muscle Model", J. Biomechanics v. 14, pp. 747 - 758.

Hof, A.L. and Van Den Berg, Jw. (1981c), "EMG to Force Processing III: Estimation of Model Parameters for the Human Triceps Surae Muscle and Assessment of the Accuracy by Means of a Torque Plate", J. Biomechanics v. 14, pp. 771 - 785

Hultborn, H. and Illert, M (1991), "How is Motor Behavior Reflected in the Organization of the Spinal Systems?" in *Motor Control: Concepts and Issues*, Ed. D.R Humphrey and H.-J. Freund, pp. 49 - 73.

Jacobs, R. A., Jordan, M. I., Nowlan, S., & Hinton, G. E. (1991). "Adaptive mixtures of local experts." in *Neural Computation, 3*, 1-12.

Jankowska, E. 1992, "Interneuronal Relay in Spinal Pathways from Proprioceptors", Progress in Neurobiology 38:335-378.

Kandel, E.R, Schwartz, J.H, Jessell, T.M (1991), "Principles of Neural Science, third edition", Elsevier Science Publishing Company, New York, ISBN 0-444-01562-0

Keynes, R.D and Aidley, D.J (1991), "Nerve and Muscle" Cambridge University Press, Cambridge. ISBN 0521 41042 8

Laskowski, M.B and Sanes, J.R (1987), "Topographic Mapping of Motor Pools onto Skeletal Muscles", *Journal of Neuroscience* v.7, pp. 252 - 260.

Lieber, R.L and Shoemaker, S.D (1988), "Muscle, joint, and tendon contributions to the torque profile of frog hip joint" ??

Lieber, R.L and Shoemaker, S.D (1988), "Muscle force and moment arm contributions to torque production in frog hindlimb", ??

Loeb, E.P, Giszter, S.F, Borghesani, P., and Bizzi, E.
Effects of dorsal root cut on the forces evoked by spinal microstimulation in the spinalized frog
Somatosensory and Motor Research v. 10 (1993), pp. 81 - 95.

Loeb, G.E, (1987) "Hard Lessons in Motor Control from the Mammalian Spinal Cord", *Trends in Neurosciences*, v. 10, pp. 108 - 113.

Loeb, G.E, He, J., Levine, W.S, "Spinal Cord Circuits: Are they Mirrors of Musculoskeletal Mechanics?", (1989) *Journal of Motor Behavior*, v. 21, pp. 473 - 491.

Macpherson, J.M (1994), "The force constraint strategy for stance is independent of prior experience", Exp. Brain Res., v. 101, pp. 397 - 405.

Masino, T, and Grobstein, P. (1989a) "The organization of descending tectofugal pathways underlying orienting in the frog, *Rana pipiens* II. Evidence for involvement of a tecto-tegmento-spinal pathway" Exp. Br. Res. v. 75, pp 245 - 264.

Masino, T, and Grobstein, P. (1989b) "The organization of descending tectofugal pathways underlying orienting in the frog, *Rana pipiens* II. Evidence for involvement of a tecto-tegmento-spinal pathway" Exp. Br. Res. v. 75, pp 245 - 264.

Masino, T, and Grobstein, P. (1990) "Tectal Connectivity in the Frog *Rana pipiens*: Tectotegmental Projections and a General Analysis of Topographic Organization" J. Comp. Neurol. v. 291, pp 102 - 127.

Matthews, Peter B.C (1981) "Muscle spindles: their messages and their fusimotor supply" in Handbook of Physiology Bethesda, Maryland ISBN 0-683-01105-7, pp 189 - 228.

Montgomery, N. M. (1988) "Projections of the Vestibular and Cerebellar Nuclei in *Rana pipiens*" Brain Behav. Evol. v 31, pp 82 - 95.

Mussa-Ivaldi, F.A (1992), "From Basis Functions to Basis Fields: Vector Field

Approximation from Sparse Data", Biological Cybernetics, v. 67, pp. 479 - 489.

Nichols, T.R and Houk, J.C (1976) The improvement in linearity and the regulation of stiffness that results from actions of the stretch reflex. J. Neurophysiol. 39:119 - 142.

Olney, A.J. and Winter, D.A (1985), "Predictions of Knee and Ankle Moments of Force in Walking from EMG and Kinematic Data", *J. Biomechanics*, v. 18, pp 9 - 20.

Ostry DJ, Feldman AG, Flanagan JR (1991) Kinematics and control of frog hindlimb movements. J Neurophysiol 65: 547-562.

Partridge, L.D, and Benton, L.A (1981) "Muscle, the motor" in Handbook of Physiology Bethesda, Maryland ISBN 0-683-01105-7, pp 43 - 106.

Palmer, K.I. (1990), "Modelling and Identification of Electrically Stimulated Muscle", M.S. Thesis, Mechanical Engineering, Massachusetts Institute of Technology, Cambridge, MA.

Pedersen, D.R, Brand, R.A, Cheng, C., Arora, J.S (1987), "Direct Comparison of Muscle Force Predictions Using Linear and Nonlinear Programming", Journal of Biomechanical Engineering, v.109, pp. 192 - 199.

Peterson, B.W. (1984) "The Reticulospinal System and Its Role in the Control of Movement" in Barnes, C.D. (ed) Brainstem Control of Spinal Cord Function Academic Press, Inc. (Harcourt Brace Jovanovich, Publishers). Orlando ISBN 0-12-079040-8, pp. 28 - 86.

Poggio, T and Girosi, F (1990), Proc. of the IEEE, v.78, pp 1481 – 1497.

Pournezam, M., Andrews, B.J, Baxendale, R.H, Phillips, G.F, and Paul, J.P (1987), "Reduction of muscle fatigue in man by cyclical stimulation" J. Biomed. Eng., v. 10, pp. 196 - 200.

Press, W.H, Teukolsky, S.A, Vetterling, W.T, Flannery, B.P, (1992), Numerical Recipes in C. The Art of Scientific Computing, 2nd Edition. Cambridge University Press. New York.

Rack. P.M.H and Westbury, D.R (1969), "The effects of length and stimulus rate on tension in the isometric cat soleus muscle", J. Physiology London, v. 240, pp. 443

- 460.

Riehle, A., and Requin, J. (1989), "Monkey Primary Motor and Premotor Cortex: Single-Cell Activity related to Prior Information About Direction and Extent of an Intended Movement", J. Neurophys., v.61, pp. 534 - 549.

Rubinson, K. (1968) "Projections of the Tectum Opticum of the Frog" Bain Behav. Evol. v. 1, pp 529 - 561.

Schotland JL, Lee WA, Rymer WZ (1989) Wiping and flexion withdrawal reflexes display different EMG patterns prior to movement onset in the spinalized frog. Exp Brain Res 78: 649-653.

Simpson, J.J. (1976) "Functional Synaptology of the Spinal Cord" in Llinas, R, and Precht, W. (eds.) Frog Neurobiology, a handbook Springer-Verlag, Berlin, Heidelberg, New York. ISBN 3-540-07606-9 pp 728 - 746

Smith, J.L., Zernicke, R.F (1987), "Predictions for Neural Control Based on Limb Dynamics", *Trends in Neuroscience*, v. 10, pp. 123 - 128.

Solomonow, M., Baratta, R., Zhou, B.H, Shoji, H., and D'Ambrosia, R.D. (1987), "The EMG-Force Model of Electrically Stimulated Muscle: Dependence on Control Strategy and Predominant Fiber Composition". IEEE Transactions on Biomedical Engineering, V. BME-34, pp. 692 - 703.

Ten Donkelar, H.J, (1982) "Organization of Descending Pathways to the Spinal Cord in Amphibians and Reptiles" Progress in Brain Research v 57, pp 25 - 67.

Wickland, C.R, Baker, J.F, Peterson, B.W, (1991) "Torque Vectors of Neck Muscles in the Cat", *Experimental Brain Research*, v. 84, pp.649 - 659.

Windhurst, U.R, Burke, R.E, Dieringer, N., Evinger, C, Feldman, A.G, Hasan, Z, Hultborn, H, Illert, M, Lundberg, A.P, MacPherson, J.M, Massion, J, Nichols, T.R, Schwarz, H.R.M, Vilis, T (1991), "Group Report: What are the Output Units of Motor Behavior and How Are They Controlled?" in Motor Control: Concepts and Issues, Humphrey, D.R and Freund, H.J (Eds), John Wiley & Sons, Ltd.

Winters, J.M. and Stark, L. (1988), "Estimated Mechanical Properties of Synergistic Muscles Involved in Movements of a Variety of Human Joints." J. Biomechanics v. 21, pp. 1027 - 1041

Wolpert, D.M., Ghahramani, Z., Jordan, M.I. (1995), "Are arm trajectories planned in kinematic or dynamic coordinates? An adaptation study", Experimental Brain Research, v. 103, pp. 460-470

Zajac, F.E and Winters, J.M (1990), "Modeling Musculoskeletal Movement Systems: Joint and Body Segmental Dynamics, Musculoskeletal Actuation, and Neuromuscular Control", in *Multiple Muscle Systems: Biomechanics and Movement*, J.M Winters and S.L-Y. Woo (eds), pp. 121 - 147.

Zajak, F.E, (1989), "Muscle and Tendon: Properties, Models, Scaling, and Application to Biomechanics and Motor Control", Critical Reviews in Biomechanical Engineering, v. 17, pp. 359 - 411.